

Assessing the effects of compaction and saturation on diffusion and diffusive fractionation of methane

Towards an improved quantification of methane oxidation in land-fill cover soil

H.P.W. Blom



Assessing the effects of compaction and saturation on diffusion and diffusive fractionation of methane

Towards an improved quantification of methane oxidation
in landfill cover soil

by

H.P.W. Blom

to obtain the degree of Master of Science
at the Delft University of Technology,
to be defended publicly on Wednesday December 12, 2018 at 14:00 PM.

Student number: 4256972
Project duration: April 23, 2018 – December 12, 2018
Thesis committee: Dr. J. Gebert, TU Delft, supervisor
Dr. H. Hajibeygi, TU Delft
Prof. dr. ir. T. Heimovaara, TU Delft

An electronic version of this thesis is available at <http://repository.tudelft.nl/>.
Cover image: Dr. Ok-Youn Yu, Appalachian State University [54]

Summary

A considerable contribution to the greenhouse effect originates from landfills. This contribution originates from the degeneration of waste in the landfill. The gas which is created during the degeneration consists of 40 to 60% methane. One mole of methane has a global warming potential which is 28 times higher than that of carbon dioxide. Therefore, emissions of methane should be reduced. One method which can be used to reduce this emission is the oxidization of methane to carbon dioxide. This can be done by the construction of a cover soil with methanotrophic bacteria in the soil. These bacteria oxidize methane as their source of carbon and energy. This oxidation process discriminates against the heavier isotopes present in the gas, this shifts the isotope signature. A method to determine the oxidation efficiency of the methane is based on the evaluation of this change in isotope signature over the cover soil. Next to the fractionation of isotopes due to oxidation, fractionation also occurs due to diffusion. However, fractionation due to diffusion is generally assumed to be negligible. Mostly, this assumption is valid, since the dominant part of transport is advective; which does not discriminate against an isotope.

In this thesis the effect of compaction and saturation on two sands are evaluated. Using this evaluation, the criteria during which diffusion becomes an important transport phenomena are determined. This is determined by a series of experiments, where the concentration of methane is monitored while the gas diffuses through a soil sample. In this thesis the effect of the soil matrix on the fractionation of methane is also evaluated. This is evaluated by performing isotope spectrometry on samples of gas, taken at different times during the experiments. These two aspects are combined to evaluate if the oxidation efficiency can still be determined using fractionation of stable methane isotopes when diffusion plays a considerable role in gas transport.

During the experiments the decrease of methane in the chamber was measured. Spread over two soils, for a total of 18 variations in compaction or saturation the decrease of methane over time was measured. The results of the experiments show that for diffusion no distinction between variation in compaction and saturation needs to be made. Compaction and saturation can be described together for both soils using the air-filled porosity. The relation between the air-filled porosity and the effective diffusion coefficient is linear for both soils. Due to the large sand fraction the share of coarse pores is high for the whole range of compaction, meaning that no significant increase of tortuosity is visible in the relation between air-filled porosity and the effective diffusion coefficient. When the effective diffusion coefficients are compared to effective permeability values of these soils, it showed that the diffusion is more important for drier and more compacted soils. Thus, diffusive transport becomes important for gas transport over a cover soil when the pressures are lower, the soil is drier, and the soil is more compacted.

The fractionation factors due to diffusion, which have been determined for a selection of experiments, showed no trend with any other measured parameters. The precision of the measured values from which the fractionation factors are determined is high. Thus, the confidence in the fractionation factors is high. The lack of a trend present means that in sand the soil matrix has no effect on the fractionation factor. This means that the fractionation factor due to diffusion in soil is the same as in free air. For the calculation of the oxidation efficiency with a relevant diffusive flux the ratio of diffusive to advective flux needs to be determined but the fractionation factor due to diffusion is constant. Before the oxidation efficiency can be calculated, first the load needs to be corrected for any loss through hot-spots. Next, the advective flux and diffusive flux are combined, this is done by adding the fluxes together. The fluxes can be added because there are no interdependent effects, each flux only increases the total flux. Thus, the oxidation efficiency can be calculated using the changes in isotope signatures, even when a significant diffusive flux is present.

Preface

Before you lies the culmination of my academic career thus far; the thesis I wrote to obtain my master thesis at the Delft University of Technology. It is ever important to reduce our impact on the environment and I hope that the findings in this thesis will find their way to make a contribution towards the reduction of the impact of old landfills. Writing this thesis would not have been possible without the devotion of the members of my graduation committee. Therefore, I would like to thank Timo Heimovaara and Hadi Hajibeygi for their support and valuable insights throughout these months. I would like to especially thank Julia Gebert for giving me the opportunity to work on this topic, for all the time she had available for me, and the continuous enthusiasm with which she always discussed the topic. The lab technicians should of course not be forgotten, I also want to thank them for their contribution to the experimental work I performed.

To the Atmospheric Physics and Chemistry Group of the University of Utrecht, and especially to Prof. dr. T. Roeckmann and M. Menoud, I want to express my gratitude for the stable isotope mass spectrometry they performed and for the explanations on the workings of the device.

Of course my gratitude also goes out to my family and friends for their continuous support during my time at the Delft University of Technology.

H.P.W. Blom
Delft, December 12th 2018

Nomenclature

Chemical formulas

CH ₄	Methane
CO ₂	Carbon dioxide
H ₂ O	Water
O ₂	Oxygen

Subscripts

<i>a</i>	In free air
<i>g</i>	Gas molecule
<i>i</i>	For species <i>i</i>
<i>p</i>	Pore
<i>w</i>	Of water
<i>atm</i>	Value at atmosphere
<i>ij</i>	For species <i>i</i> in <i>j</i>
<i>mix</i>	Of the mixture
<i>ox</i>	Due to oxidation
<i>t=0</i>	Value at time 0
<i>trans</i>	Due to transport
0	For normalized conditions, usually in free air
p	In soil

Parameters

α	Fractionation factor	-
κk_r	Effective permeability	m^2
λ	Gas mean free path	m
λ_r	Reaction rate constant	mol/s
μ	Bulk gas viscosity	Pa * s
ϕ	Porosity	-
τ	Tortuosity of the medium	-
τ_{yx}	Force in the x-direction on a unit area perpendicular to the y-direction	kg/m ²
ε	Soil air-filled porosity	-
<i>A</i>	Area	m^2

c	Concentration	mol/m^3
D	Diffusion coefficient	m^2/s
d	Diameter	m
DE	Direct emission correction factor	-
E	Energy	J
J	Flux	$mol\ m^{-2}s^{-1}$
k_B	Boltzmann constant	$m^2\ kg\ s^{-2}\ K^{-1}$
K_n	Knudsen number	-
L	Length	m
m	Mass	kg
$M\%$	Measured volume percentage of methane	
N	Knudsen diffusion flux	$mol\ m^{-2}s^{-1}$
n	Number of moles of gas	-
P	Pressure	Pa
p	Pressure	Pa
R	Ideal gas constant	$J\ mol^{-1}\ K^{-1}$
R	Ideal gas constant	J/mol/K
R	Rate of diffusion	mol/s
r_C	Kinematic fractionation constant for carbon	-
T	Temperature	K
t	Time	s
U	Voltage	V
V	Volume	m^3
v	Velocity	m/s
X	Mole fraction	-
x	Fraction of methane in the chamber	
z	Elevation from a fixed point	m

List of Figures

2.1	Schematic cross section of a biocover [20]	6
2.2	Soil gas profile over a landfill cover soil	7
2.3	Effective diffusivity plotted versus the air-filled porosity, showing the non-linear relation [17]	9
2.4	Effective diffusivity plotted versus the air-filled porosity, for different Proctor densities [17]	9
2.5	Left: Schematic view of partial saturation Right: Schematic of the permanent wilting point Source: [39]	15
3.1	The hammer used for compaction; base plate diameter: 15.1 cm	21
3.2	Picture of the test setups with soil samples in place	21
3.3	Schematic of the test setup	22
3.4	Example of raw data; shown here, soil WIE, compaction 80%, saturation 20.47%V	25
4.1	Example of the fit to the measured data, for soil HH at 85% of the Proctor density	32
4.2	Effective diffusivity plotted versus the compaction for both soils	33
4.3	Air-filled porosity plotted versus the compaction for both soils	33
4.4	Effective diffusion coefficient plotted versus the bulk density for the compaction series	33
4.5	Example of the fit to the measured data, for soil WIE at 25.53%V saturation	34
4.6	Plot of the effective diffusion coefficient versus the saturation as percentage of the total volume	35
4.7	Plot of the air-filled porosity versus the saturation as percentage of the total volume	35
4.8	Effective diffusion coefficient plotted versus the bulk density for the saturation series	35
4.9	Effective diffusivity plotted versus the porosity	36
4.10	α_{trans} plotted versus the effective diffusion coefficients from the tests	38
4.11	α_{trans} plotted versus all effective diffusion coefficients, from the performed tests and literature	38
D.1	Effective permeability plotted versus the compaction level [52]	63
D.2	Effective permeability plotted versus the saturation [52]	64
D.3	Measured gas diffusivities and air permeabilities in L3 sandy clay loam and L5 sandy clay. (a), (c) Sieved, repacked soil. (b), (d) Undisturbed soil (closed symbols) and structurally disturbed soil (open symbols). [32]	64
D.4	Fractionation factor for transport plotted against the soil gas diffusivity [16]	65
E.1	Leakage test for set-up 1	67
E.2	Leakage test for set-up 2	68
E.3	Leakage test for set-up 3	68
E.4	Leakage test for set-up 4	69
E.5	Leakage test for set-up 5	69
E.6	Raw data for soil HH at 75% of the Proctor Density	70
E.7	Raw data for soil HH at 80% of the Proctor Density	71
E.8	Raw data for soil HH at 85% of the Proctor Density	71
E.9	Raw data for soil HH at 90% of the Proctor Density	72
E.10	Raw data for soil HH at 95% of the Proctor Density	72
E.11	Raw data for soil HH at 25.49%V saturation	73
E.12	Raw data for soil HH at 18.58%V saturation	73
E.13	Raw data for soil HH at 8.59%V saturation	74
E.14	Raw data for soil HH at 5.18%V saturation	74
E.15	Raw data for soil WIE at 75% of the Proctor Density	75
E.16	Raw data for soil WIE at 80% of the Proctor Density	75
E.17	Raw data for soil WIE at 85% of the Proctor Density	76
E.18	Raw data for soil WIE at 90% of the Proctor Density	76

E.19	Raw data for soil WIE at 95% of the Proctor Density	77
E.20	Raw data for soil WIE at 31.24%V saturation	77
E.21	Raw data for soil WIE at 25.53%V saturation	78
E.22	Raw data for soil WIE at 16.74%V saturation	78
E.23	Raw data for soil WIE at 12.49%V saturation	79
F.1	The fit of α_{trans} for the soil sample at 75% of the Proctor Density	81
F.2	The fit of α_{trans} for the soil sample at 85% of the Proctor Density	81
F.3	The fit of α_{trans} for the soil sample at 95% of the Proctor Density	82
F.4	The fit of α_{trans} for the soil sample in the saturation series at 5.78% air-filled porosity	82
F.5	The fit of α_{trans} for the soil sample in the saturation series at 12.9% air-filled porosity	82
F.6	The fit of α_{trans} for the soil sample in the saturation series at 29.0% air-filled porosity	83
G.1	Results of the t-test of the effective diffusion coefficients for the compaction and saturation series of soil HH	85
G.2	Results of the t-test of the effective diffusion coefficients for the compaction and saturation series of soil WIE	86
G.3	Results of the t-test of the effective diffusion coefficients for the compaction and saturation series of both soils	86

List of Tables

2.1	Comparison of the gas transport models	13
3.1	Soil properties [52]	19
3.2	Soil hydraulic characteristics and targeted water contents, at 85% Proctor density	20
3.3	Dimensions of the test setup	22
3.4	Leakage of methane from the test setups per hour, in volume percentage methane of the whole chamber	24
3.5	Values used to determine the best value for the effective diffusion coefficient	26
3.6	Correction factors for direct emission (DE) and methane load to cover (1-DE) [18]	29
4.1	Targeted densities and levels of saturation for the parallels	31
4.2	Root mean square errors for the different literature models	39
4.3	Values used to determine the percentage of diffusive flux, as part of the total flux of methane for the compaction series	40
4.4	Values used to determine the percentage of diffusive flux, as part of the total flux of methane for the saturation series	40
4.5	Increase in calculated oxidation efficiencies when taking diffusion into account, given in percentage increase of the original value	41
C.1	Targeted densities and levels of saturation for the parallels, the saturation levels are given as percentage of the total volume	59
C.2	Actual densities and saturation levels	60
C.3	Actual densities and saturation levels	61
G.1	Coefficients of determinations for linear and exponential relations for both soils	86
H.1	The values used for the increased values for oxidation efficiency, for the paper by Cabral et al [9]	87
H.2	The values used for the increased values for oxidation efficiency, for the paper by Chanton et al [10]	87

Contents

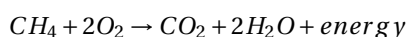
Summary	iii
Nomenclature	vii
List of Figures	ix
List of Tables	xi
1 Introduction	1
1.1 Problem definition	1
1.2 Research questions	2
1.2.1 Sub-questions	2
1.3 Hypotheses	2
2 Theoretical background	5
2.1 Methane oxidation systems	5
2.1.1 Methane oxidation	6
2.1.2 Methanotrophic activity	7
2.2 Diffusion	8
2.3 Advection	8
2.4 Drivers of diffusion in landfill cover soils	8
2.5 Types of diffusion	10
2.5.1 Molecular diffusion	10
2.5.2 Knudsen diffusion	11
2.5.3 Nonequimolar flux	12
2.6 Gas transport models	12
2.6.1 Advective-diffusion model	12
2.6.2 Maxwell-Stefan equations	12
2.6.3 Dusty gas model	13
2.6.4 Gas transport model comparison	13
2.6.5 Diffusion coefficient approximations	13
2.7 Unsaturated zone	14
2.7.1 Water retention	15
2.8 Fractionation of stable isotopes	16
3 Methodology	19
3.1 Soils	19
3.2 Soil preparation	19
3.3 Setup for the diffusion experiments	21
3.4 Measurement procedure	22
3.4.1 Leakage tests	23
3.4.2 Sensor calibration	24
3.5 Data evaluation	24
3.5.1 Calculation of the effective diffusion coefficients	24
3.5.2 Fractionation of stable isotopes	26
3.5.3 Validation	26
3.6 Literature models	27
3.7 Share of diffusive flux in total gas transport	28
3.8 Fractionation method including diffusion	28

4	Results	31
4.1	Data evaluation	31
4.1.1	Compaction series	31
4.1.2	Saturation series	34
4.1.3	Effect of air-filled porosity on the effective diffusion coefficient	36
4.1.4	Fractionation of carbon stable isotopes	37
4.2	Literature models	38
4.3	Share of diffusive flux in total gas transport	39
4.4	Including diffusion when using stable isotope fractionation to quantify methane oxidation efficiency	41
5	Discussion	43
5.1	Air-filled porosity	43
5.2	Soil diffusivity	43
5.3	Fractionation of stable methane isotopologues	44
5.4	Contribution of diffusion to the release of methane gas to the atmosphere	45
5.5	Quantifying methane oxidation in landfill cover soils	45
6	Conclusions	47
7	Recommendations for future research	49
	Bibliography	51
A	Derivation of Graham's law	55
B	Derivation of equation 3.3	57
C	Saturation and densities of used soils	59
D	Figures from literature	63
E	Raw data	67
E.1	Leakage tests	67
E.2	Experimental data	70
F	Determination of the fractionation factors	81
G	Statistical analyses	85
H	Data used to determine the increased predictions in Chapter 4.4	87

Introduction

1.1. Problem definition

In current society, more emphasis is being placed on reducing the emissions of greenhouse gasses. One example of a source of anthropogenic greenhouse gasses are old landfills. In landfills the decomposition of organic matter creates methane and carbon dioxide. In older landfills the waste is not isolated and the produced landfill gas can diffuse through the cover soil to the atmosphere. Of all methane emissions to the atmosphere, an estimated 11% originate from landfills [23]. The impact of landfills on the environment can be significantly reduced by oxidizing the produced methane to carbon dioxide. The oxidation reaction is as follows:



This reaction is beneficial from an environmental perspective, as the global warming potential of a molecule of methane is approximately 28 times higher than a molecule of carbon dioxide [24]. To combat the emissions of methane first the landfill gas is captured actively, when the gas is captured it can be used for energy recovery or simply be flared. When the production of landfill gas decreases over the years, at a point this active aftercare is not feasible anymore. When active aftercare is not feasible anymore passive aftercare is used, during this phase there is no continuous effort to reduce the emissions of methane. However, there are still methods to reduce the emissions of methane. A possible reduction strategy is microbial methane oxidation in the cover soil, which is referred to as a biowindow or biofilter. This method is based on presence of a type of bacteria which oxidizes methane as their source of energy and carbon; methanotrophic bacteria.

One method to quantify methane oxidation is by examining the carbon isotope fractionation in methane. Isotopes are the same chemical element, thus with the same number of protons but with a different number of neutrons. When a molecule contains an isotope the molecule is referred to as an isotopologue. There are two stable isotopes for carbon, ^{12}C and ^{13}C . The lighter isotope, ^{12}C , is oxidized slightly faster than the ^{13}C isotope [2]. This results in an enrichment of ^{13}C in the methane remaining in the cover soil. The ratio of ^{13}C isotopes at the surface and in the waste body can be used to estimate the degree of methane oxidation. However, not only oxidation is a cause of fractionation of stable carbon isotopes, fractionation can also be attributed to diffusion of methane. In previous work it was shown that $^{12}\text{CH}_4$ diffuses 1.9% faster than $^{13}\text{CH}_4$ due to their different diffusion coefficients [30]. In general, fractionation due to diffusion is assumed to be negligible. This assumption is made since gas transport is expected to be dominated by advection, originating from pressure difference between the landfill and the atmosphere. Advection does not discriminate based on molecular weight. When advection is the dominant transport phenomena the fractionation effects originating from the diffusion are negligible.

However, in landfills large concentration gradients occur over the landfill cover soils, the volume percentage of methane in the waste body is generally in the range of 40% to 60% and the volume percentage of methane in the atmosphere is 0.000179% [46]. As a consequence of this concentration gradient, diffusion

is expected to be a prominent gas transport process. Therefore, the effects of fractionation during the diffusive transport need to be taken into account, this fractionation occurs due to the difference in molecular weight between the isotopes. In previous research [16], it was suggested that this fractionation of methane is limited by the soil, and thus it needs to be better quantified before it is used in calculations of oxidation efficiencies. To be able to better quantify the fractionation of stable methane isotopes due to diffusion, any variation due to heterogeneity in the soil properties and variations in moisture content needs to be known. The compaction, saturation, and soil texture affect the pore system through which diffusion occurs, by either elongating the diffusive path or available volume of air for diffusion to occur in. This is used to determine if stable isotope fractionation is able to quantify methane oxidation when relevant diffusive flux is present over the landfill cover soil.

1.2. Research questions

To assess the use of stable fractionation of methane isotopes for the quantification of methane oxidation efficiencies, the effect of the soil on the rate of diffusion and thus the contribution of diffusion to the total transport of methane needs to be known. Also, the effect of the soil on the fractionation of stable methane isotopes needs to be known. For this, two research questions were formulated. To answer the two research questions, five sub-questions are formulated to facilitate in answering the research questions.

1. What is the effect of compaction and saturation on diffusion and diffusive fractionation of methane?
2. How does diffusive flux affect the quantification of methane oxidation in the landfill cover soil when using fractionation of stable methane isotopes?

1.2.1. Sub-questions

To answer the research questions above, the sub-questions will give the smaller components needed to answer these questions.

- What is the relationship between compaction or saturation and air-filled porosity?
- How does soil diffusivity relate to air-filled porosity?
- What is the effect of soil diffusivity on the fractionation of stable CH₄ isotopologues?
- Which type of existing model is most suitable for modelling the gas diffusivity at different compaction and saturation levels?
- What is the contribution of diffusion through a cover soil to the release of CH₄-gas to the atmosphere?

1.3. Hypotheses

The expected outcomes to the research questions are described below for each question separately. Then, the two hypotheses for the research questions the different hypotheses for the sub-questions are presented, to test all these hypotheses the experiments described in this thesis are used.

1. It is hypothesized that with both an increased compaction and an increased saturation level the rate of diffusion decreases due to the limitation of the available pore space for diffusive transport. The expectation is that blockage of pore throats due to the increased compaction and saturation levels will reduce the rate of diffusion, but will also limit the fractionation of stable methane isotopes. The limitation the soil has on the diffusion rate is expected to reduce the difference in the ratio of the diffusive speeds of the isotopes.
2. It is expected that quantifying the methane oxidation is also possible when the diffusive flux increases. However, when the diffusive flux becomes significant, fractionation due to transport needs to be quantified since fractionation due to diffusion affects the calculation of the oxidation efficiency. As mentioned before, the hypothesis is that the fractionation factor will vary in space due to the heterogeneity of soil in relation to the diffusivity of the soil.

These two hypotheses are based on the expected results of the sub-questions. For saturation and compaction it is known that a higher degree of either will reduce the air-filled porosity, since both will increase the volume fraction of either water or solid. It is anticipated that the soil diffusivity is positively correlated to the air-filled porosity, as volume through which diffusion can occur is reduced by the presence of the soil matrix [1]. This relation is expected to be exponential, since at a certain point an increasing number of pore throats will get blocked. This would increase the tortuosity more than the proportional decrease due to decreasing air-filled porosity. Additionally, no diffusion is expected to occur below the 10% air-filled porosity threshold [17].

For the soil diffusivity, the expectation is that a positive correlation to the fractionation of stable CH_4 isotopologues will be found. The fractionation effects will be smaller as diffusion through pores will be restricted. It is reasoned that the difference in effective diffusion coefficients for the ^{12}C and ^{13}C isotopes becomes smaller due to the restrictions imposed by the characteristics of the soil. On the other hand, the diffusive path will in general be longer when the effective soil diffusivity is lower. This could result in a longer path along which fractionation can occur. However, this effect of a longer path is expected to be smaller than the reduced rate of diffusion, resulting in a positive correlation between the soil diffusivity and the fractionation.

A variety of models has been developed to predict the diffusive behavior of gas in soil. One of the three water-induced linear reduced models described by Moldrup et al [33] are expected to be superior, these models proved to be adequate to model a wide variety of soils [33]. Each of these three models is considered a viable option to give predictions closest to reality, since they are estimations of the tortuosity of the soil. However, as these models are very similar, no distinction can be made between the different WLR models at this stage of the research. The models are given by the formulas in chapter 2.6.5. It is expected that the diffusion of CH_4 contributes significantly to the physical transport of CH_4 . At least, the contribution cannot be disregarded for landfill cover soils and will result in more realistic predictions.

2

Theoretical background

The theoretical background for this thesis is elaborated upon in this chapter. First a general overview of methane oxidation systems is given, including a general overview of methane oxidation and methanotrophic activity. Next, the transport of gas through the cover soil is discussed, by the two drivers diffusion and advection. Then, the diffusion is described by the various drivers of the process and using various models found in literature. Lastly, the water retention processes and models are explained and fractionation effects of the isotopes during diffusion are described.

2.1. Methane oxidation systems

To reduce methane emissions from landfills, different methods are used during different stages of the lifetime of the landfill. In the first decades after closure of the landfill active aftercare is used. One aspect of this active aftercare is that landfill gas is actively captured and the energy in the gas is recovered. When this energy recovery is not feasible anymore the gas is actively flared [22]. Next, when active aftercare is not feasible anymore, passive gas management systems are utilized. Methane oxidation systems are an example of such. These systems are used when energy recovery or flaring are not feasible anymore due to economic or technical limitations. Then, microbial methane oxidation can be used to reduce the impact of the landfill on the environment. Methane oxidation systems oxidize methane to carbon dioxide by the activity of methanotrophic bacteria in the cover soil. These bacteria use the oxidation as their source of energy and carbon. There are three different forms of employment of biotic methane oxidation systems, biofilters, biowindows, and biocovers [20].

- Biofilters use contained bioreactors filled with a substance to host the methane oxidizing bacteria.
- Biowindows are areas of a landfill cover which are designed and optimized for methane oxidation. To guarantee the larger part of the landfill gas passing through the biowindow it has a lower resistance to gas movement in comparison to the surrounding area of the landfill cover. The gas supply is passive, meaning that no pumps are used.
- A biocover is used on when the whole cover of the landfill is optimized for methane oxidation. A biocover spans the whole area of the landfill, resulting in a methane load to area which is smaller compared to biofilters or –windows. A homogeneous distribution of gas over the biocover area is highly linked to high removal rates. Therefore, the gas distribution system is important for the performance of biocover.

A methane oxidation system consists of two parts; the methane oxidation layer top- and subsoil, and a gas distribution layer. The biocover is presented schematically in figure 2.1. Oxidation occurs in the methane oxidation layer, the range over which this happens varies seasonally and depends on the intensity of influx of oxygen from above and the gas flux originating from the waste body. For vegetation to establish itself on top, the top soil is required. To provide a homogeneous gas flux for the methane oxidation layer, the gas is distributed using a gas distribution layer [20].

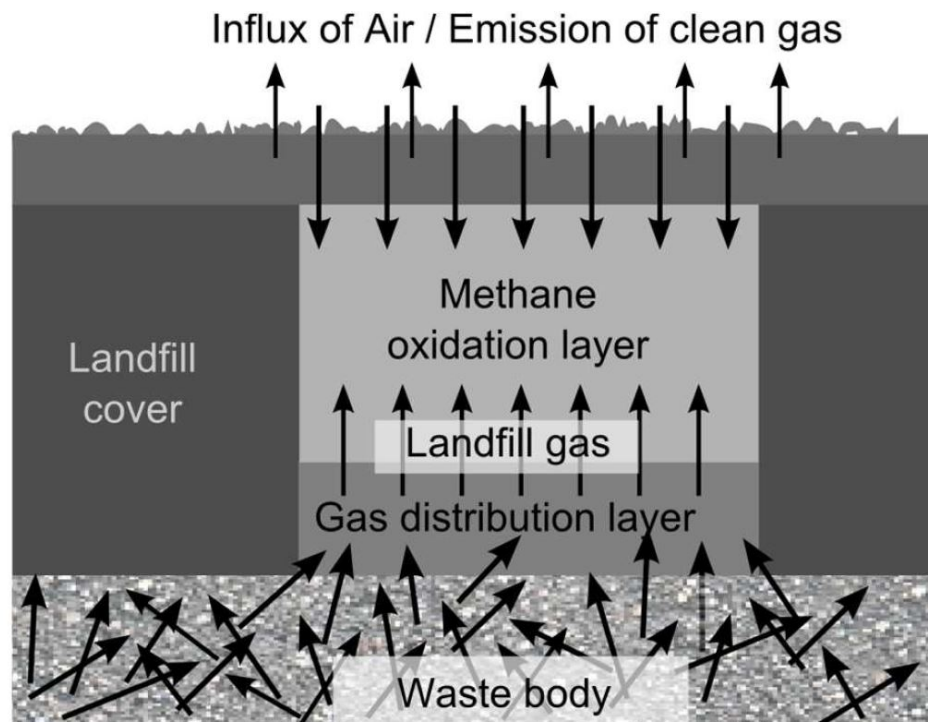


Figure 2.1: Schematic cross section of a biocover [20]

Newer landfills are constructed with a liner on top of the landfill or fully around the waste body. This liner, a low permeable barrier, is placed to isolate the waste from the environment, to prevent the release of pollutants to the surroundings. If the waste body is sealed at the top the gas which is created in the waste needs to be lead passively or actively through pipes penetrating the liner to a system oxidizing the methane. Older landfills do not have such a liner surrounding the waste body. In those cases landfill gas can migrate freely from the waste body through the cover soil.

2.1.1. Methane oxidation

The percentage of methane which is oxidized is dependent on the methane load to the cover soil and the activity of the methanotrophic bacteria in the cover soil. If the load is larger than the potential activity the oxidation efficiency will never reach a 100%. The potential activity of these methanotrophic bacteria is dependent on the temperature, which is of great importance as the activity of the microorganisms is directly related to this. An optimal temperature for activity is found at 30 degrees centigrade [36] [41] [43]. Another environmental factor, the water content in the soil, is closely related to the available pore space for gas transport and the continuity of pore space. For gas transport, the water content should ideally be as low as possible. However, when the moisture content becomes too low, the microorganisms are exposed to growing drought stress, and eventually methanotrophic activity comes to a halt due to the drying [41]. Finally, the exposure to methane and oxygen stimulates the growth of these bacteria, since methane is the source of energy for this type of microorganisms. This also means that if the influx of landfill gas from the bottom is too large the diffusion of oxygen from the top is limited, and the potential activity of the bacteria is not reached.

The performance of the methane oxidation system is highly dependent on the interface area between the aqueous and gaseous phase, and the gas transport mechanisms. Most of the governing soil parameters are deduced from the soil texture. The soil texture governs the interface area between the water and the gas, the water retention parameters, and the pore size distribution. The soil texture also governs soil mechanical properties. For optimal performance of the methane oxidation system, the air permeability should be as high as possible. Since pores that are larger than 50 μm do not hold any water and thus will not be blocked, and will in general be available for gas transport [20]. The availability of methane and oxygen for the microbes in the system should be maximized. The availability is fully dependent on the permeability of the cover soil and

the magnitude of the methane flux over the cover soil. The methane flux is dependent on the pressure and concentration differential between the waste mass and the atmosphere, originating from the decomposition of the waste and the soil permeability. The permeability, which also changes the diffusivity of the cover soil, changes due to compaction and water infiltration in the cover soil. The methane flux in itself also changes the availability of oxygen for the microbes, since too strong a flow of gas from the waste mass blocks the inflow of air from the atmosphere [9]. It is found that the degree of potential aeration is affected by the magnitude of the bottom flux in combination with the diffusivity of the soil: purely diffusive gas transport allows for maximum penetration of gaseous components from the top [16].

2.1.2. Methanotrophic activity

Methane oxidation systems have a typical soil gas profile, which is characterized by bi-directional flow of oxygen from the top and methane from the bottom. An example of the soil gas profile which follows from this bi-directional flow is shown in figure 2.2. The figure shows that at the surface the oxygen concentration has its maximum concentration and at the bottom methane has its maximum concentration. In approximately the top 25 centimeter there is only infiltration of oxygen and there is no methane present. Below this zone, the oxygen concentration drops and the methane concentration as well as the carbon dioxide concentration rise. These bi-directional fluxes result in a narrow band in the methane oxidation layer, in which there are sufficient concentrations of both oxygen and methane for effective oxidation of methane. Pawlowska and Stepniewski [37] found that the maximum methanotrophic activity was at a depth of 60 centimeters in the sample, similar to the finding by Stein and Hettiaratchi [43]. Knightley et al [27] found the maximum methanotrophic activity occurred between 20 and 30 centimeters. The variety at which depth and the variety in the nature of this band is explained by the availability of the optimal mixture of methane and oxygen for the bacteria. This optimal mixture is created by the transport rates of methane and oxygen, and is thus dependent on the permeability and diffusivity of the soil, in combination with the bottom flux of the methane and the methanotrophic activity of the bacteria.

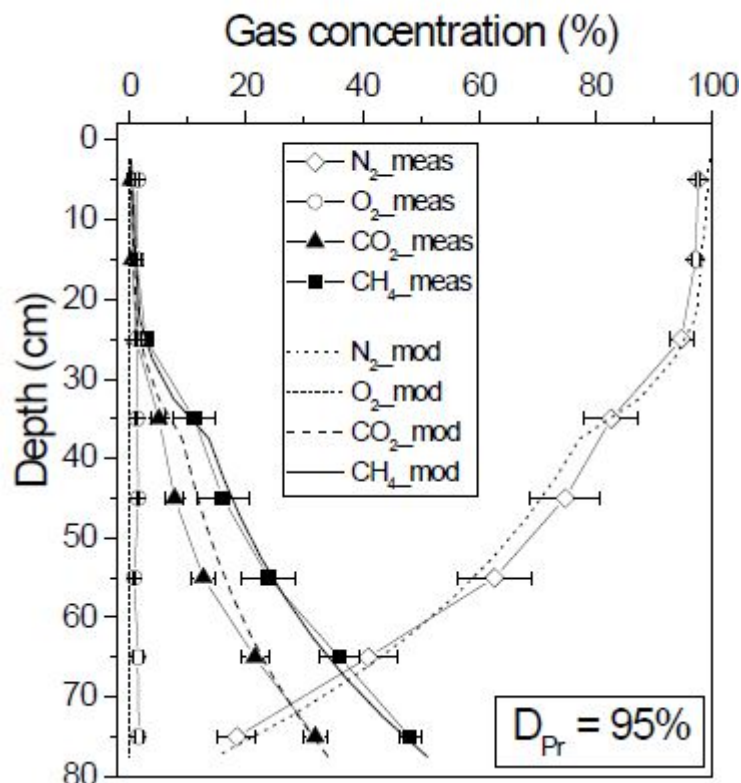


Figure 2.2: Soil gas profile over a landfill cover soil

Bender and Conrad [3] divided the methanotrophic bacteria into two groups. One is characterized by a high potential activity, but combined with a low affinity in relation to methane. The second group is char-

acterized by lower maximum methanotrophic activity. However, this is combined with a high affinity with methane. Therefore, the second type is found in soils exposed to normal atmospheric methane levels. In contrast, in soils subject to long term exposure to high concentrations of methane, like landfill cover soils or soils in methane oxidation systems, the first type of bacteria are used.

2.2. Diffusion

Transport of molecules from a location with due to the thermal motion of gas molecules in air or solution, is called Brownian movement. Diffusion is when Brownian movement results in net movement of these molecules from zones with higher concentration to zones with lower concentration. In a closed system, the end result is a homogeneous mixture. When the mixture is homogeneous, no net movement occurs anymore. In solids and liquids, the movement of molecules is significantly smaller than movement in the gaseous phase. The velocity of diffusion for methane in air is four orders of magnitude higher than in water, because solubility of methane is very low [48] [49]. In a porous medium, it is therefore assumed that all diffusion occurs through the gaseous phase. Due to the occupation of a large fraction of volume in a porous medium by the solid and liquid phases, adjustments for the volume of free air are typically accounted for by a factor multiplied by the diffusion coefficient in free air. Some findings suggest that a minimum threshold of 10% air-filled porosity is required for diffusion to occur. Below this threshold the diffusion is restricted by the low pore connectivity [17] [50].

2.3. Advection

The landfill gas which is created in the waste body results in an over-pressure, and thus a pressure difference over the landfill cover soil is created. Due to this pressure difference, gas is transported through the pores of the cover soil to the atmosphere, reducing the pressure difference. The gas transport due to this pressure difference is called advection. Where diffusive flux is described by the effective diffusion coefficient in Fick's law (equation 2.5), the advective flux is described by the effective gas permeability in Darcy's law (equation 2.1) [20].

$$N^V = -\frac{P}{RT} \frac{\kappa k_r}{\mu} \nabla P \quad (2.1)$$

In this formula, P is the gas pressure in Pascal, T is the temperature in Kelvin, R is the ideal gas constant, μ is the bulk gas viscosity, ∇P is the gas pressure gradient, and κk_r is the effective permeability. Kühne et al [29] stated that advective transport is changed by a power of four when changes in pore diameter occur. This contrasts with diffusion, which is dependent on air-filled pore volume, and is not directly influenced by the pore diameter [4]. This effect of the pore walls is the drag of the gas on the pore walls, which is described using Newton's law of viscosity. Bird, Stewart and Lightfoot [4] gave this law as given in Equation 2.2. In this equation, τ_{yx} is the force in the x-direction on a unit area perpendicular to the y-direction, v_x is the flow velocity in the x-direction, and y is the distance from the boundary. This formula accounts for half the pore, y has a value from the pore wall to the middle of the pore. Thus, the coarser a pore is the smaller the effect of drag is on the total velocity of the gas.

$$\tau_{yx} = -\mu \frac{dv_x}{dy} \quad (2.2)$$

2.4. Drivers of diffusion in landfill cover soils

The first thing which springs to mind when considering diffusion through porous media is the air-filled porosity, i.e. the volume of air through which diffusion can occur. The air-filled porosity directly affects the gas diffusion coefficient. Gebert et al [17] found the relationship to be non-linear, as shown in figure 2.3. The air-filled porosity is of course dependent on the compaction and texture of the particles, since these determine the pore size and pore size distribution. Increasing compaction will predominantly alter the coarser pores, through which diffusion will mostly occur. The effect of compaction on the diffusivity is shown in figure 2.4. The saturation also effects the air-filled porosity, since water is the other phase which fills the pores. Another factor affecting the air-filled porosity in undisturbed samples is the presence of macroporosity, originating from rootage or burrows. The macropores facilitate preferential flow paths through the soil, resulting

in a significant difference between undisturbed and repacked soils [34]. The data in this figure is all from the same soil, and thus solely shows the effect of the reduction in air-filled porosity. In figure 2.4 the compaction is given as Proctor density. The Proctor density is the maximum density of a soil, determined from a standardized test.

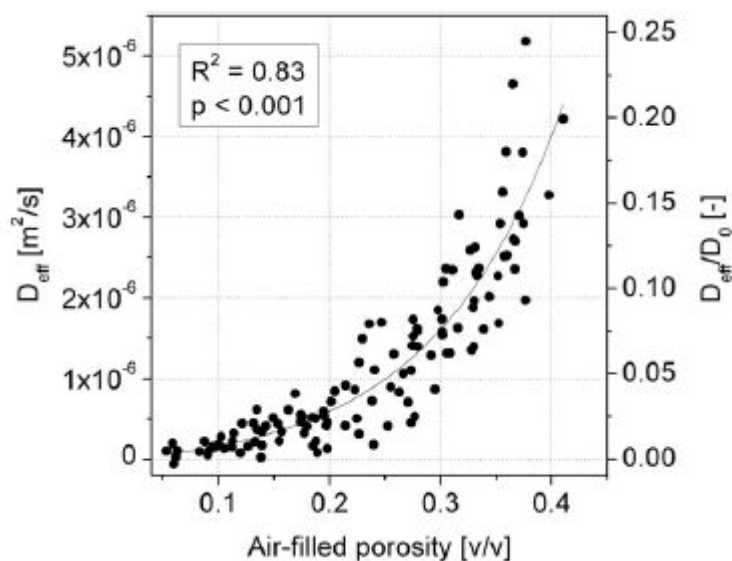


Figure 2.3: Effective diffusivity plotted versus the air-filled porosity, showing the non-linear relation [17]

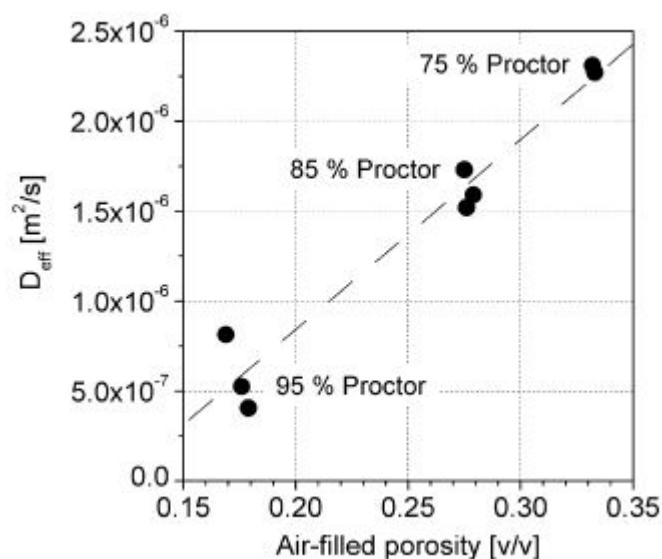


Figure 2.4: Effective diffusivity plotted versus the air-filled porosity, for different Proctor densities [17]

Papendick and Runkles [35] observed that in wet media the gas diffusivity was lower than in dry media at the same air-filled porosity. This was attributed to the change in pore shapes and occurrence of water menisci in the pore throats when there is also a wetting phase present, resulting in an increased tortuosity for the gas transport [33] [32]. As in a normal soil, the aqueous phase is generally the wetting phase and the gaseous phase the non-wetting phase, water is separating the solid and gaseous phases. The water forces the gaseous phase to the center of the pores, reducing the volume in which diffusion is possible to occur. Another effect of soil being water wet is water completely filling the smaller pores when the water film around the particles is

of sufficient thickness, which results in the gas transport to be restricted to the coarser pores [40]. The filling of the smaller pores with water means these are unavailable for diffusion of gas, increasing the tortuosity and reducing the air-filled porosity. Therefore, when the pore sizes are smaller and a wetting phase is present, the diffusivity of a gaseous phase is lower, as both the available volume for diffusion is lower and the path length of diffusion is longer. Moldrup et al [33] also concluded the same from their data. This shows that when water is absent, the relation between effective diffusivity and air-filled porosity goes more towards linearity.

Two other factors influencing the path length of the diffusion are the tortuosity and the connectivity, describing the structure of the pore space. The tortuosity is defined as the length of the flow path through the pores compared to the length of the sample, and the connectivity gives a measure for the interconnectedness of pores.

The rate of diffusion through a soil is the rate of diffusion through free air of the substance including a correction for the restrictions presented by the soil structure. The diffusion rate of a substance in free air is dependent on the mass of the molecules and the temperature of the gas. Diffusion originates from the movement of particles; the movement speed of these particles depends on the mass of and the temperature of the gas. Higher temperature originates from higher movement speed of the particles. Thus, increasing temperature has a positive effect on the rate of diffusion. In a gas mixture, the temperature is the same for all species and all particles. The rate of diffusion can still be different for the different species. This can be explained by the kinetic energy, Equation 2.3. In Equation 2.3 m is the mass of the molecules and v is the velocity of the molecules.

$$E = \frac{1}{2}mv^2 \quad (2.3)$$

From the derivation given in Appendix A, it can be seen that kinetic energy is only dependent on the temperature. For a gas mixture at a constant uniform temperature, it is thus concluded that the kinetic energy of each particle is the same, as the temperature of each particle is the same. This theory is used to formulate Graham's law, which is given in Equation 2.4.

$$\frac{R_1}{R_2} = \sqrt{\frac{m_2}{m_1}} \quad (2.4)$$

The derivation of Graham's law is also given in Appendix A. In Graham's law, the R is the rate of diffusion and the m is the corresponding molecular mass. This also explains the fractionation due to diffusion of isotopes, since isotopes have different molecular mass.

2.5. Types of diffusion

Three different diffusion mechanisms are distinguished: molecular diffusion, equimolar flux, and Knudsen diffusion. These are discussed separately.

2.5.1. Molecular diffusion

Molecular diffusion is the most fundamental type of diffusion. This is the movement of molecules from a high concentration to a low concentration, as described earlier. Molecular diffusion simply takes into account the collisions of molecules in the same phase. Steady state molecular diffusion is governed by Fick's Law, which relates the diffusive flux to the concentration gradient. Equation 2.5 shows this law.

$$J_i = -D_{ij} \frac{dc_i}{dz} \quad (2.5)$$

In this formula, J_i is the flux of the gas, D_{ij} is the diffusion coefficient for species i in species j , c_i the concentration of species i , and z the length of the diffusive path. Fick's law assumes a stationary reference frame, meaning that Fick's law assumes no advective flow occurs. However, when there is also advective transport, such as in landfill cover soils, the reference frame is moving with the advective flow to isolate the diffusive effects. When diffusion occurs through porous media, the law needs to be altered for the reduced free space through which diffusion can occur. Cabral et al [8] did this by adding a factor for the air-filled porosity and tortuosity, resulting in Formula 2.6.

$$J_i(t) = -\varepsilon D_e \frac{\delta c(t)}{\delta z} \quad (2.6)$$

In this formula, the ε is the air-filled porosity and the D_e is the effective diffusion coefficient, which is determined using Equation 2.7.

$$D_e = D_a^0 \tau \quad (2.7)$$

The D_a^0 is the diffusion of the component through free air, τ is the tortuosity of the medium. In this equation, tortuosity is defined as the length of the sample divided by the path length, resulting in a value between 0 and 1.

Fick's second law relates the unsteady diffusive flux to the concentration gradient and predicts how diffusion changes the concentration with time. Fick's second law transient state is taken into account, Equation 2.8 shows the formula. In Equation 2.8 a term for consumption of the species along the diffusive path is included.

$$\frac{\partial c}{\partial t} = D^{eff} \frac{\partial^2 c}{\partial z^2} - \lambda_r c \quad (2.8)$$

In Fick's second law, the term $-\lambda_r C$ relates to consumption of the species along the diffusive path [8].

2.5.2. Knudsen diffusion

When the pore radius is of the same order as the mean free path length of the gas molecules, i.e. when the pore radius becomes smaller than the distance between two gas molecules, Knudsen diffusion plays a key role when evaluating diffusion. The walls of the porous medium influence the collisions that occur, since the solid phase is involved in most of the collisions between molecules. To determine whether Knudsen diffusion can be neglected when diffusion is evaluated, the ratio of the gas mean free path to the pore sizes is used. Equation 2.9 shows this ratio.

$$K_n = \frac{\lambda}{d_p} \quad (2.9)$$

In this equation, d_p is the average pore diameter. The gas mean free path, λ , is calculated by Equation 2.10.

$$\lambda = \frac{k_B T}{\sqrt{2} p \pi d_g^2} \quad (2.10)$$

In this formula, k_B is the Boltzmann constant and T is the temperature. The parameter d_g is the effective molecule diameter. The equation states that if K_n is much greater than 10, Knudsen diffusion is more dominant than molecular diffusion. This means that molecular and viscous diffusion can be neglected. If K_n is much smaller than 0.1, Knudsen diffusion can be disregarded, as collisions between gas molecules becomes dominant. When K_n is between 0.1 and 10, none of the diffusion mechanisms can be disregarded [21].

The formula describing Knudsen diffusion is very similar to Fick's Law. Equation 2.11 shows the formula for Knudsen diffusion. The Knudsen effective diffusion coefficient is $D_{i,Knudsen}$.

$$N_i = -D_{i,Knudsen} \frac{dc_i}{dz} \quad (2.11)$$

The difference between both diffusion coefficients is that the coefficient for Knudsen diffusion is independent of absolute pressure or the pressure of the species. Additionally, the dependency on temperature is different, as the effect of increasing temperature is smaller for Knudsen diffusion. For Knudsen diffusion, the temperature is taken to the power 0.5; for molecular diffusion, the temperature is taken to the power 1.5 [21].

Geck [20] stated that Knudsen diffusion can be neglected for landfill cover soils, as the maximum pore size for which Knudsen diffusion is occurring is 5.3 nm. These pore sizes are not governing gas transport in landfill cover soils. The expected pore sizes in the two sands that govern gas transport are in the range between 0.2 and 50 μm . Thus, the dominant diffusion types are molecular diffusion and nonequimolar flux.

2.5.3. Nonequimolar flux

Nonequimolar diffusion occurs when gas components have different molecular weights [40]. When gas components have different molecular weights, different diffusion rates are encountered. Lighter gas molecules have a higher velocity in comparison to heavier gas molecules. In binary gas mixtures, the faster diffusion of the lighter molecules results in a pressure gradient. This effect is called nonequimolar flux, which is a diffusive flux and is different from advective flux. The effect of the nonequimolar flux is the same as that of the advective flux, however, no separation of the gas mixture occurs. These effects cannot be separated, as nonequimolar flux can only occur due to a diffusive flux. An equation for the bulk diffusive flux is given in Equation 2.12, which is the combination of the molecular diffusive flux and the nonequimolar diffusive flux [44] [40].

$$N_i^D = J_{iM}^m + x_i \sum_{j=1}^v N_j^D \quad (2.12)$$

The N_i^D is the bulk molar diffusive flux for component i , J_{iM}^m is the molar diffusive flux for component i . The nonequimolar diffusion is described by the factor $x_i \sum_{j=1}^v N_j^D$. In nonequimolar gas mixtures, the molar gas flux moves in the direction in which the lighter gas molecules are moving, since latter molecules move faster. The center of mass of this gas mixture moves with the diffusion of the heavier molecules.

2.6. Gas transport models

To describe the diffusive processes mentioned before, several models are presented in literature. The models which are expected to perform best are discussed in this section. First, models predicting the diffusive flux are given; these are the advective-diffusion model, the Stefan-Maxwell equations, and the dusty gas model. Secondly, models approximating the effective diffusion coefficient are given.

2.6.1. Advective-diffusion model

The advective-diffusion model is the simplest of the four models discussed here. It is an extended version of Fick's law for diffusion, in which a term for advection is added to Fick's law. These terms can be added, since diffusion and advection are independent processes. When considering a one-dimensional situation, diffusion will randomly move a molecule either with or against the direction of flow. Advection will move the molecules with the direction of flow. Thus, a combination of both will only change the magnitude of this movement; no interdependent processes involved [42]. The combination of Fick's law and flow is shown in Equation 2.13.

$$J_i = - \left(D_{ij} \frac{dc}{dz} + vc \right) \quad (2.13)$$

In this formula, the v is the flow velocity of the fluid and c is the concentration. The part of the formula for the movement due to flow is written in this form to assure that the units are equal. However, both the advective-diffusion model and Fick's Law only take unidirectional diffusion in binary gasses into account. Neither is valid for ternary or concentrated gas systems, in which molecular interactions cannot be neglected.

2.6.2. Maxwell-Stefan equations

The Maxwell-Stefan equations can be used in situations where ternary or concentrated gas systems are present, in which molecular interactions cannot be neglected. The equations as described by Bird, Stewart and Lightfoot [4] are shown in Equation 2.14.

$$\frac{dX_i}{dz} = \sum_{j=1}^n \frac{X_i J_j - X_j J_i}{c D_{ij}^{eff}}, \quad i = 1, 2, \dots, n \quad (2.14)$$

In these equations, the X_i is the mole fraction of species i , D_{ij}^{eff} is the effective gas diffusivity, and c is the total concentration. A downside of these equations is that interactions with the solid-gas boundary are not taken into account, since these equations were developed for gases at low densities. Thus, if Knudsen diffusion is not negligible, these equations should not be used. The Maxwell-Stefan equations can also not be used to describe the relationship between pressure gradient and total flux [13].

2.6.3. Dusty gas model

The dusty gas model was developed to also take Knudsen diffusion into account. The dusty gas model takes all possible collisions and interactions into account. The walls are considered as giant molecules in the dusty gas model [45], i.e. the dust. However, the model is not widely used due to its complexity [21]. Equation 2.15 presents the model.

$$\sum_{j=1, j \neq i}^n \frac{X_i J_j^T - X_j J_i^T}{D_{ij}} - \frac{J_i^T}{D_{iK}} = \frac{p_t \nabla X_i}{RT} + \left(1 + \frac{k_0 p_t}{D_{iK} \mu_g}\right) \frac{X_i \nabla p_t}{RT} \quad (2.15)$$

2.6.4. Gas transport model comparison

For different situations, the models are required to take all relevant effects into account. The advective-diffusion model can only be used when the simplest forms of advection and diffusion are involved. The model only considers unidirectional diffusion in a binary gas mixture. In more complex situations, when a mixture consists of multiple gasses or involves concentrated gas, the Stefan-Maxwell equations will be more realistic. In situations where interactions between the gas and walls cannot be neglected, the dusty gas model should be applied [40]. Table 2.1 presents an overview of a few situations. However, as mentioned before, the governing pore sizes in landfill cover soils are of a diameter that Knudsen diffusion can be neglected [20]. The diffusion in landfills assumes binary gas, therefore, the advective-diffusion model will be sufficient to model the diffusion in the cases considered in this thesis.

Table 2.1: Comparison of the gas transport models

Concentration	Permeability	Binary gas	Ternary(+) gas
Low	Low	Dusty Gas	Dusty Gas
High	Low	Dusty Gas	Dusty Gas
Low	High	Advective-diffusion	Stefan-Maxwell
High	High	Stefan-Maxwell	Stefan-Maxwell

2.6.5. Diffusion coefficient approximations

The most basic diffusion models for porous media are the models created by Penman, Marshall, and Millington [33]. Each of these models relates the ratio of gas diffusivity in the porous media over the diffusivity in free air to the porosity. However, this thesis involves unsaturated soils and no completely dry soils. This implies that the Penman, Marshall, and Millington models are themselves not sufficient. Moldrup et al [33] modified these models to also be suitable to model the diffusivity of a soil in unsaturated conditions, i.e. to account for the increased tortuosity due to the presence of water within the pores. These models are the so called WLR Penman, WLR Marshall, and WLR Millington models; WLR is short for Water-Induced Linear Reduction. This is done by the addition of the term ε/ϕ to the original equations, resulting in Equations 2.16, 2.17, and 2.18.

WLR Penman model:

$$\frac{D_p}{D_0} = 0.66\varepsilon \left(\frac{\varepsilon}{\phi}\right) \quad (2.16)$$

WLR Marshall model:

$$\frac{D_p}{D_0} = \varepsilon^{3/2} \left(\frac{\varepsilon}{\phi}\right) \quad (2.17)$$

WLR Millington model:

$$\frac{D_p}{D_0} = \varepsilon^{4/3} \left(\frac{\varepsilon}{\phi}\right) \quad (2.18)$$

In these equations, D_p is the effective diffusion coefficient in soil, compared to the D_0 , which is the effective diffusion coefficient in free air. The porosity is given by ϕ and the air-filled porosity is ε .

Moldrup et al [33] found all models to perform adequately for most practical purposes. The tested data sets showed that WLR(Penman) and WLR(Marshall) models performed better for the porosity range which is customary in soils, when compared to the WLR(Millington) model and the models without the WLR correction. At low gas diffusivities, i.e. $D_p/D_0 < 0.1$, the WLR(Marshall) model was found to give superior results. However, the WLR models should not be used to predict the effective diffusion coefficient of gas in undisturbed soils. They can be used to fit data and give predictions for repacked and disturbed samples [33].

An alternative to the WLR models is the Millington and Quirk model [31], which is very similar to the WLR models. In this formula, the parameters used are the same as those used in the WLR model, shown in Equation 2.19.

$$\frac{D_p}{D_0} = \frac{\varepsilon^{10/3}}{\phi^2} \quad (2.19)$$

An empirical formula which was found to best fit the effective diffusivity data in tests from previous work is only dependent on the air-filled porosity. This relation was fitted by Gebert et al [16] to a data set with all samples at -6 kPa. Thus, any air-filled porosity consisted only of pores larger as 50 μm . The relation is given in Equation 2.20.

$$D^{eff} = 1.319 \times 10^{-7} \times e^{(\varepsilon/0.116)} - 1.477 \times 10^{-7} \quad (2.20)$$

Contrary to the predictive models for the diffusion coefficient given before, Troeh et al [50] created a model which needs to be fitted to data using two fitting parameters u and v . The u can be taken as an initial threshold for the diffusion and v is the shape of the curve. This initial threshold is the point when pores start to be interconnected. The formula is given by equation 2.21.

$$\frac{D_p}{D_0} = \left(\frac{\phi - u}{1 - u} \right)^v \quad (2.21)$$

Allaire et al [1] stated that it is not possible to determine the best relationship to describe diffusivity of soils a priori. The decision for a certain model must be supported by a few measurements of the soil material in question.

2.7. Unsaturated zone

As mentioned before, the bacteria needs some water in the pores but also an adequate share air-filled pores, since they require a supply of oxygen and methane. This explains why methane oxidation occurs easiest in the unsaturated zone, which is the transition zone between the fully saturated and fully dry areas. In this transition zone, the pores are filled with both a fluid phase and a gaseous phase, shown schematically in the left picture in Figure 2.5. In this figure the field capacity and the permanent wilting point are shown. Field capacity describes the point where pores are of a size where they drain freely with gravity. The permanent wilting point is the point where plants are not able to extract water from the pores, since the water tension is too high.

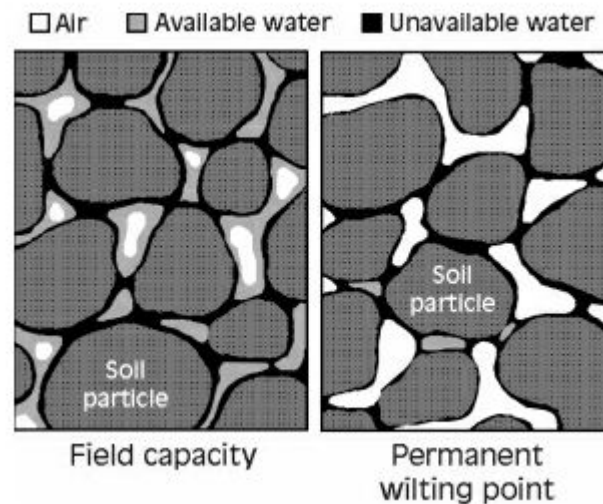


Figure 2.5: Left: Schematic view of partial saturation Right: Schematic of the permanent wilting point Source: [39]

The degree of saturation for soil is calculated by dividing the volume of water by the volume of the pores, as shown in Equation 2.22. The saturation of air is then simply calculated by using Equation 2.23 [53].

$$S = \frac{V_w}{V_p} \quad (2.22)$$

$$S_a = 1 - S \quad (2.23)$$

In these equations, S is the degree of saturation, V_w is the total volume of water, and V_p is the total volume of pores. The subscript a gives either the porosity, volume, or saturation of air. A completely dry sample has a value for S of 0, and a sample which is fully saturated has a value for S of 1. The air-filled porosity is determined using Equation 2.24. The air-filled porosity is determined by dividing the volume of air by the total volume of the sample.

$$\varepsilon = \frac{V_a}{V_T} \quad (2.24)$$

2.7.1. Water retention

The transition zone mentioned before, in which the soil is partly saturated, originates from the heterogeneity of the pore sizes. Different pore sizes are attributed to different water tensions in the pores, this is explained by the Law of Young-Laplace. The Law of Young-Laplace describes the capillary pressure difference, based on differences in radius. A pore diameter smaller than $0.2 \mu\text{m}$ corresponds to a water tension of 1500 kPa, and is known as the permanent wilting point, since plants generally cannot extract water from the pores at this water tension. The permanent wilting point is schematically shown in Figure 2.5 (right). To stop water moving against gravitational force, a water tension of 30 kPa is necessary. At this point, water is available for plants and the corresponding pore sizes are between 0.2 and $10 \mu\text{m}$. When pore sizes are between 10 and $50 \mu\text{m}$, water is draining from the pores due to gravitational forces. However, it drains slow enough to be accessible for uptake by plant roots. Pores that are any larger, are usually air-filled, as they drain free with gravity. The corresponding water tension is 6 kPa, which is called field capacity [20]. In literature, several methods are given to measure and describe these curves, known as water retention curves. Below a short summary on a few methods is given.

For well-graded media and fine-textured soils, assumptions of uniform water content and one-dimensional flux may be sufficient for modelling gas diffusion under quasi steady-state conditions. For coarse-textured materials with a narrow pore-size distribution, the hydrostatic component of water potential induces substantial changes in water content within a shallow sample thickness [26].

A commonly used and effective parametric model for relating water content to matrix suction is proposed by Van Genuchten [51]. The relation is given in Equation 2.25.

$$\Theta = \frac{\theta - \theta_r}{\theta_s - \theta_r} = \left[\frac{1}{1 + (a|h|^n)} \right]^m \quad (2.25)$$

In this equation, θ is the water content; with subscript s , this becomes the water content when fully saturated, and with subscript r , this is the residual water content. This relationship either relates the saturated and residual water contents or empirical parameters to the saturation. For the formulation using empirical parameters, the matrix suction is given as h ; the other parameters are determined when fitting the formula to a data set for that specific soil [51].

An alternative is the Brooks-Corey relationship, relating capillary pressure to water phase saturation. This relation is given by Brooks and Corey [7], as shown in Equation 2.26.

$$\Theta = \left(\frac{h}{h_b} \right)^{-\lambda} \quad (2.26)$$

In this equation, h_b is the bubbling pressure and the λ is a fitting parameter. The Brooks-Corey relation proved to model the pressure heads accurately for the two soils used in this thesis [52].

2.8. Fractionation of stable isotopes

In general, metabolisms process lighter isotopes faster. This also applies to methanotrophic bacteria when oxidizing methane. The lighter isotope, $^{12}\text{CH}_4$, oxidizes slightly faster than $^{13}\text{CH}_4$ [11]. At levels closer to the surface in a cover soil, the fractionation of ^{13}C was not affected. The relative concentration of $^{13}\text{CH}_4$ compared to $^{12}\text{CH}_4$ increased. An approach to assess the efficiency of microbial methane oxidation has been developed, using that the methanotrophic bacteria discriminate against the heavier isotope. This method is based on the fractionation of stable isotopes which naturally occur due to the oxidation process. The method also takes into account that additional fractionation is caused by the faster diffusion of $^{12}\text{CH}_4$ than $^{13}\text{CH}_4$, because of a difference in their respective diffusion coefficients. Fractionation due to diffusion leads to the preferential release of $^{12}\text{CH}_4$, and thus the enrichment of $^{13}\text{CH}_4$ in the gas left behind in the soil. The fractionation of stable methane isotopes can be calculated by [5], as given in Equation 2.27.

$$f_{ox} = \frac{\delta_S - \delta_A}{1000 * (\alpha_{ox} - \alpha_{trans})} \quad (2.27)$$

The δ_S is the fraction of ^{13}C in the sample taken at the surface, δ_A is the fraction of ^{13}C in the source, α_{ox} is the fractionation factor for oxidation, and α_{trans} is the fractionation factor for transport. The numerator gives the difference between the measured isotope signatures for the emitted and produced methane. The values for the isotope signature is given relative to an international standard, the VPDB or Vienna Pee Dee Belemnite. The fractionation factor for α_{trans} is usually assumed to be equal to 1, meaning that no fractionation due to diffusion occurs. However, Marrero and Mason [30] found that α_{trans} can be as high as 1.0195 due to molecular diffusion in methane. These fractionation factors can be determined by the ratio of stable isotope reaction rates or diffusion rates [15], as given in Equation 2.28. This ratio is dependent on either the reaction rate constants for oxidation or the rate constants for transport.

$$\alpha_{ox} = \alpha_{trans} = k_{12}/k_{13} \quad (2.28)$$

The fractionation occurs due to the faster diffusion of $^{12}\text{CH}_4$ compared to $^{13}\text{CH}_4$ due to its lower mass. It was also suggested that the fractionation is lower than expected when compared to the diffusion coefficients in free air. This suggests that the difference in soil-based diffusion rates is reduced by the restrictions imposed by the soil [16]. When assuming that the fractionation due to oxidation is 0, the relation shown in Equation 2.29 given by Coleman et al can be used to determine the fractionation factor due to transport [11].

$$\delta^{13}\text{C}_t \cong 1000 * (\alpha_{trans} - 1) * \ln(M/M_0) + \delta^{13}\text{C}_{t=0} \quad (2.29)$$

In this formula, M/M_0 is the fraction of CH_4 remaining at time t . To determine the fraction of $\delta^{13}\text{C}$ compared to the standard value, the VPDB standard, equation 2.30 is used. In this equation, R is the isotope ratio ^{13}C to ^{12}C .

$$\delta^{13}\text{C} [\text{‰}] = \left[\left(\frac{R_{sample}}{R_{standard}} \right) - 1 \right] * 1000 \quad (2.30)$$

Both fluxes, advective and diffusive, are often considered separately. However, advection and diffusion are not independent of each other. Advective flux could transport gas of high methane concentration to the surface, thereby shortening the pathway of diffusion resulting in an increased concentration gradient [20].

3

Methodology

In this chapter, the soils are described first, followed by the experimental setup. Next, the procedures used when preparing the soils and the procedures during measurements are described. Finally, the methods used to process the data obtained are given.

3.1. Soils

In this thesis soil from two different landfill sites are used. One originates from the Wieringermeer landfill, the Netherlands, which is operated by Afvalzorg Deponie B.V.. The second soil originates from the Hamburg area, Germany, and is operated by the Hamburg Port Authority. They are respectively referred to as soil WIE and soil HH. These soils are selected as they are also used in the thesis by Van Verseveld, to facilitate in further research [52]. Van Verseveld researched the effects of compaction and saturation on advective transport. These soils proved to be suitable methane oxidation layers at the locations where they are used. Table 3.1 gives the soil properties for soil WIE and soil HH, as determined by Van Verseveld [52]. Both soils consist mostly of sand. The sand in soil HH is a bit coarser when compared with soil WIE, which consists mostly of fine sand. Soil HH contains more silt than soil WIE, but soil WIE contains more clay than soil HH. This larger presence of clay in soil WIE shows as clay lumps in the soil, which give local zones of lower porosity. However, soil HH consists of a larger fraction of fines (clay and silt). Additionally, soil WIE has CaCO_3 present and soil HH does not. The Proctor density of soil HH is 1.90 g/cm^3 and that for soil WIE is 1.76 g/cm^3 .

Table 3.1: Soil properties [52]

Soil	Soil HH	Soil WIE	Unit
Clay	2.8	8.8	%dw
Silt	18.3	7.2	%dw
Sand	79.1	82.4	%dw
Coarse	15.87	3.42	%dw sand
Medium	27.88	16.38	%dw sand
Fine	45.22	75.21	%dw sand
Very Fine	11.02	4.99	%dw sand
Organic content	1.1	1.34	%dw
CaCO_3	0	5.5	%dw
Proctor density	1.90	1.76	g/cm^3

3.2. Soil preparation

The variations in compaction and saturation have been subdivided into two different series. The compaction series varies the compaction rate but has a constant saturation level. For soil HH the saturation is constantly

targeted at 12.35%V and for soil WIE the saturation is constantly targeted at 20.47%V. For the saturation series the water content is varied between the different tests and the degree of compaction is kept constant. Both soils are compacted to 85% of the Proctor density for all samples in the saturation series.

The available soils have been divided over buckets that are closed with a lid, each of these buckets were saturated to different gravimetric water contents. The different gravimetric water contents are based on the targeted degrees of saturation given in Appendix C. This was done by adding a specific amount of demineralized water or by allowing the bucket dry due to contact with the air. The air drying was done by leaving the bucket at room temperature with the lid removed for a set period of time. To check if the saturation was at an adequate level, three soil samples were taken after the soil samples were homogenized. The three samples were dried in an oven to determine the gravimetric water content.

The targeted water contents are the same as those approximated in the thesis by Van Verseveld [52]. These water contents are based on capillary pressures, which relate to certain pore sizes. The used water tensions are given in Table 3.2. The value of 1500 kPa is selected, since this is the permanent wilting point. A common pressure plotted in water retention curves is 100 kPa. The pores larger than 10 μm drain at a pressure of 30 kPa. The pressure where all water drains freely is 6 kPa. Therefore, 12 kPa was included.

Table 3.2: Soil hydraulic characteristics and targeted water contents, at 85% Proctor density

Water tension (kPa)	Saturation WIE (%V)	Saturation HH (%V)	Reason
1500	12.47	5.18	Permanent wilting point
300	16.74	8.59	To ensure a good spread
100	20.47	12.35	Commonly plotted pressure
30	25.53	18.58	Coarser pores drained
12	31.24	25.49	Twice field capacity

The degrees of saturation in Table 3.2 had been determined by Van Verseveld from the water tensions using a HYPROP device (HYPROP-UMS, 2013) and a Dewpoint meter (Decagon Devices) [52]. These values were fitted using the Brooks-Corey water retention model. The HYPROP device measures the water tensions over the evaporation process and during this time it also measures the changes in mass of the sample [38]. Thereby, both the water retention curves are obtained.

After the soil is brought to the selected saturation levels, the soil is compacted to the required compaction levels. The desired compaction levels are the same as in the thesis by Van Verseveld [52]: 75, 80, 85, 90 and 95% of the Proctor density. The compaction was done during packing of soil into the metal cylinders. All the soil is poured at once, there are not multiple cycles of compaction used. The goal of the packing was to create a soil sample which is 10 centimeters high. To make sure there is no effects of compaction on soil-air interface and to create a more homogeneous sample, the cylinder is first overfilled. The initial column of compacted soil has a height of 11 centimeters. After compaction the upper centimeter is scraped loose, and removed with a spoon. If this is done correctly, it should limit the effects of the compaction process on the soil-air interface, and result in a column of soil of 10 centimeters high at the desired degree of compaction.

The soil is compacted using the hammer shown in Figure 3.1. The hammer has a massive square block which can be moved along the rod, and two base plates. The lower base plate rests on the soil and the upper base plate takes the force of the falling hammer. The rod and two base plates are referred to as the static part of the hammer. The hammer is operated by letting a weight of 4.951 kilogram fall from 10 centimeters high on a base plate with a diameter of 15.1 centimeters. The static part of the hammer weighs 3.382 kilograms. The weight of the hammer is dropped on the base plate as often as required to create a soil sample of 11 centimeters high.

Thus summarizing, the first step is to determine how much weight of soil is needed to obtain the desired degree of compaction. Secondly, the soil is poured in the cylinder, after which it is being compacted using the hammer to a height of 11 centimeters. Finally, the top centimeter is scraped loose and removed using a spoon.



Figure 3.1: The hammer used for compaction; base plate diameter: 15.1 cm

3.3. Setup for the diffusion experiments

The test setup consists of a gas chamber, a cylinder with the soil sample, and a data collection system. A picture of the setup is shown in Figure 3.2 and a schematic representation in Figure 3.3. The gas chamber is constructed from a PVC cylinder with a metal slider on top. On top of this slider the metal cylinder containing the soil samples is placed. As seen in these figures, the PVC cylinder containing the gas mixture has several objects attached. There is a methane sensor connected in the middle of the gas chamber, which is of the type INIR-ME-100% made by SGX Sensortech. This sensor is designed to measure methane concentrations between 0 and 100%. Opposite of the sensor, a sampling port has been installed through which small quantities of gas can be extracted from the chamber. The sampling port consisted of a fitting with a rubber septum inside, through this septum the gas samples can be taken using a syringe.

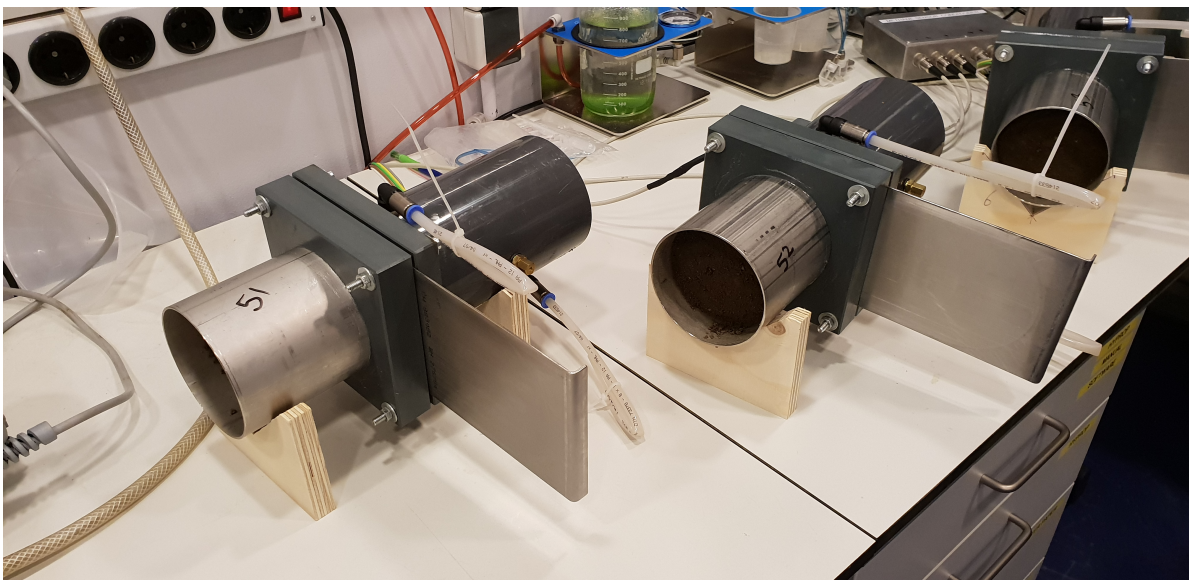


Figure 3.2: Picture of the test setups with soil samples in place

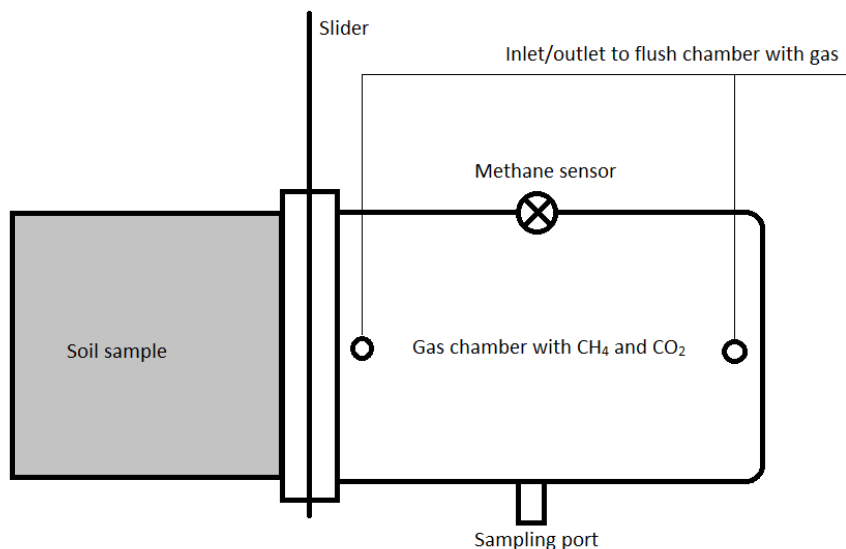


Figure 3.3: Schematic of the test setup

There are also two connections for 8-mm tubing installed on the PVC cylinder, which are used for the flushing of the chamber. On top of this cylinder, two square blocks of PVC are present with a slider in between. This slider has a cut-out on one end with the same diameter as the metal cylinder. This slider is added to be able to open and close the gas chamber. In both PVC square blocks a similar cut-out is made, with a diameter slightly larger than the cylinder filled with the soil sample. The metal cylinder containing the soil sample is placed in the cut-out in the PVC block, the connection is sealed using an O-ring and petroleum jelly. As is seen in Figure 3.2, during a diffusion experiment the connections for the 8-mm tubing are closed by bending them and tying them down using a tie-wrap. This created sufficient gas tightness for these connections for the duration of the tests.

The dimensions of the test setup are given in Table 3.3. This is subdivided in the dimensions of the gas chamber and cylinder.

Table 3.3: Dimensions of the test setup

Dimensions		
Gas chamber		
Diameter	10.3	cm ³
Height	19.0	cm
Cylinder with soil sample		
Diameter	10.0	cm ³
Height	10.0	cm

3.4. Measurement procedure

The diffusion chambers are flushed with the gas, after the soil samples are prepared. The gas consist of 50% methane and 50% carbon dioxide, a good representation of landfill gas. The gas has been created by Linde Gas. Flushing of the 1.5 liter chamber takes 30 seconds, which completely fills the chamber. Before the test can start the sensors take 45 minutes to warm-up, after which the soil samples are placed in the test setups. The soil samples are weighed before and after the test to check how much water weight is lost due

to evaporation. Due to their exposure to air during testing, the samples will likely dry out a little. After the soils are in place, the chamber is injected with 1.5 milliliters of C_2H_2 to incapacitate any bacteria which are still present in the soil samples. After all possible leakage points have been smeared with petroleum jelly, the measurement is started.

Every second for the duration of a test, the computer stores the voltage the methane sensor gives. After the measurement is started the sliders are opened. Following the concentration gradients, the gas mixture diffuses from the chamber through the soil into the atmosphere, while air diffuses from the atmosphere through the soil into the chamber. The concentrations of the gas used for the experiments consists of 50% CO_2 and 50% CH_4 . When the concentration of methane drops below approximately 15% the tests are stopped. The tests are usually repeated twice to produce their respective parallel data sets. This is done for each individual variation in saturation and compaction.

The gas in the gas chamber was sampled for the analysis of stable carbon isotopes during a series of the performed tests. The fractions of each isotopologue in the sample are determined using stable isotope spectrometry at the University of Utrecht; by Prof. dr. T. Roeckmann from the working group "Atmospheric physics and chemistry". Only a limited number of stable isotope spectrometry tests are available. Therefore, a selection of tests are sampled. The samples are only taken for a selection of tests on the Wieringermeer soil. From the compaction series one test of the 75%, the 85%, and the 95% of the Proctor Density has been sampled. From the saturation series one test of the 8.34%dw, the 17.04%dw, and the 20.86%dw are sampled. These compaction levels include the most compacted, least compacted, and the middle value of the compaction series. The saturation levels are selected to include the driest and wettest samples. The saturation level in the middle of the series is already in the compaction series. Therefore, the soil sample at 17.04% saturation is also sampled, since it is expected that in this range the diffusion coefficient will show a sudden decrease in value. This sudden decrease in value was found in the thesis by Van Verseveld [52].

For the selected soil samples, gas samples are taken at concentrations of approximately 40%, 35%, 30%, 25%, and 20% CH_4 in the gas chamber. The 40% value is after any initial effects which occur after opening the slider. The 20% is selected as concentrations much lower will significantly increase the duration of the experiments. The ratio of the isotopes ^{13}C and ^{12}C is determined using isotope ratio mass spectrometry, during which the molecules are isolated based on their molecular weight. For this, a fixed volume of the sample gas is injected into the system. First, the CH_4 is separated from the air. Next, the CH_4 is focused more using a cryofocus to guarantee a peak with a large enough amplitude for the isotope ratio measurement. Cryofocussing is a process which relies on the difference of condensation temperatures of the gas. Next, any remaining gas components are separated from the CH_4 using gas chromatography. After the separation the CH_4 is combusted to CO_2 and H_2 , after which the CO_2 is introduced into the isotope ratio mass spectrometer [6].

3.4.1. Leakage tests

To determine the maximum magnitude of the error of the effective diffusion coefficients, the leakage of methane from the gas chamber needs to be determined. The leakage is independent of the diffusion of gas through the soil. The leakage occurs through small gaps and slits between the different parts of the setup, which are unavoidable as some parts of the setup need to be able to move or be removed. The procedure of the leakage tests is as follows; first the five chambers are flushed with methane and the setups are left for 45 minutes to warm up. After 45 minutes the measurement is started and ran for at least three hours. When processing the data, the loss of methane over that period is used as an indication of diffusion of gas from the chamber. For the duration of the leakage tests the setups are used in combination with a cylinder which has a plastic stopper on top of it, this clogs up the cylinder and prevents any leakage through this way. This stopper only allows leakage through the slits and gaps in the test setup.

The leakage of methane from the test setups is determined over a period of at least three hours. The obtained results are given in Table 3.4. The results are given as absolute concentration percentages of methane that have leaked from the chamber per hour. As shown, four of the setups have a leakage of less than 0.2 percent of methane. Only setup four has a leakage which is more considerable, however, at 1.0 volume percent

leakage per hour it is still considered to perform adequately. The graphs which are obtained from the leakage tests are given in Appendix E.

Table 3.4: Leakage of methane from the test setups per hour, in volume percentage methane of the whole chamber

Test setup	Leakage per hour (%V)
1	0.106
2	0.159
3	0.0929
4	1.002
5	0.128

3.4.2. Sensor calibration

The output of the sensors is given in voltage versus time. These voltages first have to be converted to volume percentages of methane. This is done by applying the formula given in 3.1, which is determined by the performed zero-measurements. For the zero-measurements readings of the voltage were taken at different methane concentrations for each soil sensor; 50%, 40%, 30%, 20%, 10%, and 0%. These concentrations were created by injection a calculated volume of atmospheric air to the 50/50 concentration from the gas bottle. There is a different conversion for each sensor, Equation 3.1a corresponds to sensor 1, Equation 3.1b to sensor 2, etc. Plots of concentration in volume percentage of CH₄ versus the time are obtained from the measurements. From these plots the diffusion coefficients are determined by fitting Fick's Law, (2.5). In these equations, M% is the measured volume percentage of methane and U is the voltage the sensor gives.

$$M\% = 72.082 * U - 88.133 \quad (3.1a)$$

$$M\% = 71.163 * U - 87.011 \quad (3.1b)$$

$$M\% = 68.301 * U - 82.476 \quad (3.1c)$$

$$M\% = 81.543 * U - 100.78 \quad (3.1d)$$

$$M\% = 72.243 * U - 87.736 \quad (3.1e)$$

3.5. Data evaluation

The used methods to evaluate the data acquired during the performed tests is explained in this section. The data evaluation consists of two parts: the determination of the effective diffusion coefficient and the determination of the fractionation of the stable methane isotopes. After these two aspects are explained, the validity of any assumptions during the data evaluation are given.

3.5.1. Calculation of the effective diffusion coefficients

To fit Fick's law to the measured methane concentrations a derivation of Fick's law is used. An example of a raw data plot is shown in Figure 3.4. In this derivation the amount of moles which flow out of the gas chamber is equal to the drop of moles of gas in the chamber, since the only possibility for gas to leave the chamber is through the soil sample. The amount of moles in the gas chamber is calculated using the ideal gas law, thus it is also assumed that the gas will behave as an ideal gas. The ideal gas law is given in Equation 3.2. In this equation, P is the pressure, V is the volume, n is the number of moles of gas, R is the ideal gas constant, and T is the temperature.

$$PV = nRT \quad (3.2)$$

The rate at which the amount of moles changes in the gas chamber is limited by the dimensions of the soil sample and the effective diffusion coefficient of the soil. This effective diffusion coefficient is a parameter which originates from the soil sample. The derivation is written in such a way that the fraction of methane

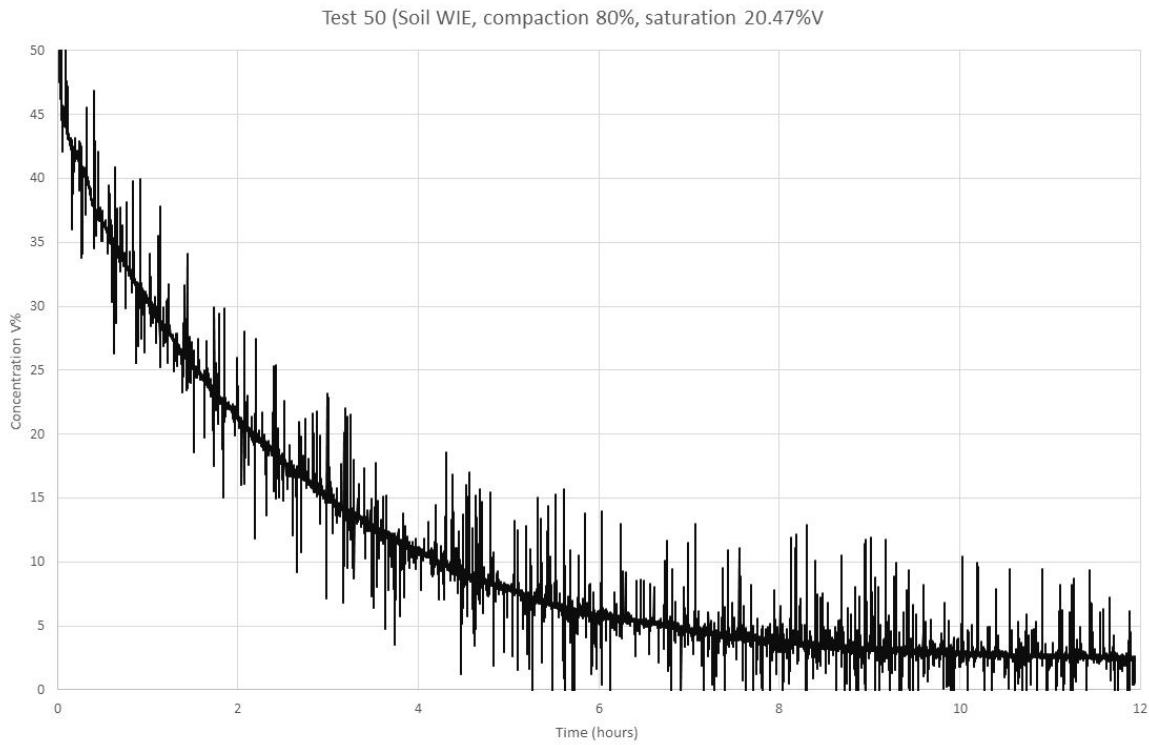


Figure 3.4: Example of raw data; shown here, soil WIE, compaction 80%, saturation 20.47%V

in the chamber and the time are the only two variables. As the changes of the fraction of methane in the chamber over a period of time is known, the effective diffusion coefficient can be derived. To determine the optimal value of the effective diffusion coefficient a least-square method is used. The smallest least-square error corresponds to the optimal value for effective diffusion coefficient.

Fick's first law rewritten to a formula dependent on the change in mole fraction over time is given in Equation 3.3. This is then rewritten to the final formula, a relation between fraction of methane in the chamber and time ($x = f(t)$). This is used to determine the effective diffusion coefficient. This final formula is given in Equation 3.4. The full derivation of Equation 3.4 is shown in Appendix B.

$$\frac{dx}{dt} = -D_{eff} \frac{A}{LV} (x - x_{atm}) \quad (3.3)$$

$$x = (x_{t=0} - x_{atm}) * e^{C*t} + x_{atm} \quad \text{with} \quad C = -D_{eff} \frac{A}{VL} \quad (3.4)$$

In the formula, $x_{t=0}$ is the fraction of methane at time 0 in the chamber and the x_{atm} is the fraction of methane in the atmosphere. For x_{atm} a value of approximately 2 ppm is used [46]. The area through which diffusion can occur, i.e. the area of the base of the soil sample, is included through A . The length of the soil sample and the volume of the chamber are respectively accounted for by L and V . All these parameters for the dimensions are given in meters, square meters, or cubic meters. The values in Equation 3.4 are given in Table 3.5.

Table 3.5: Values used to determine the best value for the effective diffusion coefficient

Parameter	Value	Unit
x	Measured	-
t	Measured	s
$x_{t=0}$	Measured	-
x_{atm}	0.00000179	-
D_{eff}	Best fit determined	m^2/s
A	0.007854	m^2
L	0.10	m
V	0.001583	m^3

The raw data files, found in Appendix E, show that at the start of the tests, after the slider has been opened, a steep drop in the fraction of methane in the chamber is measured by the sensors. This is caused by a small strip of air which is in between the soil sample and the slider. Once the slider is opened this air mixes with the gas in the chamber, thus directly dropping the amount of methane in the chamber. To ignore this effect in the data evaluation the first six minutes, or 360 data points, are removed when determining the effective diffusion coefficients. This also resulted in better fits for Equation 3.4. These first six minutes are selected to be removed because somewhere near the end of that period the curves show a sudden change in slope. This sudden change is taken as the point on the curve after which the gas in the chamber is homogeneous.

3.5.2. Fractionation of stable isotopes

The gas samples taken during the specified tests are analyzed at the University of Utrecht, the Netherlands. Stable isotope mass spectrometry is used to determine the amount of ^{13}C present compared to a standard value (this is the Vienna PeeDee Belemnite). This difference is denoted as $\delta^{13}C$. How these values change with changing fractions of methane, is then evaluated to determine the α_{trans} .

To determine the α_{trans} , the formula by Coleman et al [11] is used. Using the equation given in 3.5 the values of α_{trans} are determined. To acquire the α_{trans} , the difference between $\delta^{13}C$ and $\delta^{13}C_{t=0}$ is plotted against $\ln\left(\frac{M}{M_0}\right)$. The $\delta^{13}C_{t=0}$ is the difference between the measured isotope signature and the Vienna PeeDee Belemnite. The M is the total amount of methane and M_0 is the total amount of methane at the start of the test. This slope is used to determine the values of α_{trans} . This is done by using the rewritten form of equation 3.5, given in Equation 3.6. In this equation, S is the best representation of the slope of the plot of $(\delta^{13}C - \delta^{13}C_{t=0})$ versus $\ln\left(\frac{M}{M_0}\right)$. In this equation, r_C is the kinematic fractionation constant for the carbon.

$$\delta D_t \approx 1000 \left(\frac{1}{r_C} - 1 \right) \ln \left(\frac{M}{M_0} \right) + \delta D_{t=0} \quad (3.5)$$

$$\alpha_{trans} = \frac{1000}{S + 1000} \quad \text{with} \quad S = \frac{\delta^{13}C - \delta^{13}C_{t=0}}{\ln\left(\frac{M}{M_0}\right)} \quad (3.6)$$

3.5.3. Validation

Fick's law was used in the derivation used to determine the effective diffusion coefficients. Fick's law assumes that no advective flow is present. This is the case for the test setup, since there is no pressure difference in the system. Additionally, it is assumed that no Knudsen diffusion is present. This is calculated using the ratio of the gas mean free path to the pore size, calculated in Equation 3.8. The gas mean free path in this equation is calculated in Equation 3.7. In this calculation a value of $50 \mu m$ is used for the diameter of the pores, since this corresponds to the size of the pores which make up the largest part of the air-filled porosity, and thus predominantly controls the gas transport [17]. For the effective diameter of a gas molecule a value of $3.8 * 10^{-10}$ meter is used [25]. The calculated ratio has a value of $4.8 * 10^{-13}$. This is much smaller than 0.1, meaning that Knudsen diffusion can be ignored and Fick's law is valid.

$$\lambda = \frac{k_B T}{\sqrt{2} p \pi d_g^2} = \frac{1.38 * 10^{-23} * 292.35}{sqr{2} * 101325 * \pi * 3.8 * 10^{-10}} = 2.4 * 10^{-17} \quad (3.7)$$

$$K_n = \frac{2.4 * 10^{-17}}{5.0 * 10^{-5}} = 4.8 * 10^{-13} \quad (3.8)$$

The ideal gas law is used to determine the amount of moles of methane in the gas chamber. The validity of the assumption that methane behaves as an ideal gas is dependent on the pressure and the temperature. The pressure should be below the critical gas pressure and the temperature should be above the critical temperature. Methane has a critical temperature of -82.59°C , which is well below the temperature of 19.2°C at which the tests are performed. The critical pressure of methane is 4.599 MPa , which is also well above the pressure during the tests, being 0.101 MPa [47]. Therefore, methane can be considered to behave like an ideal gas.

3.6. Literature models

In Chapter 2.6.5, there are six models given to approximate the effective diffusion coefficient of the soils. These models are given again in Equations 3.9. These models are all used to determine their respective predicted values of D_{eff} , which is then compared to the derived values from the test results. All these models are solely based on the air-filled porosity, and the total porosity. The root mean square error is used as a quantification of the error of the different models, the root mean square error is calculated using Equation 3.10.

WLR Penman model [33]:

$$\frac{D_{eff}}{D_0} = 0.66\varepsilon \left(\frac{\varepsilon}{\phi} \right) \quad (3.9a)$$

WLR Marshall model [33]:

$$\frac{D_{eff}}{D_0} = \varepsilon^{3/2} \left(\frac{\varepsilon}{\phi} \right) \quad (3.9b)$$

WLR Millington model [33]:

$$\frac{D_{eff}}{D_0} = \varepsilon^{4/3} \left(\frac{\varepsilon}{\phi} \right) \quad (3.9c)$$

Millington and Quirk model [31]:

$$\frac{D_{eff}}{D_0} = \frac{\varepsilon^{10/3}}{\phi^2} \quad (3.9d)$$

Gebert et al empirical equation [17]:

$$D_{eff} = 1.319 \times 10^{-7} \times e^{(\varepsilon/0.116)} - 1.477 \times 10^{-7} \quad (3.9e)$$

Troeh et al model [50]:

$$\frac{D_{eff}}{D_0} = \left(\frac{\phi - u}{1 - u} \right)^v \quad (3.9f)$$

$$RMSE = \sqrt{\frac{\sum_{i=1}^n (M_i - P_i)^2}{n}} \quad (3.10)$$

In Equation 3.10, the M_i is the measured value at point i , and P_i is the predicted value at point i . The sum of these squared differences is divided by n , the number of points which are in the series. The model giving the smallest value for the root mean square error is deemed the best model to predict the effective diffusion coefficients of these soils.

3.7. Share of diffusive flux in total gas transport

In this section the influence of diffusion on the transport of methane is evaluated. To do this the magnitude of the diffusive flux is compared to the magnitude of the advective flux. If the diffusive flux is a considerable part of the total flux it cannot be ignored when Equation 3.13 is used to determine the oxidation efficiency. To determine the importance of diffusion for gas transport, the advective flux needs to be calculated, for which Equation 3.11 is used. In this equation, P is the pressure of the gas in the landfill, R is the ideal gas constant, T is the temperature, κ_{eff} is the effective permeability, μ is the bulk gas viscosity, and ∇P is the gas pressure gradient. The bulk gas viscosity, μ_{mix} , is calculated by Graham's model and is given in Equation 3.12 [12]. The outcome of Equation 3.11 needs to be compared to the calculated diffusive fluxes, for this Fick's law is used again.

$$N^V = -\frac{P}{RT} \frac{\kappa_{eff}}{\mu} \nabla P \quad (3.11)$$

$$\mu_{mix} = \sum_i (x_i * \mu_i) \quad (3.12)$$

3.8. Fractionation method including diffusion

The final aspect that is checked is the effect of including diffusion when assessing the oxidation efficiency using the fractionation method. The formula which is used to determine oxidation efficiency is given again in Equation 3.13. Currently, the factor for fractionation due to transport, α_{trans} , is assumed to be 1. However, when diffusion has relevant flux it is hypothesized that diffusion cannot be disregarded. Therefore, the increase in fractionation efficiency is determined to check if the difference is relevant.

$$f_{ox} = \frac{\delta_S - \delta_A}{1000 * (\alpha_{ox} - \alpha_{trans})} \quad (3.13)$$

In Equation 3.13 the α_{trans} is the general term for fractionation due to transport phenomena, thus due to advection and diffusion. There is no fractionation happening due to advection as this process does not discriminate against molecular weight [16]. Therefore, the α_{trans} due to advection is taken as 1. For diffusion, the values are obtained from the stable isotope analysis on the gas samples. However, the α_{trans} is a parameter for the bulk flux, thus the $\alpha_{advection}$ and the $\alpha_{diffusion}$ need to be combined. Considering the advective-diffusion model, described in chapter 2.6.1, the bulk flux is calculated by adding the diffusive and advective flux. To determine the total α_{trans} , the ratio of the flux compared to the total flux is multiplied with the respective fractionation factor, these two values are then added. This relation is shown in Equation 3.14.

$$\alpha_{trans} = \frac{J_{advection}}{J_{total}} * \alpha_{advection} + \frac{J_{diffusion}}{J_{total}} * \alpha_{diffusion} \quad (3.14)$$

This corrects the fractionation factor for the magnitude of the diffusive flux compared to the advective flux. However, this would assume a perfect cover soil with no cracks or other hot-spots of emission, resulting in an overestimation of the oxidation efficiency. Hot-spots are highways for transport of gas, so emission through these hot-spots is assumed to be advective. This results in another reduction factor for α_{trans} which should be used in Equation 3.13. To apply the correction factor for direct emission through these hot-spots, Equation 3.15 should be used to adjust for the loss of methane due to direct emission.

$$\alpha_{diffusion} = \alpha_{advection} * DE + \alpha_{diffusion} * (1 - DE) \quad (3.15)$$

In this equation, DE is the direct emission correction factor and taken from Table 3.6. These values have been estimated by Gebert et al [18]. To determine the best estimate for α_{trans} , the methane load to the cover should be determined first, by using Equation 3.15. Next, the calculated $\alpha_{diffusion}$ should be combined with the $\alpha_{advection}$ in Equation 3.14. Then the improved predictions for the oxidation of methane are calculated using Equation 3.13, included the complete α_{trans} .

Table 3.6: Correction factors for direct emission (DE) and methane load to cover (1-DE) [18]

	(DE) [-]	(1-DE) [-]
No cover or daily cover <30 cm, no gas distribution layer	0.90	0.10
Temporary cover >30 cm, porosity <0.10, no gas distribution layer	0.80	0.20
Temporary cover >30 cm, porosity 0.10-0.20, no gas distribution layer	0.70	0.30
Temporary cover >30 cm, porosity >0.20, no gas distribution layer	0.60	0.40
Permanent cover >100 cm, porosity <0.10, gas distribution layer	0.50	0.50
Permanent cover >100 cm, porosity 0.10-0.20, gas distribution layer	0.30	0.70
Permanent cover >100 cm, porosity >0.20, gas distribution layer	0.10	0.90

4

Results

In this chapter the results obtained from the different aspects of the tests are given and elaborated upon. First, the fit of the curves to the measured data are discussed. Next, the test data are evaluated, this evaluation is split into four different parts. These four parts are the compaction series, the saturation series, the effect of air-filled porosity, and the fractionation of stable methane isotopes. Next, the data obtained from the tests are compared to predictions made by models found in literature to check which best describes the data. The following step is to relate the obtained data back to the field scale, thus determining the importance of diffusion for gas transport over landfill cover soils. Lastly, the effect of including fractionation due to diffusion in a prediction of methane oxidation is given.

4.1. Data evaluation

As mentioned before, the data evaluation is split in four individual parts. First, the compaction series for the Wieringermeer and Hamburg soils are discussed, followed by the discussion of the saturation series for both soils. Next, the effect of air-filled porosity is related to the effective diffusion coefficient. Lastly, the observed fractionation of stable isotopes for both soils is shown.

Table 4.1: Targeted densities and levels of saturation for the parallels

Density (% of Proctor Density)	Saturation for soil HH (%V)	Saturation for Soil WIE (%V)
75	12.35	20.47
80	12.35	20.47
85	12.35	20.47
90	12.35	20.47
95	12.35	20.47
85	25.49	31.24
85	18.58	25.53
85	8.59	16.74
85	5.18	12.49

4.1.1. Compaction series

For the compaction series of both soils the compaction is varied. The saturation is kept constant at the central value; for all samples of soil WIE this is around 20.47%V, and for soil HH around 12.35%V. This is the The compaction of the samples are as close as possible to the targeted densities given in Table 4.1. The compaction levels which were actually obtained are given again in Table C.2 in Appendix C. In this table the densities are given as a percentage of the Proctor Density and the saturation levels as volume percentages. The densities are in the same range as the target density, having a maximum deviation of 3% of the Proctor Density. It proved difficult to consistently produce soil samples closer to the target density. This spread in degrees of compaction is what explains the difference between the target saturations, which can be found in Appendix

C, and the actual saturation levels which are used during the experiments. For both soils the level of saturation turned out higher than intended, for soil HH the saturation levels are approximately 1% point higher, and for soil WIE the saturation levels are approximately 3% point higher with a few saturation levels turning out 4% point higher.

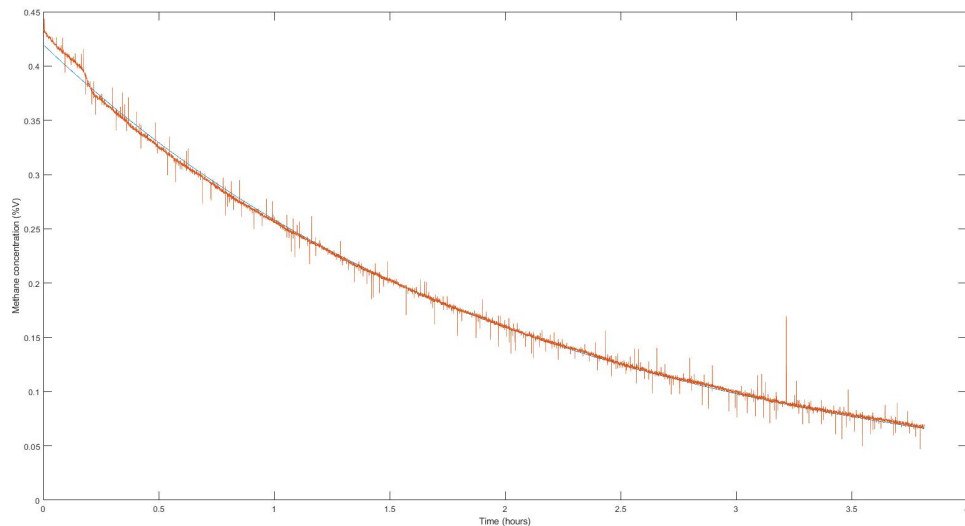


Figure 4.1: Example of the fit to the measured data, for soil HH at 85% of the Proctor density

In Appendix E all the measured data are shown. The data show that an increase in density results in a slower decrease in methane concentration. This corresponds to a decreasing effective diffusion coefficient with an increasing degree of compaction. The error in the fit to the data proved to be minimal for all tests performed. An example of a fitted curve to the measured data is given in Figure 4.1. In this figure, Equation 3.4 is fitted to the data of soil HH at 85% of the Proctor Density. In the figure some outliers are seen, since these outliers are both positive and negative they and multiple are present the fit is still considered to be good.

The plot of the effective diffusion coefficient versus the degree of compaction is given in Figure 4.2. It is seen that the slope of the relation between the effective diffusion coefficient and the degree of compaction is linear. The decreasing values of the effective diffusion coefficient with increasing density are approximately the same for both sands. However, the values for the effective diffusion coefficients are higher for soil HH over the complete range of tested densities. Figure 4.2 shows that the data points are mostly in groups of three, with vertical variation between them. This is explained by the fact that the samples dried slightly during the experiments. The densities stayed constant, but the air-filled porosity increased due to the evaporation of water during the three runs of each soil sample. This effect is compensated for when plotting the air-filled porosity versus the effective diffusion coefficient, as is done in Figure 4.9 for each individual data point. The air-filled porosity takes small changes in both the compaction and saturation into account, also those variations due to evaporation. In Figure 4.3 the compaction is plotted against the air-filled porosity. Again both soils give linear trends, in this plot however the deviation from the trend line is minimal. In Figure 4.4 the effective diffusion coefficients are plotted versus the bulk density to compensate for the difference in specific weight.

In Van Verseveld [52], a relation between the effective permeability and the compaction level was found for both soil HH and soil WIE. This relation is plotted in figure D.1 in Appendix D, where it can be seen that the relation for pressure-induced transport is exponential. This is in contrast to the linear relation found between compaction and effective diffusion coefficient.

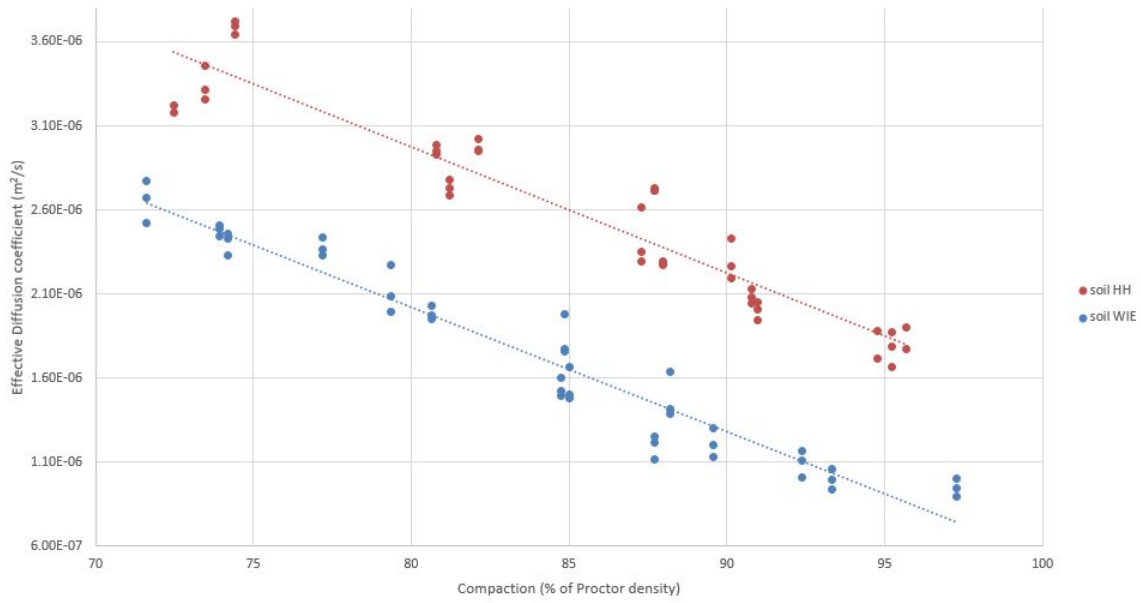


Figure 4.2: Effective diffusivity plotted versus the compaction for both soils

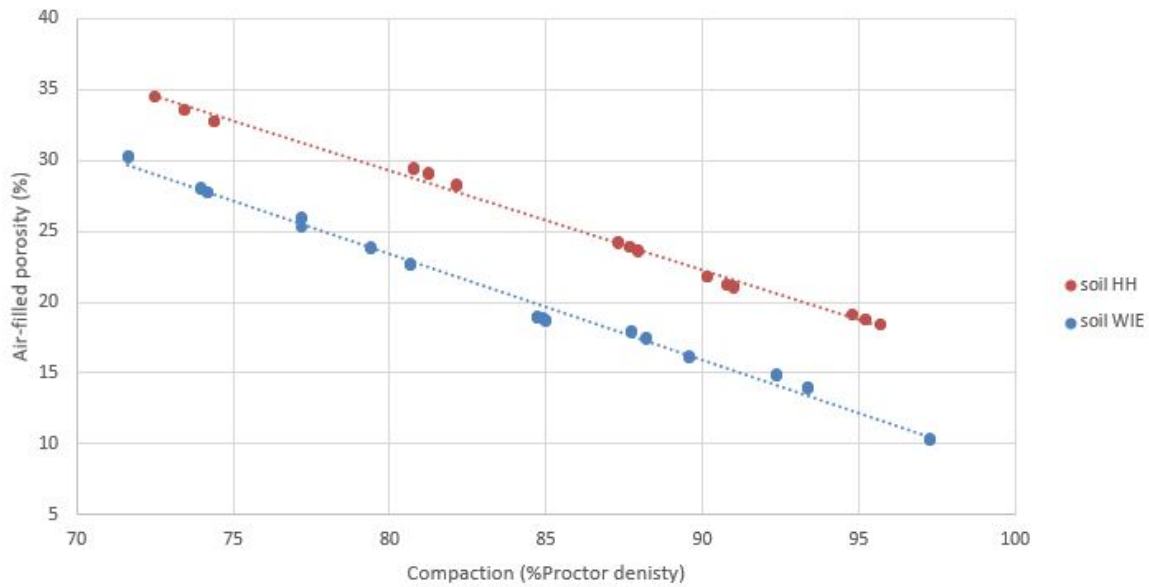


Figure 4.3: Air-filled porosity plotted versus the compaction for both soils

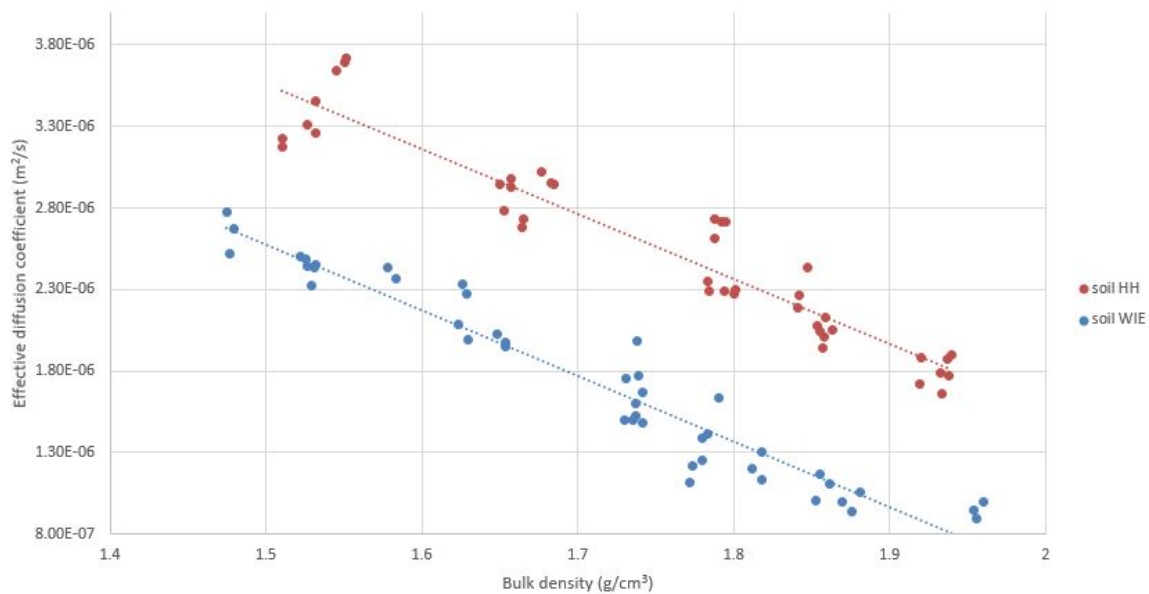


Figure 4.4: Effective diffusion coefficient plotted versus the bulk density for the compaction series

4.1.2. Saturation series

For the series of experiments with a varying level of saturation, the samples are all compacted to approximately 85% of the Proctor Density and the water content is varied. Also for the saturation series the targeted values are given in Table 4.1. The degrees of compaction and the levels of saturation which were actually obtained are given in Table C.3 in Appendix C. In this table it is shown that for soil WIE the levels of saturation in volume percentages are higher than targeted. Which stems from small variations in the gravimetric water content during preparation of the soil, since soil WIE proved to be more difficult to accurately dry and compact. The volumetric water content is more susceptible to variations in density than to the gravimetric water content. For soil HH the saturations of the samples with a target of 25.49%V are higher than the target. However, the samples for the other four targeted saturation values are reasonably close.

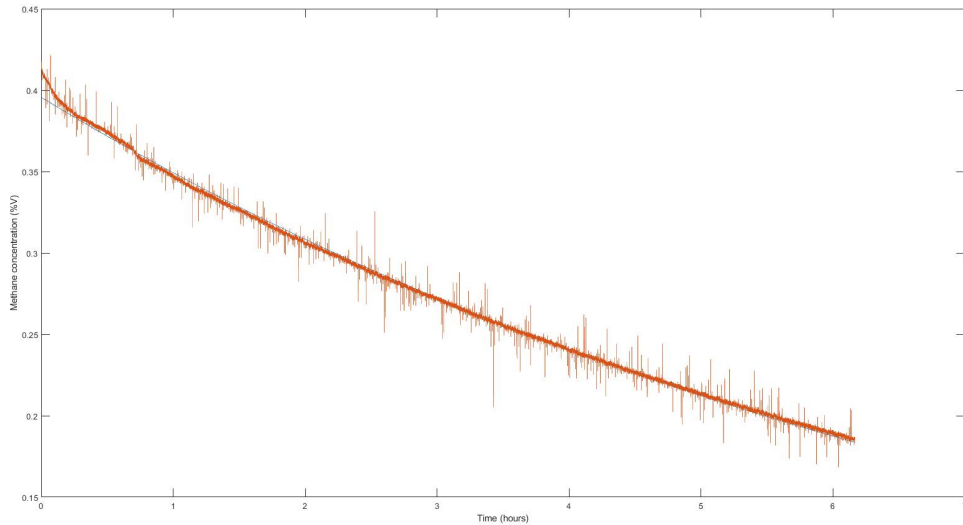


Figure 4.5: Example of the fit to the measured data, for soil WIE at 25.53%V saturation

In Figure 4.7 the air-filled porosity is plotted against the level of saturation. This shows a decreasing air-filled porosity with an increasing level of saturation. When comparing Figure 4.7 to Figure 4.3, the first observation is that for both soils the compaction and the saturation series follow linear relationships. For both soils however, the relation between saturation and air-filled porosity is much steeper. The comparison between percentages is not directly possible, since the Proctor density generally only has values between 70 and 100 % and the saturation can have values ranging from 0 to 100%.

In Appendix E all measured data are given. These figures show a relatively large spread in diffusion rates between the different parallels. For both soils, the samples with the largest water content result in the longest time for the gas in the chambers to diffuse. The trend which is found in the raw data, for higher levels of saturation the methane concentration in the gas chamber decreases slower, corresponds to the trend found in Figure 4.6. In Figure 4.6 the effective diffusion coefficients are plotted against the saturation. The effective diffusion coefficients are again determined by fitting Equation 3.4. An example of a fitted curve to the measured data for the saturation series is given in Figure 4.5. Figure 4.6 shows that the relationship between the saturation and the effective diffusion coefficients increases with a decreasing level of saturation. The values for the effective diffusion coefficient decrease faster for soil HH, compared to soil WIE. In the compaction series the decrease of the effective diffusion coefficient seemed more similar for both soils.

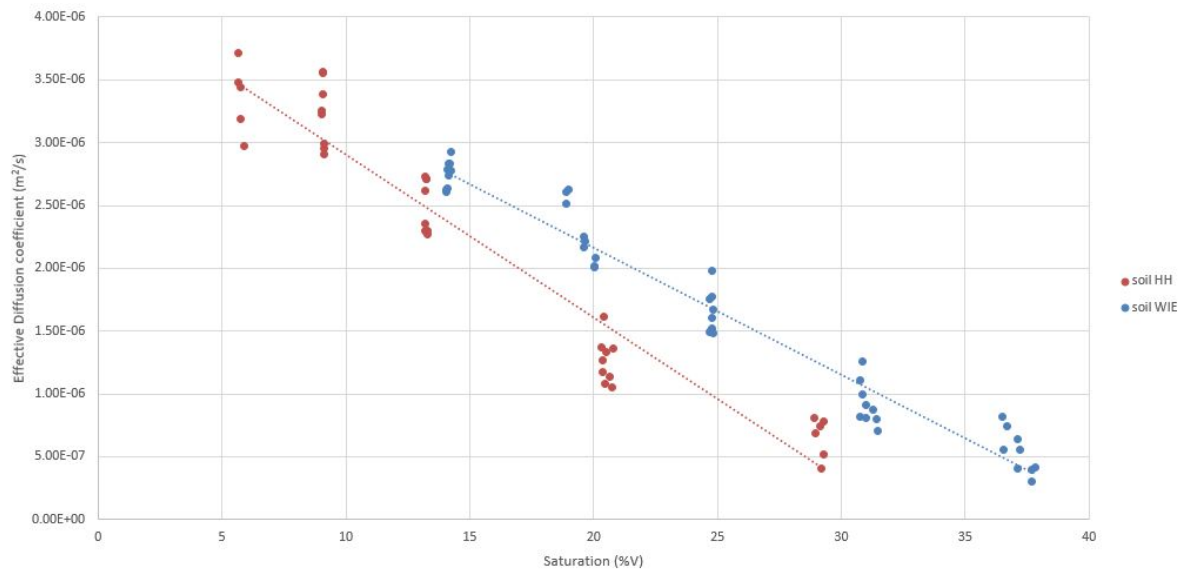


Figure 4.6: Plot of the effective diffusion coefficient versus the saturation as percentage of the total volume

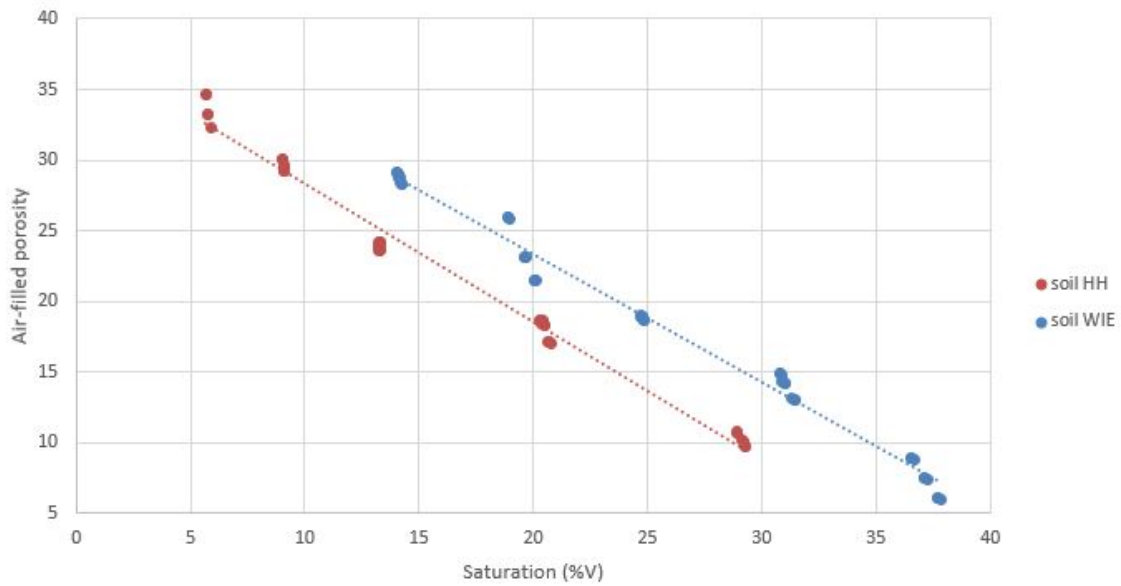


Figure 4.7: Plot of the air-filled porosity versus the saturation as percentage of the total volume

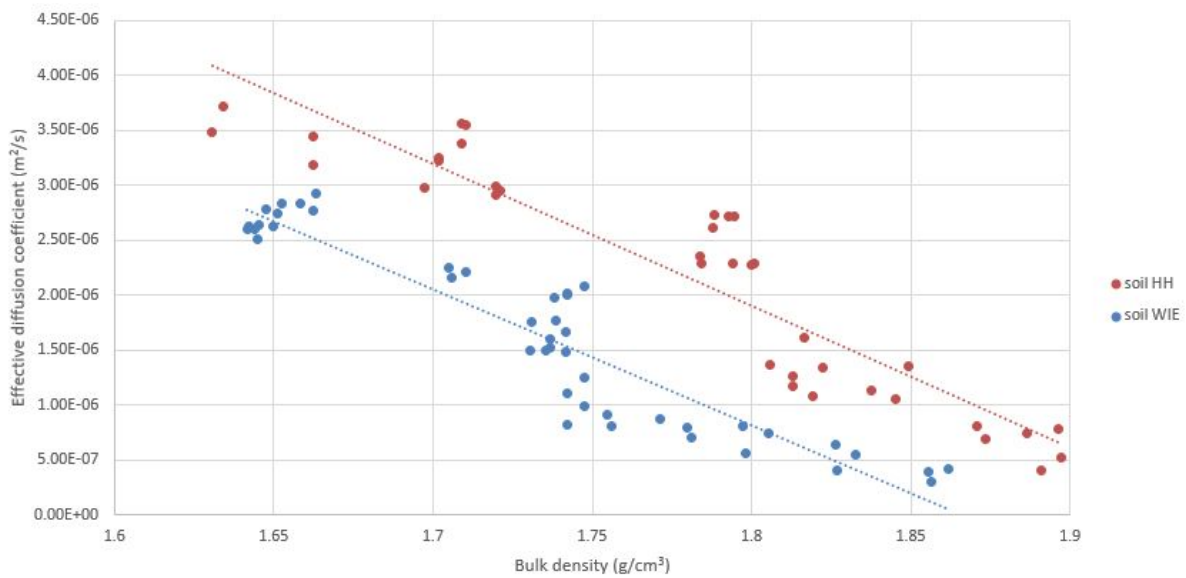


Figure 4.8: Effective diffusion coefficient plotted versus the bulk density for the saturation series

In the saturation series soil WIE has higher values for the effective diffusion coefficient, but for the compaction series soil HH shows higher effective diffusion coefficients. The two soils have a different Proctor Density, to remove any effects due to this difference the effective diffusion coefficients are plotted against the bulk densities. The figure showing the bulk density plotted against effective diffusion coefficients is given in Figure 4.8. In Figure 4.4 and Figure 4.8 soil WIE has lower values for both the compaction and saturation series.

As was seen in the compaction series, the saturation series also shows that there is a variation in air-filled porosity for one single value of saturation. This is explained by the variation in densities between the different parallels tested, and by small differences in saturation level between the different runs on those parallels.

Van Verseveld [52], also found a relation between saturation and effective permeability for both soil HH and soil WIE. This relation is plotted in Figure D.2 in Appendix D, where it is seen that the relation between water content and effective permeability suddenly drops between 25% and 30% water content. The diffusion tests do not show any sudden drops, the relations are linear over the whole range. There is no sudden drop visible in the data collected in this thesis.

4.1.3. Effect of air-filled porosity on the effective diffusion coefficient

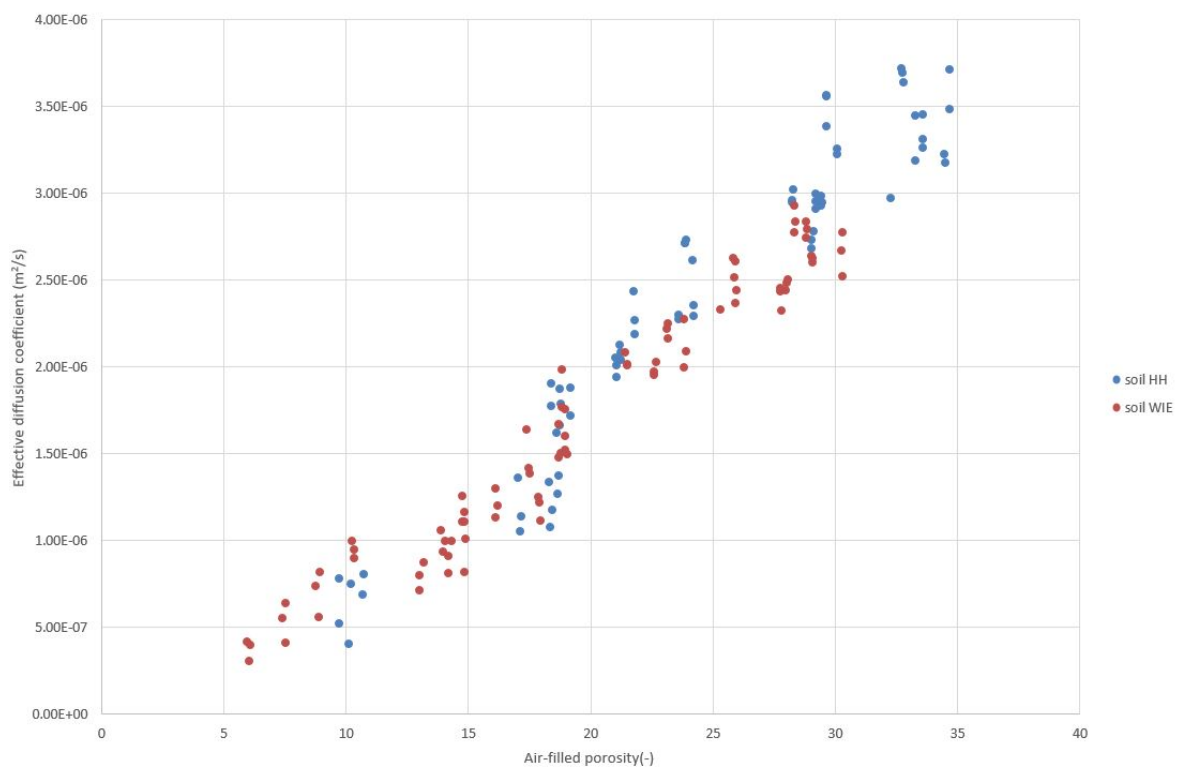


Figure 4.9: Effective diffusivity plotted versus the porosity

As mentioned before in the saturation and compaction series small variations are found between the data points of the different runs and parallels which cannot be explained using the plots they are presented in. The data of both soils is generalized by calculating the air-filled porosity for all data points. The variations in compaction and the small variations between the individual runs due to evaporation of pore water during testing account for changes in air-filled porosity. In Figure 4.9 the effective diffusion coefficients is plotted against the air-filled porosity. In this plot there seems to be no difference between air-filled porosity from the saturation or compaction series because all data points align along the same linear relationship. Figure 4.9 also suggests that there is no distinction between soil HH and soil WIE. Both these apparent relations are tested using t-tests, the results are given in Appendix G. This shows that for both soils the difference between the compaction and saturation series is not statistically relevant. However, it does show that the

values for the effective diffusion coefficient of both soils are statistically different. Using the coefficient of determination, R^2 , the level of explained variance is assessed when relations are fitted; these results are also given in Appendix G. The coefficients of explained variance show that for both soil HH and soil WIE the relation between air-filled porosity and effective diffusion coefficient is linear. The relations to which these trends abide are given in Equations 4.1 and 4.2 for soil HH and soil WIE respectively. A program called Eureqa, created by Nutonian Inc, is used to find the best relation between the air-filled porosity and the effective diffusion coefficients.

$$D_{eff} = 1.24 * 10^{-7} * \phi_a - 6.34 * 10^{-7} \quad (4.1)$$

$$D_{eff} = 1.05 * 10^{-7} * \phi_a - 3.69 * 10^{-7} \quad (4.2)$$

In these formulas the scaling factors are in the same order as those found by Gebert et al [16]. However, this relation was found to be exponential. These three empirical formulas (Equations 2.20, 4.1, and 4.2) fit their respective data well. The difference does not seem explainable by simply looking at the air-filled porosity. The only clear difference between both tests is that Gebert et al [16] used only soils where the air-filled porosity consisted of pores larger as $50 \mu\text{m}$, due to the capillary pressure in the sample. In this thesis both soils consisted predominantly of sand, with varying capillary pressures.

In Figures 2.3 and 2.4 two relations between air-filled porosity and effective diffusion coefficients are given, both from Gebert et al [17]. Figure 2.3 gives a relation found for undisturbed soils, and Figure 2.4 shows a relationship found in repacked soils. The relationship for the repacked soil also is linear, however gives lower values for the effective diffusion coefficient. Additionally, in the dissertation of Geck [20] there is a plot which also shows an exponential relationship between the effective diffusion coefficient and air-filled porosity.

4.1.4. Fractionation of carbon stable isotopes

The samples of gas which were collected during the predetermined experiments had been sent to the University of Utrecht, where isotope-ratio mass spectrometry was performed. From the measurements by the spectrometer α_{trans} is calculated using Equation 3.6. The calculated values of α_{trans} are plotted against the effective diffusion coefficients. This plot is shown in Figure 4.10. This plot does not show any trend between any of the data points. In literature four values for fractionation of stable methane isotopes are given. In free air a value of 1.195 for α_{trans} is given [30]. The three other values available for α_{trans} in literature are: 1.0178 for diffusion through glass beads [14], 1.016 at 85% of the Proctor Density, and 1.008 at 95% of the Proctor Density. These four data points suggest an asymptotic fit, as shown in Figure D.4 in Appendix D. However, when the data points from literature are plotted together with the values for α_{trans} obtained in this thesis, a more complete picture is created. In Figure 4.11 all the values of α_{trans} are plotted against the effective diffusion coefficients. When the literature and experimental data are plotted together the values of α_{trans} show some scatter. One point has a value significantly lower than the rest, being 1.008. When considering the data acquired in this thesis there seems to be no restriction for the α_{trans} by a changing effective diffusion coefficient. The absence of an effect on the fractionation factor due to diffusion with change in effective diffusion coefficient is seen for the entire range of air-filled porosity tested in this sand.

In Appendix F the plots which are used to determine the values for α_{trans} are given. α_{trans} is derived from the slope of the trend lines, using Equation 3.6. In these plots the magnitude of the error of the fits are also given. The magnitude of the error is small, which suggests that the accuracy of the measurements are high.

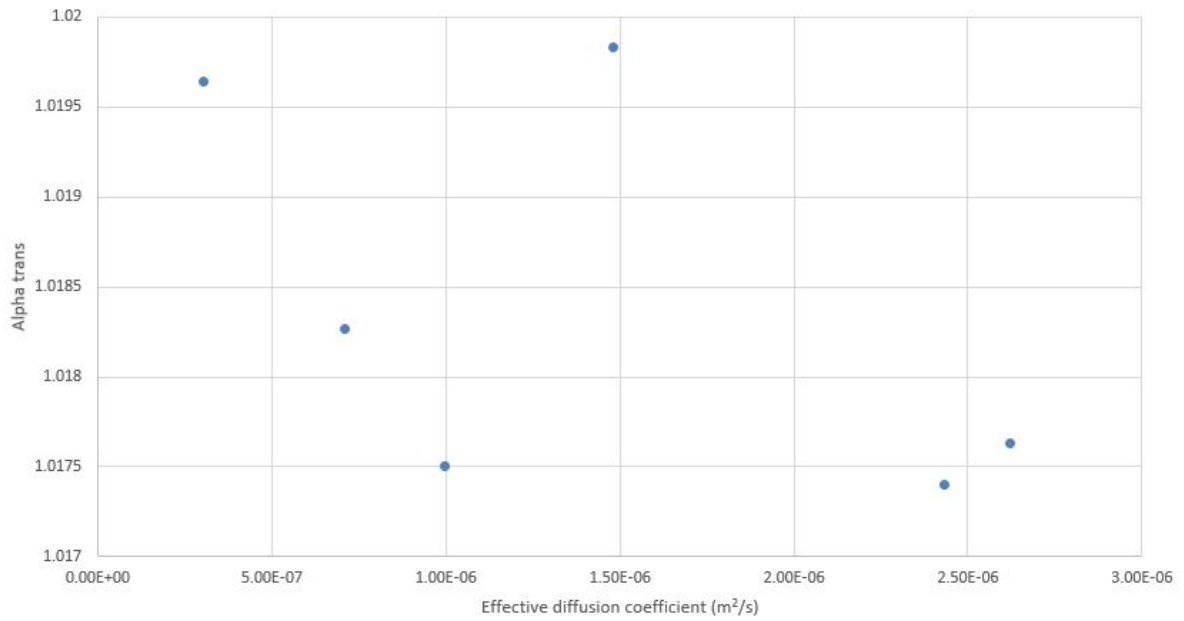


Figure 4.10: α_{trans} plotted versus the effective diffusion coefficients from the tests

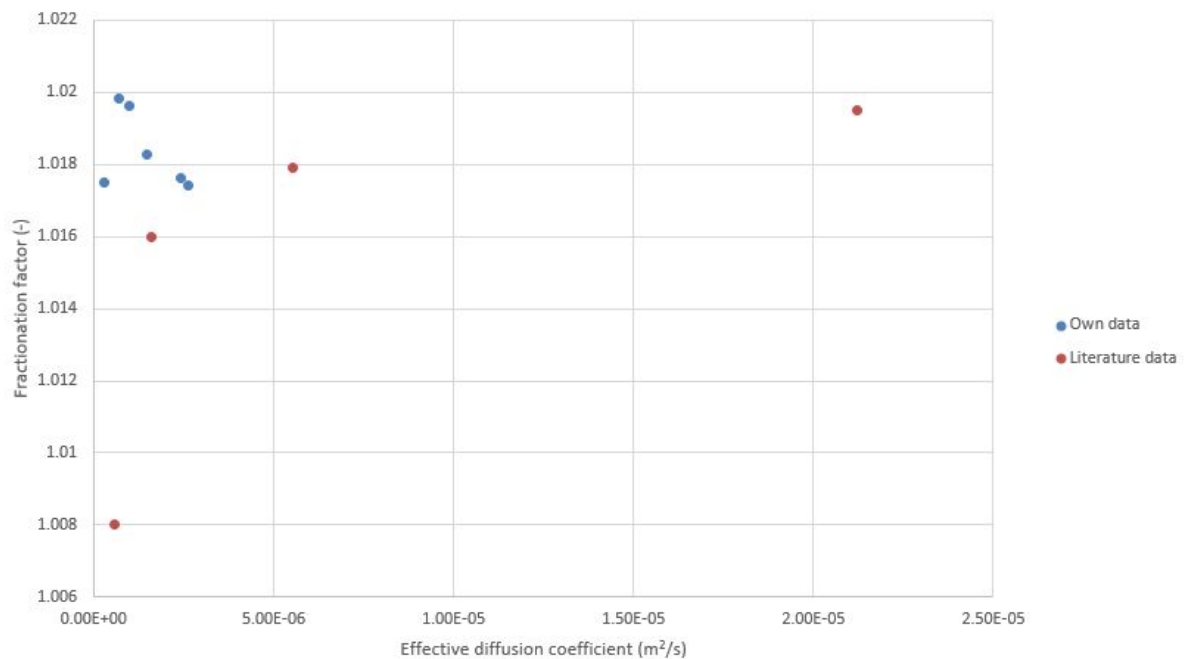


Figure 4.11: α_{trans} plotted versus all effective diffusion coefficients, from the performed tests and literature

4.2. Literature models

In this section the predictions by the models given in Section 2.6.5 are compared to the effective diffusion coefficients which are determined from the measured data. The model from literature which gives the most accurate prediction is then determined. The choice was made to not distinguish between the compaction and saturation series, since these models should be capable to model the variation in both the saturation and compaction. For this reason the model by Troeh et al (Equation 2.21) proved to be unable to model the range of available data, since this model does not include a factor taking the changing water content into account. For the other five models, and the equation determined in Section 4.1.3, the root mean square errors are given in Table 4.2. A lower root mean square error corresponds to a better fit of the model to the data.

Table 4.2: Root mean square errors for the different literature models

Model	Soil HH RMSE	Soil WIE RMSE
WLR Penman	$4.052 * 10^{-7}$	$4.779 * 10^{-7}$
WLR Marshall	$8.000 * 10^{-7}$	$8.100 * 10^{-7}$
WLR Millington	$4.875 * 10^{-7}$	$5.672 * 10^{-7}$
Millington & Quirk	$1.044 * 10^{-6}$	$1.120 * 10^{-6}$
Gebert et al	$1.317 * 10^{-6}$	$1.042 * 10^{-6}$
Equations 4.1 & 4.2	$2.446 * 10^{-7}$	$1.716 * 10^{-7}$

The values of the effective diffusion coefficient are between $5 * 10^{-7}$ and $4 * 10^{-6}$. Therefore, the empirical model by Gebert et al is not applicable to the soils considered in this thesis, since the root mean square error is in the same order as the predicted values. The model by Millington and Quirk has a root mean square error which is in the same order as the empirical relation by Gebert et al, and thus also seems not suitable to model soil HH and soil WIE. The WLR Penman, WLR Marshall and WLR Millington models all give values of reasonable accuracy. This becomes more evident when compared to the empirical relations created for the data, these have a root mean square error of $2.446 * 10^{-7}$ and $1.716 * 10^{-7}$ respectively. The root mean square errors of the empirical relations are the minimal error which can be found. The root mean square errors of the WLR models are 2 to 3 times larger than these empirical relations. For this selection of models the WLR Penman model gives the smallest error for both soil HH and soil WIE, therefore, it is deemed most suitable to model the soils considered in this thesis. It is also seen that soil HH is better modelled by the theoretical models than to soil WIE. This is in agreement with what was found in literature; Moldrup et al [33] also found that the three WLR models all perform adequately. In those tests the WLR Penman and WLR Marshall models performed best, but that was for a different sand. Therefore, in most situations the WLR Penman model is expected to be the best model for predicting the effective diffusion coefficient in sands. However, as also mentioned in literature [1], no best relationship to describe soil diffusivity can be determined in advance.

4.3. Share of diffusive flux in total gas transport

In this section, the importance of diffusion towards the transport of landfill gas is discussed. First, the points at which the fluxes are calculated are discussed, after which the ranges in which the diffusion actually plays a considerable role are shown.

The values for the diffusive and advective flux are calculated at four different pressure differences over the landfill cover soil; at 8.0 hPa, 5.0 hPa, 2.0 hPa, and 1.0 hPa. The concentrations of methane in the landfill are assumed to be constant as the production of gas is ongoing, also near the end of life of the landfill. The fluxes at these four different pressures are calculated for three levels of compaction and three levels of saturation. Using this the diffusive flux, as part of the total flux, is calculated. The calculated percentages of diffusion, as part of the total flux, are also given in Tables 4.3 and 4.4. The concentration of methane is determined based on a mixture consisting of 50% methane and the number of moles in a cubic meter of gas according to the ideal gas law. For the conditions during the performed laboratory tests the ideal gas law gives that 41.69 moles per cubic meter. Thus, the concentration of methane in the landfill is taken as 20.85 mol/m^3 .

The data in Table 4.3 show that for a higher compaction the effect of diffusion becomes more relevant for gas transport. Table 4.4 shows that diffusion becomes more relevant for gas transport when considering drier samples. Next, both Table 4.3 and Table 4.4 suggest an exponential relation between reducing pressure and increasing importance of diffusive flux. In the data four factors show to increase the importance of diffusion as a gas transport phenomena.

- Compaction of the soil
- Saturation of the soil
- Pressure of methane in the waste body
- Concentration of methane in the waste body

Table 4.3: Values used to determine the percentage of diffusive flux, as part of the total flux of methane for the compaction series

Soil HH - Saturation: 12.35%V		
Compaction level (% D _{pr})	Pressure (Pa)	Percentage diffusion of total flux (%)
75	8000	0.227
75	5000	0.340
75	2000	0.679
75	1000	1.35
85	8000	1.43
85	5000	2.13
85	2000	4.19
85	1000	8.05
95	8000	3.43
95	5000	5.07
95	2000	9.67
95	1000	17.66
Soil WIE - Saturation: 20.47%V		
75	8000	0.269
75	5000	0.404
75	2000	0.806
75	1000	1.60
85	8000	0.526
85	5000	0.788
85	2000	1.57
85	1000	3.09
95	8000	1.06
95	5000	1.58
95	2000	3.12
95	1000	6.06

Table 4.4: Values used to determine the percentage of diffusive flux, as part of the total flux of methane for the saturation series

Soil HH - Compaction: 85% of the Proctor density		
Saturation level (%V)	Pressure (Pa)	Percentage diffusion of total flux (%)
25.49	8000	0.184
25.49	5000	0.276
25.49	2000	0.552
25.49	1000	1.10
12.35	8000	1.43
12.35	5000	2.13
12.35	2000	4.19
12.35	1000	8.05
5.18	8000	2.42
5.18	5000	3.60
5.18	2000	6.96
5.18	1000	13.03
Soil WIE - Compaction: 85% of the Proctor density		
31.24	8000	0.170
31.24	5000	0.255
31.24	2000	0.510
31.24	1000	1.02
20.47	8000	0.526
20.47	5000	0.788
20.47	2000	1.57
20.47	1000	3.09
12.49	8000	2.73
12.49	5000	4.05
12.49	2000	7.79
12.49	1000	14.47

4.4. Including diffusion when using stable isotope fractionation to quantify methane oxidation efficiency

In the final section of this chapter the oxidation efficiency of methane is recalculated for two cases described in literature. For this calculation two papers have been selected. The first paper is written by Cabral et al [9] and includes data of a landfill near Quebec, Canada. The second paper is written by Chanton et al [10] and includes data of the Nashua landfill in the Northeastern part of the United States.

The oxidation efficiency is first calculated for the cases where fractionation due to diffusion is assumed to be negligible, i.e. where α_{trans} equals 1. Next, the oxidation efficiency is calculated for the case where fractionation due to diffusion is assumed to have a significant role. When fractionation due to diffusion is assumed to be of importance, the average value for the fractionation factor which is found in the performed tests in this thesis is used. The calculation is made using Equations 3.6, 3.13, and 3.14.

The cases described in both papers are near the end of life of the landfills, in which cases the pressures would have largely dissipated. Therefore, the pressure difference used in the calculations for both landfills is taken as 1.0 hPa. The values used for the calculations are given in Table H.1 and Table H.2 in Appendix H; those values are the $D^{13}C$ (in the landfill and the atmosphere), α_{ox} , and α_{trans} at different diffusive flux percentages of the total flux. The corresponding distribution of the total flux is given in Table 4.3 and Table 4.4. In Table 4.5 the average increase of the predicted value when diffusion is included is given for the cases of both papers, for a range of percentages of diffusive flux from the total flux due to transport.

Thus summarizing, diffusive fractionation significantly improves the calculation of the methane oxidation efficiency when diffusive flux is a considerable part of the total flux. The magnitude of the improvement increases with increasing share of diffusive flux of the total flux.

Table 4.5: Increase in calculated oxidation efficiencies when taking diffusion into account, given in percentage increase of the original value

Percentage of total flux due to diffusion (%)	Cabral	Chanton
2.5	1.36	1.16
7.5	4.20	3.57
12.5	7.20	6.10
17.5	10.38	8.76

5

Discussion

In this chapter the results are combined with the applied methodology and theoretic background, which is then discussed. Based on this discussion the conclusions are given in the next chapter. The recommendations which follow from this discussion are given in Chapter 7.

5.1. Air-filled porosity

In this thesis it is found that both the compaction and the saturation are linearly related to the air-filled porosity. The error when plotting the effective diffusion coefficient obtained in the compaction and saturation series against the air-filled porosity proved to be small. This is also reasonable, since the air-filled porosity is equal to the volume of air in the sample divided by the total volume of the sample. Any deviations from the linear relation could account for part of the scatter in the effective diffusion coefficients. In this, the volume of air is calculated by taking the total volume and subtracting the volume of sand and the volume of water. The total volume is the same for all soil samples, thus this value does not change. In the case of the compaction series the volume of the soil is the variable which changes, since with higher degrees of compaction more soil is compacted in the soil sample. For the saturation series the volume of water is the variable that changes. As the changing variable is linearly related to the air-filled porosity, the results of the compaction and wetting of the samples fit the theory.

5.2. Soil diffusivity

In the experiments performed the soil diffusivity proved to be linearly related to the air-filled porosity, and thus linearly related to both the compaction and saturation. In Figure 4.9 the linear trend is shown, after performing t-tests it was proved that the compaction and saturation series for one soil are related. This seems plausible as for diffusion the air-filled porosity and pore shapes are important, and since in a sand the major pathways are not altered much by any addition of water the major pore shapes stay constant. However, the performed t-tests did show that the effective diffusion coefficients of both soils are statistically different. This is explained by the difference in the fraction of fines between both soils, a larger fraction of fines increases the tortuosity of the soil. The path length of the molecules is important for diffusion; this is dependent on the fraction of fines. In this thesis the tests have been performed on sands, which generally have more coarse pores than finer textured materials. The linear reduction which is found for both soils proves that the limiting factor for the diffusion is the volume of air in the samples, since no increased effects due to tortuosity or connectivity are visible in the data. From the fact that the volume of air is the limiting factor it also follows that the size of the pore throats are linearly related to the volume of air in the soil, as these are the narrowest points of the soil and thus the limiting factor for the diffusion.

In the thesis by Van Verseveld [52] the relation between air-filled porosity and effective permeability has been researched for advective transport. This showed that a sudden drop in effective permeability when the air-filled porosity is decreased for the saturation series. The compaction series showed a trend which approached zero when the compaction level increased. This difference is explained the water first filling the finer pores; at one point the coarse pores are also filled, which shows the sudden decrease. Where for the

compaction series the share of coarse pores is reduced immediately, thus in the beginning of compacting the values more rapid. Thus for advection it is important what share of the air-filled porosity consists of coarse pores. The difference between the saturation and compaction series was not found for the relation between the effective diffusion coefficient and the air-filled porosity. Thus, for diffusion the total air-filled porosity is important and there is no effect of pore sizes on the effective diffusion coefficient. This is also supported by evaluating the relations for advective flux and diffusive flux (Equation 2.1 and Equation 2.5). In the relation for advective flux a term for viscosity is included, through which the advective flux is combined with the drag of the gas with the walls. Through the dependency of advection on the drag on the wall the advective flux is related to the pore diameter. The diffusive flux is not dependent on the viscosity or pore diameter. Thus, for diffusion there is no difference between the saturation and the compaction series.

As mentioned in Moldrup et al [32], water in sandy soils is mostly present in water films around the particles and creates menisci in the pore throats. The smaller pores in the soil also get completely filled with water when the water film surrounding the particles reaches a sufficient thickness, coarser pores initially have a very limited effect of increasing water content. These effects occur due to the fact that in soils water is generally the wetting phase, and the gaseous phase is the non-wetting phase, per Scanlon et al [40]. The forming of menisci in the pore throats and the complete filling of the smaller pores with water restrict the diffusion of gas. Partly because the soil is water-wet, and therefore the films of water surrounding the particles become thicker with increasing water content, the gaseous phase is forced to the middle of the pores, effectively decreasing the volume of air available for diffusion. However, what gives increasing saturation an additional effect on the diffusion, is the formation of water menisci in the pore throats. The presence of these menisci blocks any diffusion through that pore throat, and thus increases the tortuosity [33] [32]. Per Equations 2.6 and 2.7 the relation of tortuosity to diffusion is given.

The result when plotting the effective diffusion coefficient versus the air-filled porosity obtained in this thesis matches the trend in the results found in Gebert et al [17], as shown in Figure 2.4. However, the results given in Figure 2.3, are also found by Gebert et al [17], show an exponential relationship between air-filled porosity and the effective diffusion coefficient. This difference can be explained by the size of the sand fraction present in the specific soils. Gebhardt et al [19] found that sandy soils are only slightly compressible. Which means that the fraction of coarse pores remains large, even after compaction [19]. As both soils that were tested in this thesis consist of sand, the linear relation can be explained by the fact that there is still a large fraction of coarser pores present. For finer grained material the soil is more compressible, which proved to dramatically reduce the presence of air-filled porosity. This reduction of air-filled porosity for a compressible soil reduces the continuity and increases the tortuosity [17]. These effects have been proven to be related to the effective diffusion coefficient. For soils consisting of finer particles compaction also fills pores and blocks pore throats, since the finer particles are likely to fit in the pore throats and inside the pores.

Summarizing, the difference between the results found in the tests and in different literature is attributed to the difference in compressibility of a soil. In this thesis the air-filled porosity is used as a measure for the connectivity and tortuosity. This ignores variations between the connectivity and tortuosity at the same air-filled porosity, which could be done since mainly coarse pores are present in the system and they are not very tortuous. Ultimately, the connectivity and tortuosity are also important measures for the diffusion, since they determine the path length of the gas molecules. When a soil is more compressible the relation between the compaction and the air-filled porosity becomes more non-linear. On top of the linear reduction of the air-filled porosity more pore throats get blocked, thus increasing the tortuosity and reducing the connectivity more. When the fraction of smaller particles is larger the probability that pore throats get blocked also increases.

5.3. Fractionation of stable methane isotopologues

In Section 4.1.4 it is shown that in the tests no effect of the reduced air-filled porosity was found for the fractionation of the stable methane isotopes, for both the compaction and saturation series. This does not correspond with what was hypothesized at the start of this work. The hypothesis was that the fractionation effect would be less for soils with lower air-filled porosity. This hypothesis was based on results found in two experiments performed by Gebert et al [16], combined with a fractionation factor for diffusion through glass beads, and the fractionation factor of methane isotopes in free air.

The relations between the soil parameters and diffusion found in the literature are considered. These relations describe the effective diffusion coefficient to be dependent on the air-filled porosity, porosity, and thus also the tortuosity of the sample. All the parameters which are used in models in literature are dependent on the soil. When considering that the fractionation factor is dependent on the effective diffusion coefficients, as shown in Equation 5.1, the conclusion is made that α_{trans} is independent of soil properties.

$$\alpha_{trans} = \frac{D_{eff}^{12C}}{D_{eff}^{13C}} \quad (5.1)$$

The effective diffusion coefficient for ^{12}C and ^{13}C are corrected for the effects of the soil matrix with the same factors, thus the ratio of diffusion coefficients stays constant. This explains why there is no trend found in the performed tests. The value of 1.008 for α_{trans} as given in Figures D.4 and 4.11 corresponds to the value found by Knox et al [28] for fractionation during air-water gas transfer. The value for fractionation, α_{diff} , during air-water gas transfer is also 1.008. Therefore, it is hypothesized that diffusion of methane in the loams tested by Gebert et al [16] has a large fraction through the aqueous phase. Especially for the value at 95% of the Proctor Density the diffusion predominantly occurs through the water phase.

5.4. Contribution of diffusion to the release of methane gas to the atmosphere

The evaluation of both the diffusive flux and the advective flux for soil HH and soil WIE proved that at low pressures, especially at higher compaction and lower saturation levels, diffusive flux plays an important role. However, the soil which is used for this calculation is a sand, and as argued before the low compressibility of sand prevents to an extent the blockage of pore throats. Since advective transport is also dependent on the viscosity of the gas, and therefore the width of the pores, the effect of a larger fraction of fines will have a larger effect on advection than on diffusion. Diffusion does not depend on the viscosity, and thus is less impacted by the reduction of pore sizes.

It is also shown that the predicted values of the oxidation efficiency increase by approximately 4% when diffusion makes up only 7.5% of the total flux. The importance of including diffusion when determining the oxidation efficiencies, logically becomes larger when the percentage of diffusive flux in the total flux increases. When considering situations where pressures are sufficiently low and thus diffusion is a significant factor for gas transport, the increase in predicted values becomes of sufficient magnitude to require inclusion of fractionation due to diffusion.

5.5. Quantifying methane oxidation in landfill cover soils

In this thesis it is shown that stable isotope fractionation can be used to quantify the oxidation efficiency of methane in landfill cover soils, even at ranges when diffusion becomes a more dominant factor for gas diffusion. During the performed tests it was shown that the relation between air-filled porosity and effective diffusion coefficient proved to be linear for sands. When this is compared to the relation between air-filled porosity and effective permeability, for determining advective flux, it shows that towards more compacted and drier soils diffusion plays a more important role.

Soil HH consists of a larger fraction of fines (i.e. clay, silt, and organic content) which can also be seen from the fact that for soil HH the contribution of diffusion to the total flux is greater. This is explained by the fact that the greater fraction of fines reduces the pore sizes, this affects the advection more than diffusion, since advection is dependent on viscosity.

6

Conclusions

Finally, the sub-questions and research questions can be answered fully. In this chapter, first the answers to the sub-questions presented in Section 1.2.1 are handled separately. After which the answers to the research questions in Section 1.2 are given.

What is the relationship between compaction or saturation and air-filled porosity?

The air-filled porosity decreases linearly with increasing compaction level; this effect is found for both soils analyzed for the tests in this thesis. Additionally, the results of the series of tests with varying saturation levels show a similar linear decrease of air-filled porosity when the saturation increases, and again the effect for both soils is similar. It is also shown that an increase of water content results in a larger decrease of the air-filled porosity. The effect of compaction on changes in pore size distribution was not investigated.

How does soil diffusivity relate to air-filled porosity?

It proved that the effective diffusion coefficient is linearly related to the air-filled porosity for the two sands tested. When evaluating this relationship no distinction between the compaction and saturation series needed to be made for both soils. When evaluating the effective diffusion coefficient versus the air-filled porosity both soils follow a linear trend. No distinction needs to be made between the compaction and saturation series. There is a distinction between both soils tested, these also have different linear relations. The linear relation means that the pore structure is not affected strongly when the air-filled porosity is changed, if the experiments are performed on sands. The larger pore particles limit the compressibility, and the relatively large pore throats limit the amount of blockage that can occur due to the forming of water menisci or blockage with fines.

What is the effect of soil diffusivity on the fractionation of stable methane isotopologues?

The samples of gas which are taken from the chamber during the selected tests showed a high correlation between the change in $d^{13}C$ and the change in methane concentration. Using this it is concluded that calculated the fractionation factors for diffusion, α_{trans} , are also accurate. However, the fractionation factor showed no visible trend when compared with any soil parameters. The spread of values found in this thesis are interpreted as noise, meaning that from the obtained data no change of the fractionation factor for stable methane isotopes occurs due to changing compaction and soil water content. This means that fractionation through the investigated soils equals fractionation as is observed in air. Thus, the diffusion rates of the isotopes are not impacted differently by the soil properties. In turn this means that when diffusion is relevant more accurate predictions of the oxidation efficiency are obtained if the α_{trans} is not set to 1.

Which type of existing model is most suitable for modelling the gas diffusivity at different compaction and saturation levels?

When fitting the data obtained in this thesis to the selected literature models, it showed that the WLR models predicted the trend in the data with reasonable accuracy. For sands it was seen that only taking the air-filled porosity and the total porosity into account is sufficient to give accurate predictions when modelling the effective diffusion coefficients. When using the empirical relations found in this thesis the found relation

does improve the accuracy, but these are only applicable to the soils which are tested and cannot be used in general. Additionally, the WLR Penman model was shown to be the best approximation of the tortuosity in both sands used during the tests performed. These relations approximate the tortuosity by the ratio of the effective diffusion coefficient and the diffusion coefficient in free air.

What is the contribution of diffusion through a cover soil to the potential release of methane to the atmosphere?

The diffusive fluxes are calculated from the effective diffusion coefficients found in this thesis and on concentration gradients known from literature. These diffusive fluxes are compared to the advective fluxes, which are calculated based on a range of assumed pressures and the effective permeabilities found in Van Verseveld [52]. This showed that a higher degree of compaction, lower water content, larger fraction of fines, and a smaller pressure gradient over the landfill cover soil. All increased the importance of diffusion for gas transport through a landfill cover soil. Particularly near the end of life of a landfill diffusion starts playing an important role in gas transport. The comparison also showed that for the same air-filled porosity the diffusion is more important for transport in soil HH, at the same concentration and pressure differences. This is explained by the fact that soil HH has a larger fraction of fines.

What is the effect of compaction and saturation on diffusion and diffusive fractionation of methane?

Diffusion in the tested sands is linearly related to the air-filled porosity; the effective diffusion coefficient decreases linearly with decreasing air-filled porosity. Both the compaction and saturation are also linearly related to the air-filled porosity and the rate of diffusion for the sands tested. Both higher rates of compaction and higher saturation levels result in a reduced air-filled porosity, and thus in a reduced effective diffusion coefficient. It was also shown that both the compaction and the saturation is linearly related to the effective diffusion coefficient. Therefore, it is concluded that in the tested sands no significant restrictions of pore throats, and thus any significant increase of tortuosity, occur.

When assessing the effect of compaction and saturation on diffusive fractionation of stable methane isotopes it is shown that no definitive effect on the fractionation factor can be found. Thus it is concluded that for sand the fractionation factor due to diffusion is not altered by any change in effective diffusion coefficient. The effects of the soil matrix present does not have a different effect on the diffusion rates for the individual isotopes, resulting in the absence of a trend between the fractionation factor due to transport and the effective diffusion coefficients.

How does diffusive flux affect the quantification of methane oxidation in the landfill cover soil when using fractionation of stable methane isotopes?

When using the fractionation of stable methane isotopes to quantify the oxidation of methane, usually no fractionation due to transport is assumed to occur. However, when the diffusive flux increases and becomes of greater importance for gas transport, a correct estimation of the fractionation factor due to transport, α_{trans} , is required. When the diffusive flux is an increasing part of the total flux, the effects of fractionation affect the prediction accuracy of the method using stable isotope fractionation. In this thesis it is shown that when the diffusive flux is at 10% of the total flux, the prediction already increased by approximately 6%. To incorporate this effect of diffusive fractionation the only thing which needs to be taken into account is the ratio of diffusive flux to advective flux, since there is no effect of compaction or saturation on the fractionation of stable methane isotopes.

The fractionation factor due to transport, α_{trans} , which is used in the method, is a combination of the fractionation due to diffusion and due to advection. There is no fractionation occurring due to advection, since pressure based transport does not discriminate against molecular weight, and therefore the effect of fractionation due to transport becomes smaller when the magnitude of the advective flux increases more in comparison with the diffusive flux. This fractionation factor due to transport can be combined using the simple Advection-Diffusion model for these soils, as this model suffices when predicting the total total flux.

Recommendations for future research

- In this study, different relations between air-filled porosity and the effective diffusion coefficient were found than given in literature. The different relations were not found for different ranges of air-filled porosity, however the difference was attributed to the difference in the percentage of fines present in the soil. There are no data available on the fraction of coarse pores that are present in the soil samples, this makes it difficult to relate the findings of the tests to different soils. Therefore, it is recommended to perform diffusion tests on a range of soils, with varying fractions of fines, and also different organic contents. When performing these tests the tortuosity of the used soils needs to be taken into account, to ensure that the effect of the changing tortuosity on the effective diffusion coefficient can be quantified more directly. Additionally, it is recommended that a more extensive evaluation of the pore structure is performed on these samples. All this should facilitate in the study of the effect of pore size distribution and pore morphology on the diffusion.
- Secondly, in this study the fractionation of stable isotopes was tested for two different sands with a small fraction of fines present. As argued in the point above, this only gives a limited view of pore structures, since sand has a very low compressibility. It is possible that isotopes might experience some restriction due to the formation of bottlenecks in the soil. To test this, stable isotope analysis should also be performed for different soils (e.g. clays, loams, etc.), during which not only the air-filled porosity is measured but also the pore structure (thus the tortuosity and connectivity) and the pore size distributions are also quantified. These tests can then be used to determine if there is also no effect of the finer soils on the fractionation of stable methane isotopes. In other words, it should be investigated whether the observed lack of impact of the soil on the diffusive fractionation is also found in soils with a different pore size distribution.
- With the experiments carried out in the framework of this thesis, the fractionation of stable methane isotopologues due to diffusive methane transport was assessed. The results did not suggest any effect of the soil on the fractionation factor. However, the molecules which were assessed are $^{13}\text{CH}_4$ and $^{12}\text{CH}_4$, the difference in weight is caused by only one neutron. This is a very small difference in molecular weight, which could have resulted in a difference in transport rates not large enough to be considered outside of the accuracy range of the measurement. To evaluate this effect, it should be tested if any effect on the level of fractionation does occur when the molecule masses differ more. In other words, an experiment should be carried out in which two different types of molecules are assessed. However, this is not applicable anymore for quantification of methane oxidation efficiency in landfill cover soils, but could prove interesting when evaluating the diffusive behaviour of various molecules. A possibility is to compare the difference between diffusion of bulk methane and diffusion of bulk carbon dioxide. This was not done in this thesis as there was no carbon dioxide sensor available.
- When the ratio of diffusion to advection was determined for both soil HH and soil WIE in this thesis a difference between the importance of diffusion was found. Soil HH shows a considerably greater importance of diffusion, compared to the importance of diffusion for soil WIE at the same air-filled porosity, concentration gradient, and pressure gradient. This is attributed to the fact that soil HH also has a larger fraction of fines present. When this is extrapolated it is hypothesized that for soils with

a larger fraction of fines the importance of diffusion becomes larger, at the same concentration and pressure gradient. Therefore, it is recommended to evaluate the effects of different soils on the relation between diffusive and advective flux, especially when considering soils with larger fractions of smaller particles (e.g. clay, silts, etc.) and what the effect of the different types of fines is.

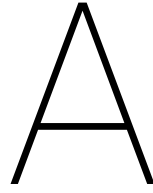
- As mentioned in the conclusion, it is clear that the prediction of methane oxidation efficiency using stable isotope fractionation does get more accurate when diffusion is included, but by how much the accuracy increases is unsure. To determine the accuracy of the stable isotope fractionation method a full field test should be performed. In this test the actual methane oxidation efficiency should be determined. In the same test the accuracy of the Advective-Diffusion model should also be evaluated, in order to be able to give the exact accuracy when the methane oxidation efficiency is calculated.

Bibliography

- [1] S.E. Allaire, J.A. Lafond, A.R. Cabral, and S.F. Lange. Measurement of gas diffusion through soils: comparison of laboratory methods. *Journal of Environmental Monitoring*, 10(11):1326–1336, 2008.
- [2] J.F. Barker and P. Fritz. Carbon isotope fractionation during microbial methane oxidation. *Nature*, 293(5830):289, 1981.
- [3] M. Bender and R. Conrad. Kinetics of methane oxidation in oxic soils. *Chemosphere*, 26(1-4):687–696, 1993.
- [4] R.B. Bird, W.E. Stewart, and E.N. Lightfoot. *Transport Phenomena.(4th edn)*. Wiley and Sons: New York, 2006.
- [5] N. Blair, A. Leu, E. Muñoz, J. Olsen, E. Kwong, and D. Des Marais. Carbon isotopic fractionation in heterotrophic microbial metabolism. *Applied and Environmental Microbiology*, 50(4):996–1001, 1985.
- [6] M. Brass and T. Röckmann. Continuous-flow isotope ratio mass spectrometry method for carbon and hydrogen isotope measurements on atmospheric methane. *Atmospheric Measurement Techniques*, 3(6): 1707–1721, 2010.
- [7] R. Brooks and T. Corey. Hydraulic properties of porous media. *Hydrology Papers, Colorado State University*, 24:37, 1964.
- [8] A.R. Cabral, P. Tremblay, and G. Lefebvre. Determination of the diffusion coefficient of oxygen for a cover system including a pulp and paper by-product. *Geotechnical Testing Journal*, 27(2):184–197, 2004.
- [9] A.R. Cabral, M.A. Capanema, J. Gebert, J.F. Moreira, and L.B. Jugnia. Quantifying microbial methane oxidation efficiencies in two experimental landfill biocovers using stable isotopes. *Water, Air, & Soil Pollution*, 209(1-4):157–172, 2010.
- [10] J.P. Chanton, C.M. Rutkowski, and B. Mosher. Quantifying methane oxidation from landfills using stable isotope analysis of downwind plumes. *Environmental science & technology*, 33(21):3755–3760, 1999.
- [11] D.D. Coleman, J.B. Risatti, and M. Schoell. Fractionation of carbon and hydrogen isotopes by methane-oxidizing bacteria. *Geochimica et Cosmochimica Acta*, 45(7):1033–1037, 1981.
- [12] T.A. Davidson. A simple and accurate method for calculating viscosity of gaseous mixtures. 1993.
- [13] A. De Visscher and O. Van Cleemput. Simulation model for gas diffusion and methane oxidation in landfill cover soils. *Waste Management*, 23(7):581–591, 2003.
- [14] A. De Visscher, I. De Pourcq, and J. Chanton. Isotope fractionation effects by diffusion and methane oxidation in landfill cover soils. *Journal of Geophysical Research: Atmospheres*, 109(D18), 2004.
- [15] J. Gebert and J. Streese-Kleeberg. Coupling stable isotope analysis with gas push-pull tests to derive in situ values for the fractionation factor α_{ox} associated with the microbial oxidation of methane in soils. *Soil Science Society of America Journal*, 81(5):1107–1114, 2017.
- [16] J. Gebert, C. Knoblauch, and A. Gröngröft. Impact of gas transport in soils on the fractionation of stable carbon isotopes. unpublished.
- [17] J. Gebert, A. Groengroeft, and E.M. Pfeiffer. Relevance of soil physical properties for the microbial oxidation of methane in landfill covers. *Soil Biology and Biochemistry*, 43(9):1759–1767, 2011.
- [18] J. Gebert, M. Huber-Humer, H. Oonk, and H. Scharff. Methane oxidation tool—an approach to estimate methane oxidation on landfills. 2011. URL <https://www.afvalzorg.nl/diensten-stortlocaties/stortgas/methaanoxidatie/>.

- [19] S. Gebhardt, H. Fleige, and R. Horn. Effect of compaction on pore functions of soils in a saalean moraine landscape in north germany. *Journal of Plant Nutrition and Soil Science*, 172(5):688–695, 2009.
- [20] C. Geck. Temporal and spatial variability of soil gas transport parameters, soil gas composition and gas fluxes in methane oxidation systems. 2017.
- [21] W. He, W. Lv, and J.H. Dickerson. Gas diffusion mechanisms and models. In *Gas Transport in Solid Oxide Fuel Cells*, pages 9–17. Springer, 2014.
- [22] M. Huber-Humer, J. Gebert, and H. Hilger. Biotic systems to mitigate landfill methane emissions. *Waste Management & Research*, 26(1):33–46, 2008.
- [23] IPCC. Climate change 2013: The physical science basis. working group 1 contribution to the fifth assessment report of the intergovernmental panel on climate change. 2013.
- [24] IPCC. Climate change 2014: Synthesis report. contribution of working groups 1, 2 and 3 to the fifth assessment report of the intergovernmental panel on climate change. 2014.
- [25] A.F. Ismail, K.C. Khulbe, and T. Matsuura. *Gas separation membranes*, volume 7. Springer, 2015.
- [26] S.B. Jones, D. Or, and G.E. Bingham. Gas diffusion measurement and modeling in coarse-textured porous media. *Vadose Zone Journal*, 2(4):602–610, 2003.
- [27] D. Kightley, D.B. Nedwell, and M. Cooper. Capacity for methane oxidation in landfill cover soils measured in laboratory-scale soil microcosms. *Applied and Environmental Microbiology*, 61(2):592–601, 1995.
- [28] M. Knox, P.D. Quay, and D. Wilbur. Kinetic isotopic fractionation during air-water gas transfer of o₂, n₂, ch₄, and h₂. *Journal of Geophysical Research: Oceans*, 97(C12):20335–20343, 1992.
- [29] A. Kühne, H. Schack-Kirchner, and E.E. Hildebrand. Gas diffusivity in soils compared to ideal isotropic porous media. *Journal of Plant Nutrition and Soil Science*, 175(1):34–45, 2012.
- [30] T.R. Marrero and E.A. Mason. Gaseous diffusion coefficients. *Journal of Physical and Chemical Reference Data*, 1(1):3–118, 1972.
- [31] R.J. Millington and J.P. Quirk. Permeability of porous solids. *Transactions of the Faraday Society*, 57: 1200–1207, 1961.
- [32] P. Moldrup, T. Olsen, T. Komatsu, and R.E. Schjønning. Tortuosity, diffusivity, and permeability in the soil liquid and gaseous phases. *Soil Science Society of America Journal*, 65:613–623.
- [33] P. Moldrup, T. Olesen, J. Gamst, P. Schjønning, T. Yamaguchi, and D.E. Rolston. Predicting the gas diffusion coefficient in repacked soil water-induced linear reduction model. *Soil Science Society of America Journal*, 64(5):1588–1594, 2000.
- [34] P. Moldrup, T. Olesen, P. Schjønning, T. Yamaguchi, and D.E. Rolston. Predicting the gas diffusion coefficient in undisturbed soil from soil water characteristics. *Soil Science Society of America Journal*, 64(1): 94–100, 2000.
- [35] R.I. Papendick and J.R. Runkles. Transient-state oxygen diffusion in soil: I. the case where rate of oxygen consumption is constant. *Soil Science*, 100:251–261, 1965.
- [36] S. Park, C.H. Lee, C.R. Ryu, and K. Sung. Biofiltration for reducing methane emissions from modern sanitary landfills at the low methane generation stage. *Water, air, and soil pollution*, 196(1-4):19–27, 2009.
- [37] M. Pawłowska and W. Stępniewski. An influence of methane concentration on the methanotrophic activity of a model landfill cover. *Ecological Engineering*, 26(4):392–395, 2006.
- [38] Plant and Soil Sciences eLibrary. Manual hyprop, 2015. http://ums-muc.de/static/Manual_HYPROP.pdf.

- [39] Plant and Soil Sciences eLibrary. Irrigation management, 2018. <http://croptechnology.unl.edu/pages/informationmodule.php?idinformationmodule=1130447123&topicorder=3&maxto=13&mineto=1>.
- [40] B.R. Scanlon, J.P. Nicot, and J.W. Massmann. Soil gas movement in unsaturated systems. *Soil physics companion*, 389:297–341, 2002.
- [41] C. Scheutz and P. Kjeldsen. Environmental factors influencing attenuation of methane and hydrochlorofluorocarbons in landfill cover soils. *Journal of Environmental Quality*, 33(1):72–79, 2004.
- [42] S.A. Socolofsky and G.H. Jirka. Special topics in mixing and transport processes in the environment. *Engineering–Lectures. 5th Edition. Texas A&M University*, pages 1–93, 2005.
- [43] V.B. Stein and J.P.A. Hettiaratchi. Methane oxidation in three alberta soils: influence of soil parameters and methane flux rates. *Environmental technology*, 22(1):101–111, 2001.
- [44] D.C. Thorstenson and D.W. Pollock. Gas transport in unsaturated porous media: The adequacy of fick’s law. *Reviews of Geophysics*, 27(1):61–78, 1989.
- [45] D.C. Thorstenson and D.W. Pollock. Gas transport in unsaturated zones: Multicomponent systems and the adequacy of fick’s laws. *Water Resources Research*, 25(3):477–507, 1989.
- [46] Engineering Toolbox. Air - composition and molecular weight [online], 2003. URL https://www.engineeringtoolbox.com/air-composition-d_212.html.
- [47] Engineering Toolbox. Methane - thermophysical properties [online], 2008. URL https://www.engineeringtoolbox.com/methane-d_1420.html.
- [48] Engineering Toolbox. Diffusion coefficients of gasses in water [online], 2008. URL https://www.engineeringtoolbox.com/diffusion-coefficients-d_1404.html.
- [49] Engineering Toolbox. Air - diffusion coefficients of gasses in excess of air [online], 2018. URL https://www.engineeringtoolbox.com/air-diffusion-coefficient-gas-mixture-temperature-d_2010.html.
- [50] F.R. Troeh, J.D. Jabro, and D. Kirkham. Gaseous diffusion equations for porous materials. *Geoderma*, 27(3):239–253, 1982.
- [51] M.T. Van Genuchten. A closed-form equation for predicting the hydraulic conductivity of unsaturated soils 1. *Soil science society of America journal*, 44(5):892–898, 1980.
- [52] C.J.W. van Verseveld. Gas flow through methane oxidation systems. Master thesis, University of Technology Delft, 2018.
- [53] A. Verruijt. *Soil Mechanics*. 2001.
- [54] O.Y. Yu. Real-time monitoring of landfill gas using remote monitoring technology [online]. URL <http://ok.tec.appstate.edu/landfill/>.



Derivation of Graham's law

In this appendix the kinetic energy is first proven to be solely dependent on temperature. This is then used to provide the derivation of Graham's law.

To find an expression in which the temperature is dependent on the mass of the particles the ideal gas law is used.

$$PV = nRT \quad (\text{A.1})$$

The pressure and volume of a gas relates to the kinetic energy of the particles through the formula given below, taken from kinetic theory.

$$PV = \frac{2}{3}N \left[\frac{1}{2}mv^2 \right] \quad (\text{A.2})$$

Combining A.1 and A.2 for the temperature gives A.3.

$$T = \frac{2}{3} \frac{N}{nR} \left[\frac{1}{2}mv^2 \right] = \frac{2}{3} \frac{1}{k} \left[\frac{1}{2}mv^2 \right] \quad (\text{A.3})$$

Rewriting A.3 for velocity gives A.4.

$$v^2 = 3kT \frac{1}{m} \quad (\text{A.4})$$

When A.4 is combined with A.5, the equation for kinetic energy, the relation between kinetic energy and temperature is obtained, given in A.6. As can be seen the kinetic energy is solely dependent on the temperature and therefore it can be concluded that in a gas mixture the kinetic energy of each particle is the same. This conclusion is used to derive Graham's law.

$$E = \frac{1}{2}mv^2 \quad (\text{A.5})$$

$$E = \frac{3}{2}kT \quad (\text{A.6})$$

Taking that the kinetic energy is the same for all particles in a gas mixture at uniform temperature the statement in A.7 is valid.

$$\frac{1}{2}m_1v_1^2 = \frac{1}{2}m_2v_2^2 \quad (\text{A.7})$$

Which results in the condition given in A.8.

$$\frac{v_1^2}{v_2^2} = \frac{m_2}{m_1} \quad (\text{A.8a})$$

$$\frac{v_1}{v_2} = \sqrt{\frac{m_2}{m_1}} \quad (\text{A.8b})$$

B

Derivation of equation 3.3

In this appendix the derivation of the formula which was used to determine the effective diffusion coefficients of the soil samples is provided. First the ideal gas law is used to determine the amount of moles methane in the gas chamber. This is done by rearranging the formula, as given below. In this formula the x is the fraction of methane the sensors measure.

$$n_m = \frac{PVx}{RT} \quad (\text{B.1})$$

Then, Fick's law is rewritten into components of the units of the parameters. As can be seen, the dx is replaced by $x - x_{atm}$, as this is the difference in concentration over the soil sample.

$$\frac{n_m * dx}{dt} = -D_{eff} * \frac{A}{L} * \frac{Pdx}{RT} \quad (\text{B.2})$$

$$\frac{PV}{RT} * \frac{dx}{dt} = -D_{eff} \frac{PA}{RTL} (x - x_{atm}) \quad (\text{B.3})$$

$$\frac{dx}{dt} = -D_{eff} \frac{A}{LV} (x - x_{atm}) \quad (\text{B.4})$$

This formula rewritten, with all the x at the left side, and then including the integrals gives the following equation.

$$\int_0^x \frac{1}{x - x_{atm}} dx = -D_{eff} \frac{A}{VL} \int_0^t dt \quad (\text{B.5})$$

When this integral is solved it gives the formula below.

$$\ln\left(\frac{x - x_{atm}}{x_{atm}}\right) + C = -D_{eff} \frac{A}{VL} t \quad (\text{B.6})$$

Solving for $t = 0$, gives the values of C.

$$C = -\ln\left(\frac{x_{t=0} - x_{atm}}{x_{atm}}\right) \quad (\text{B.7})$$

Which, if included in the formula, gives the formula below.

$$\ln\left(\frac{x - x_{atm}}{x_{atm}} \frac{x_{atm}}{x_{t=0} - x_{atm}}\right) = -D_{eff} \frac{A}{VL} t \quad (\text{B.8})$$

Rewriting this formula gives the equation used to determine the best fit for effective diffusivity, D_{eff} . This equation is given in B.9.

$$x = (x_{t=0} - x_{atm}) * e^{(-D_{eff} \frac{A}{VL} t)} + x_{atm} \quad (\text{B.9})$$

C

Saturation and densities of used soils

In this appendix the targeted degrees of compaction and levels of saturation are given in table C.1. In table C.2 and table C.3 the actual values which are created during preparation of the soils and on which the tests are performed.

Table C.1: Targeted densities and levels of saturation for the parallels, the saturation levels are given as percentage of the total volume

Density (% of Proctor Density)	Saturation for soil HH (%V)	Saturation for Soil WIE (%V)
75	12.35	20.47
80	12.35	20.47
85	12.35	20.47
90	12.35	20.47
95	12.35	20.47
85	25.49	31.24
85	18.58	25.53
85	8.59	16.74
85	5.18	12.49

Table C.2: Actual densities and saturation levels

Sample	Density ($\%D_{pr}$)	Saturation ($\%V$)	Air content ($\%V$)
HH 75% parallel 1	72.48	13.57	34.46
HH 75% parallel 2	74.41	13.93	32.72
HH 75% parallel 3	73.46	13.75	33.58
HH 80% parallel 1	80.78	12.70	29.38
HH 80% parallel 2	82.13	12.91	28.20
HH 80% parallel 3	81.23	12.77	28.99
HH 85% parallel 1	87.70	13.30	23.82
HH 85% parallel 2	87.96	13.34	23.59
HH 85% parallel 3	87.31	13.24	24.16
HH 90% parallel 1	90.77	13.73	21.19
HH 90% parallel 2	90.98	13.76	21.01
HH 90% parallel 3	90.13	13.63	21.75
HH 95% parallel 1	95.23	12.99	18.72
HH 95% parallel 2	94.77	12.93	19.12
HH 95% parallel 3	95.70	13.06	18.33
WIE 75% parallel 1	71.63	22.24	30.19
WIE 75% parallel 2	74.18	23.03	27.70
WIE 75% parallel 3	73.94	22.95	27.94
WIE 80% parallel 1	77.20	22.87	25.86
WIE 80% parallel 2	80.64	23.88	22.56
WIE 80% parallel 3	79.38	23.51	23.77
WIE 85% parallel 1	85.00	24.88	18.67
WIE 85% parallel 2	84.74	24.80	18.91
WIE 85% parallel 3	84.86	24.84	18.81
WIE 90% parallel 1	89.57	24.44	16.07
WIE 90% parallel 2	88.21	24.07	17.34
WIE 90% parallel 3	87.70	23.94	17.82
WIE 95% parallel 1	93.35	24.14	13.87
WIE 95% parallel 2	92.40	23.89	14.74
WIE 95% parallel 3	97.29	25.16	10.23

Table C.3: Actual densities and saturation levels

Sample	Density (%D_{pr})	Saturation (%V)	Air content (%V)
HH 25.49% parallel 1	84.19	29.22	10.42
HH 25.49% parallel 2	85.04	29.51	9.52
HH 25.49% parallel 3	84.63	29.37	9.95
HH 18.58% parallel 1	85.05	20.47	18.55
HH 18.58% parallel 2	85.36	20.54	18.26
HH 18.58% parallel 3	86.68	20.54	16.99
HH 12.35% parallel 1	87.70	13.30	23.82
HH 12.35% parallel 2	87.96	13.34	23.59
HH 12.35% parallel 3	87.31	13.24	24.16
HH 8.59% parallel 1	85.49	9.09	29.62
HH 8.59% parallel 2	86.04	9.15	29.17
HH 8.59% parallel 3	84.94	9.03	30.06
HH 5.18% parallel 1	83.22	5.68	34.66
HH 5.18% parallel 2	85.02	5.80	33.24
HH 5.18% parallel 3	86.25	5.89	32.27
WIE 31.24% parallel 1	82.17	36.85	8.58
WIE 31.24% parallel 2	84.68	37.98	5.78
WIE 31.24% parallel 3	83.35	37.38	7.26
WIE 25.53% parallel 1	83.63	31.56	12.89
WIE 25.53% parallel 2	82.52	31.15	14.05
WIE 25.53% parallel 3	81.88	30.90	14.71
WIE 20.47% parallel 1	85.00	24.88	18.67
WIE 20.47% parallel 2	84.74	24.80	18.91
WIE 20.47% parallel 3	84.86	24.84	18.81
WIE 16.74% parallel 1	86.14	19.70	23.09
WIE 16.74% parallel 2	88.04	20.13	21.39
WIE 16.74% parallel 3	83.09	19.00	25.81
WIE 12.49% parallel 1	85.62	14.11	29.02
WIE 12.49% parallel 2	85.89	14.16	28.80
WIE 12.49% parallel 3	86.46	14.25	28.33

D

Figures from literature

In this appendix the figures from literature which are referred to in the main text, and not included somewhere else, are given.

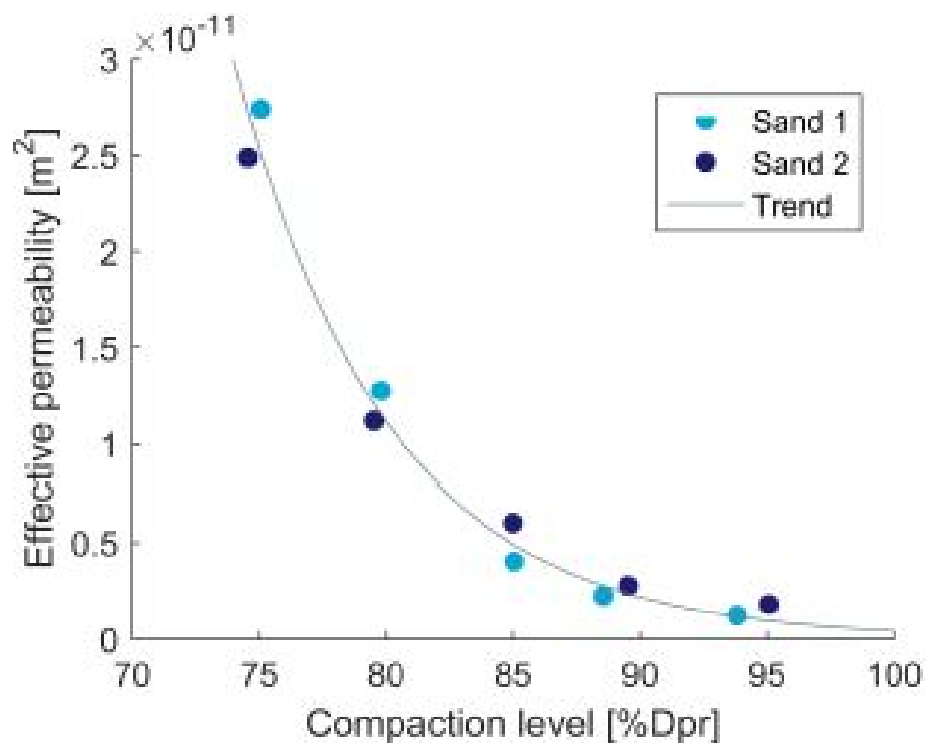


Figure D.1: Effective permeability plotted versus the compaction level [52]

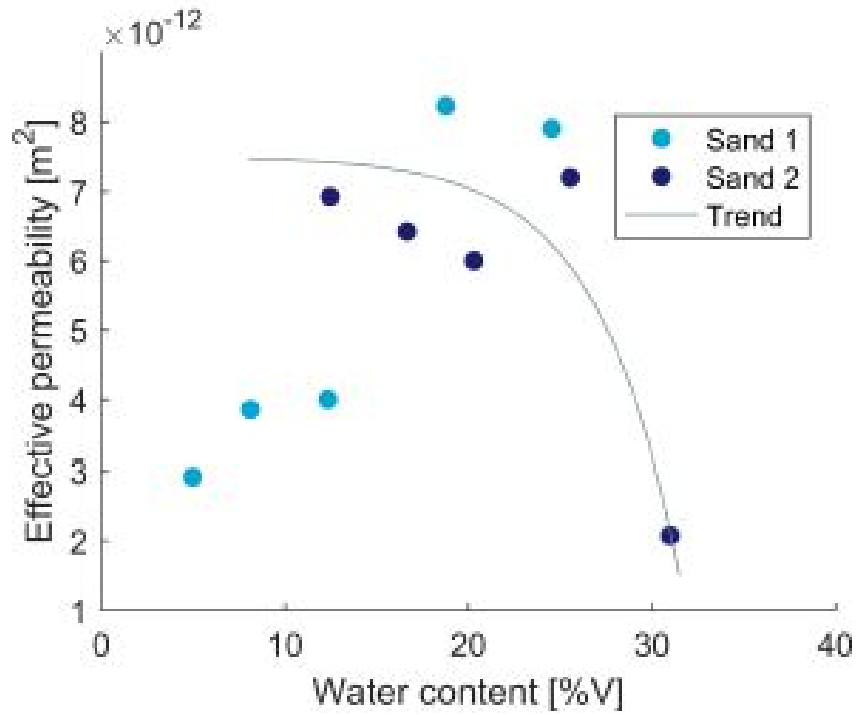


Figure D.2: Effective permeability plotted versus the saturation [52]

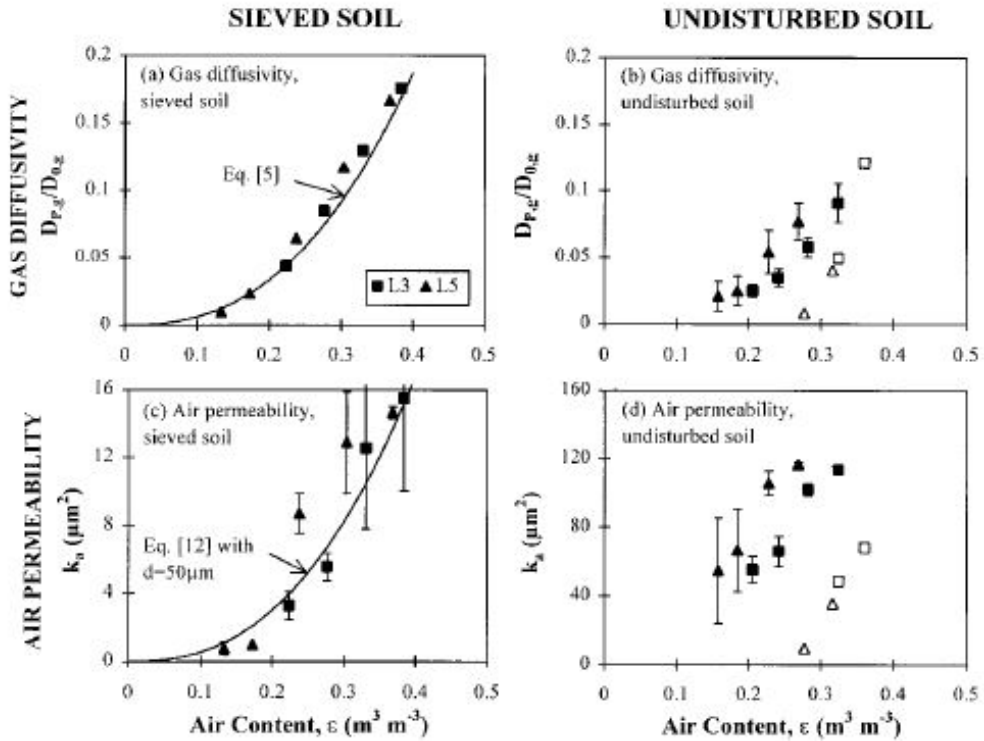


Figure D.3: Measured gas diffusivities and air permeabilities in L3 sandy clay loam and L5 sandy clay. (a), (c) Sieved, repacked soil. (b), (d) Undisturbed soil (closed symbols) and structurally disturbed soil (open symbols). [32]

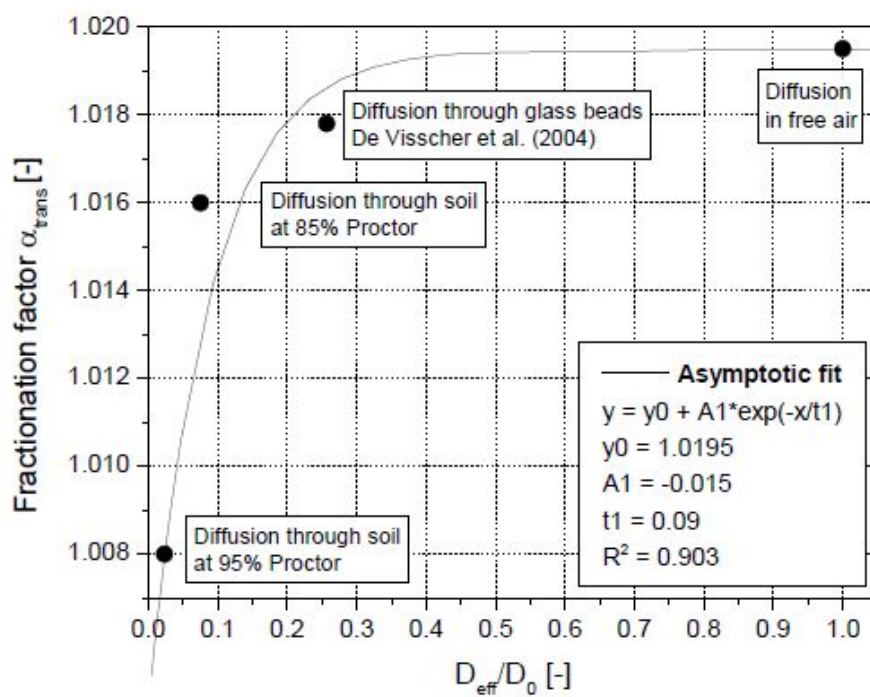


Figure D.4: Fractionation factor for transport plotted against the soil gas diffusivity [16]

E

Raw data

In this appendix the results of the leakage tests are shown first. Secondly, the experimental data from the performed tests is shown.

E.1. Leakage tests

Below in figures E.1 up to figure E.5 the results of the leakage tests are given. As can be seen the leakage is minimal.

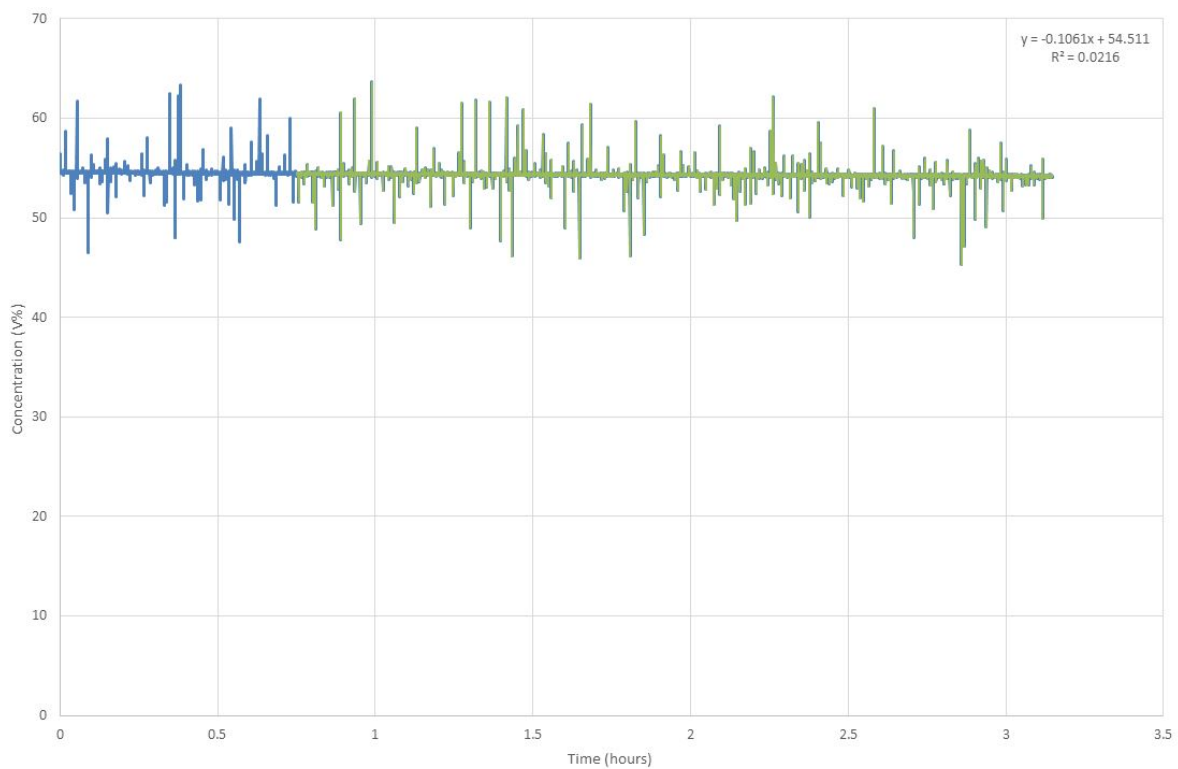


Figure E.1: Leakage test for set-up 1

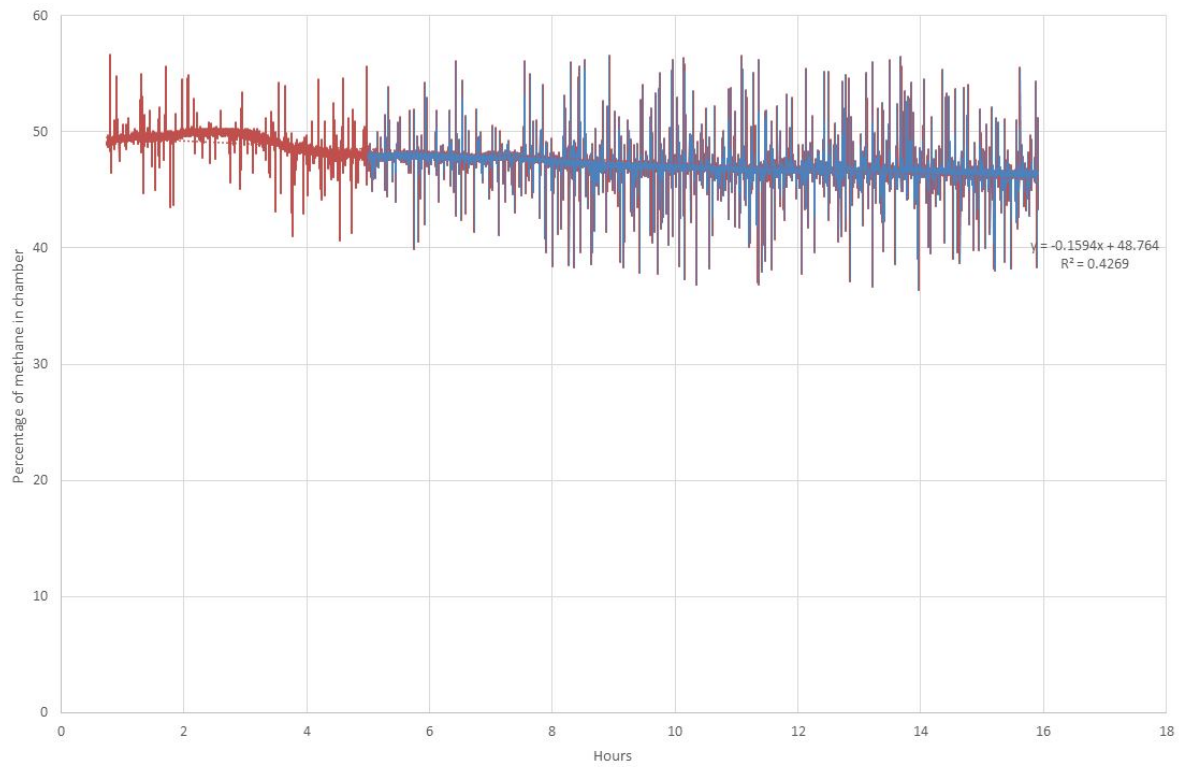


Figure E.2: Leakage test for set-up 2

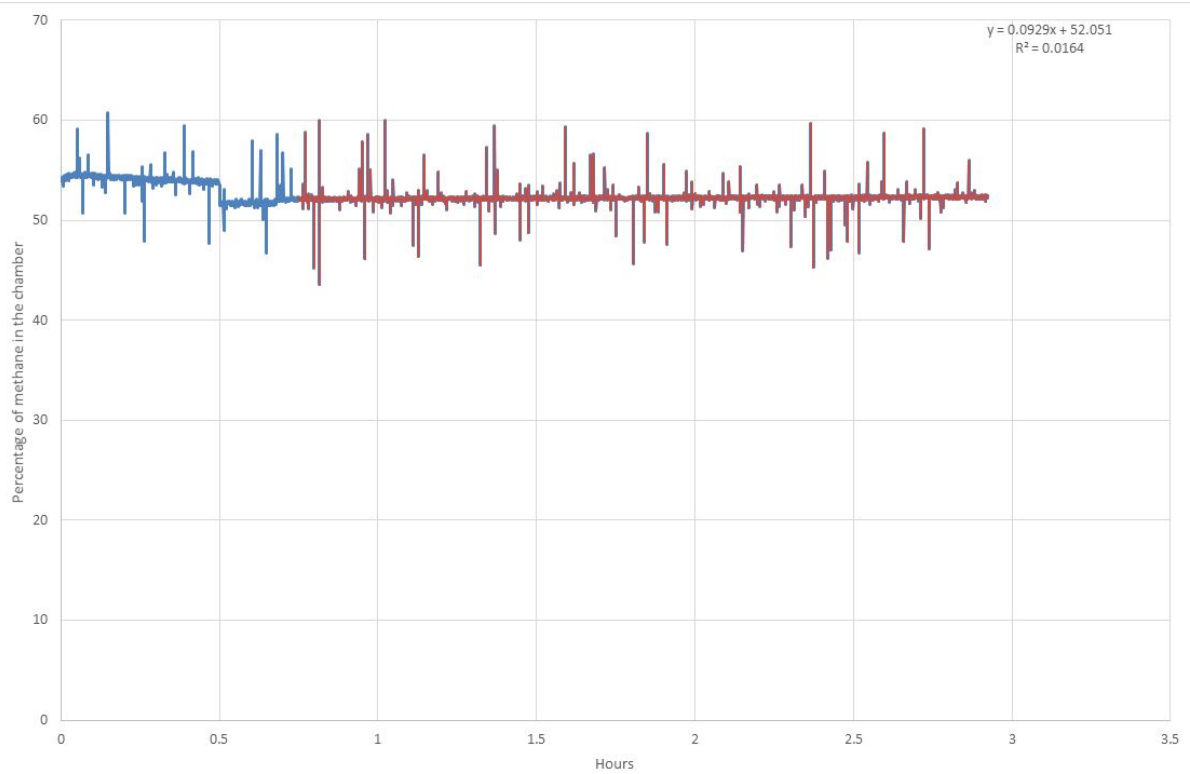


Figure E.3: Leakage test for set-up 3

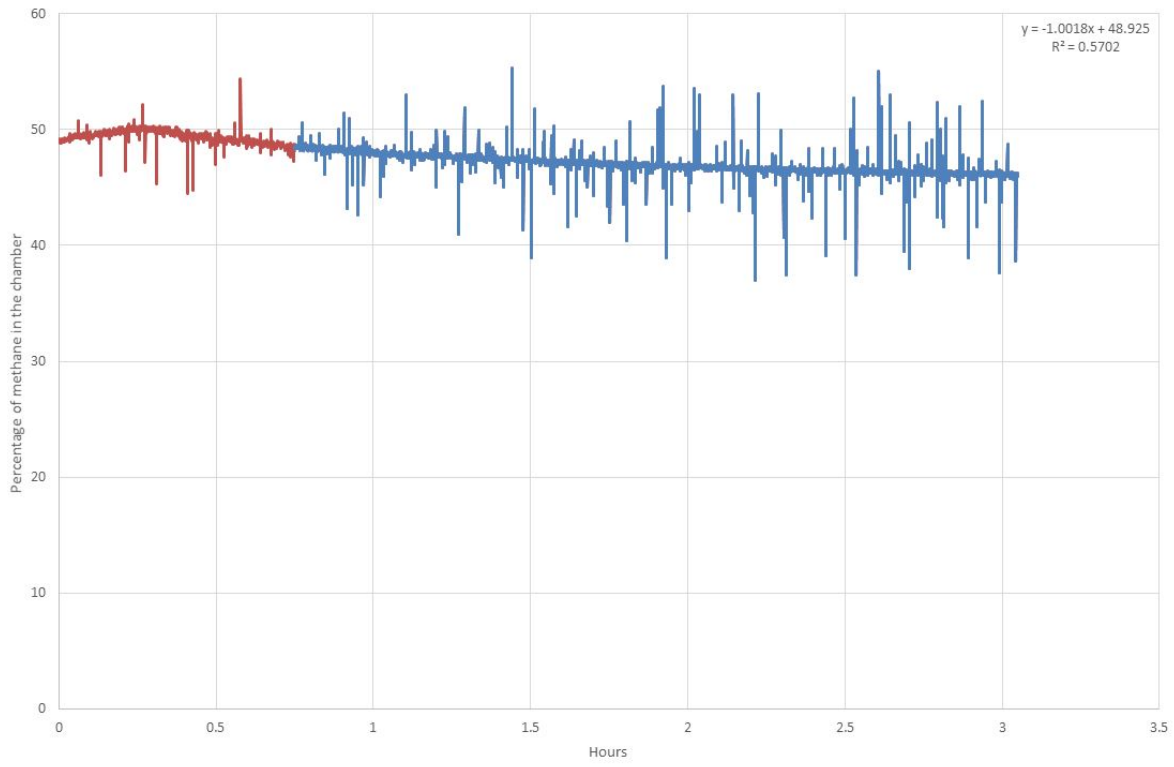


Figure E.4: Leakage test for set-up 4

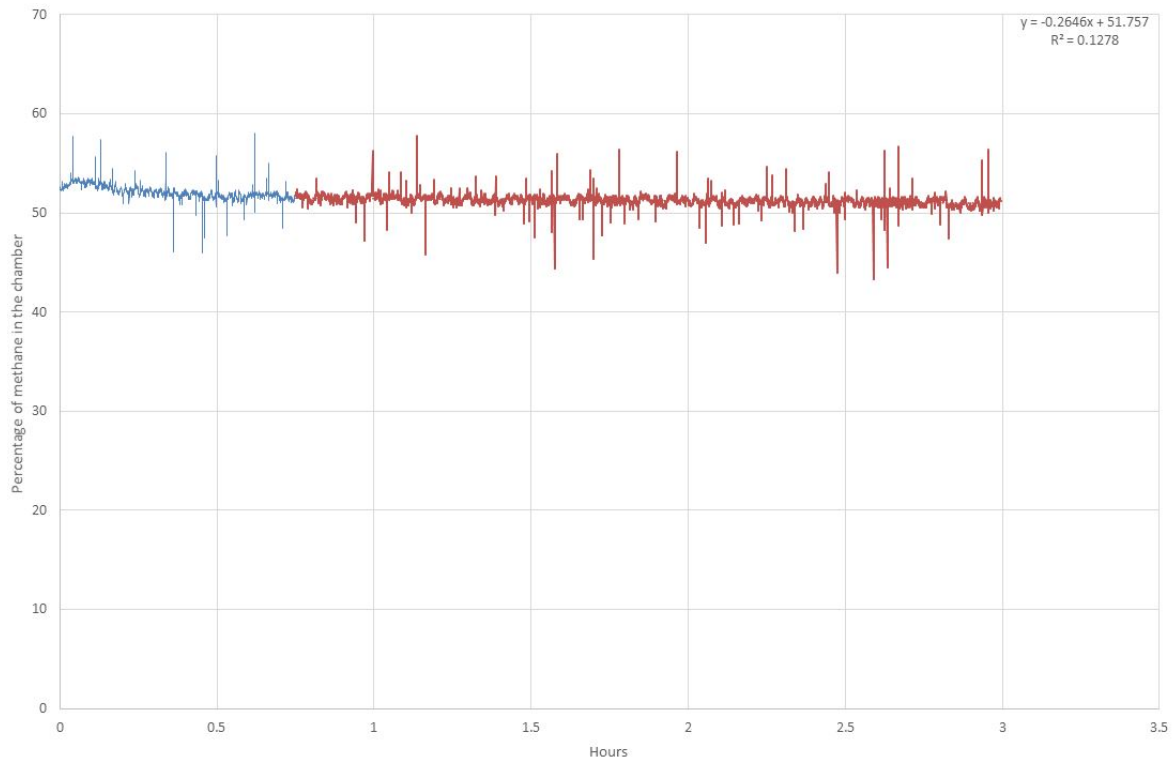


Figure E.5: Leakage test for set-up 5

E.2. Experimental data

In the rest of this appendix the measurements during all tests has been given. In each figure the results of the three runs of the three parallels for that specific targeted density and saturation are plotted. First the compaction series for soil HH is given, followed by the saturation series. After that the compaction and saturation series of soil WIE are given.

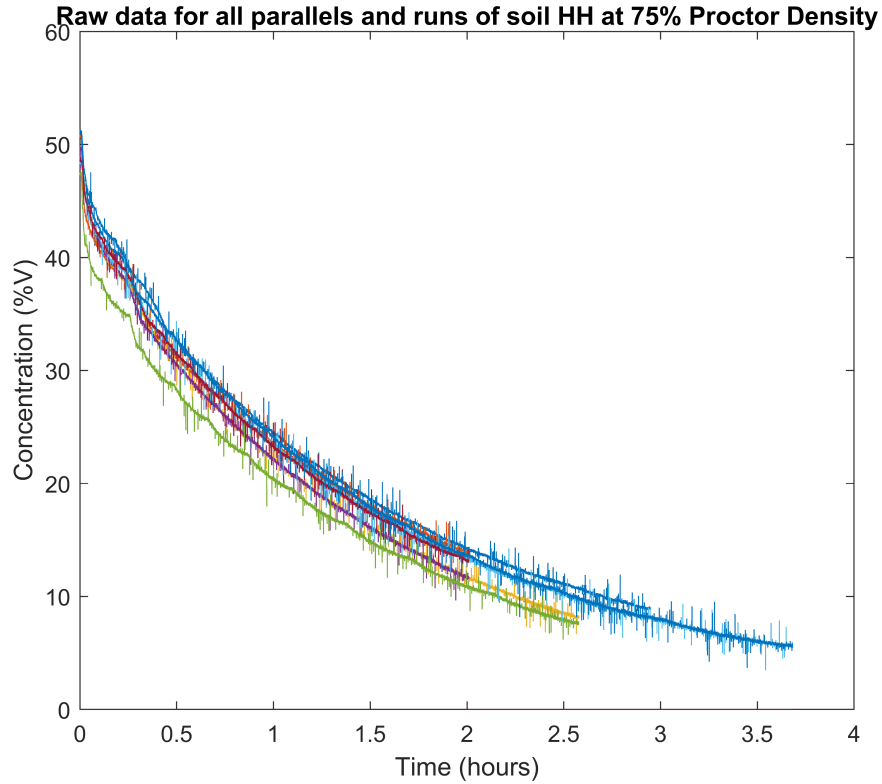


Figure E.6: Raw data for soil HH at 75% of the Proctor Density

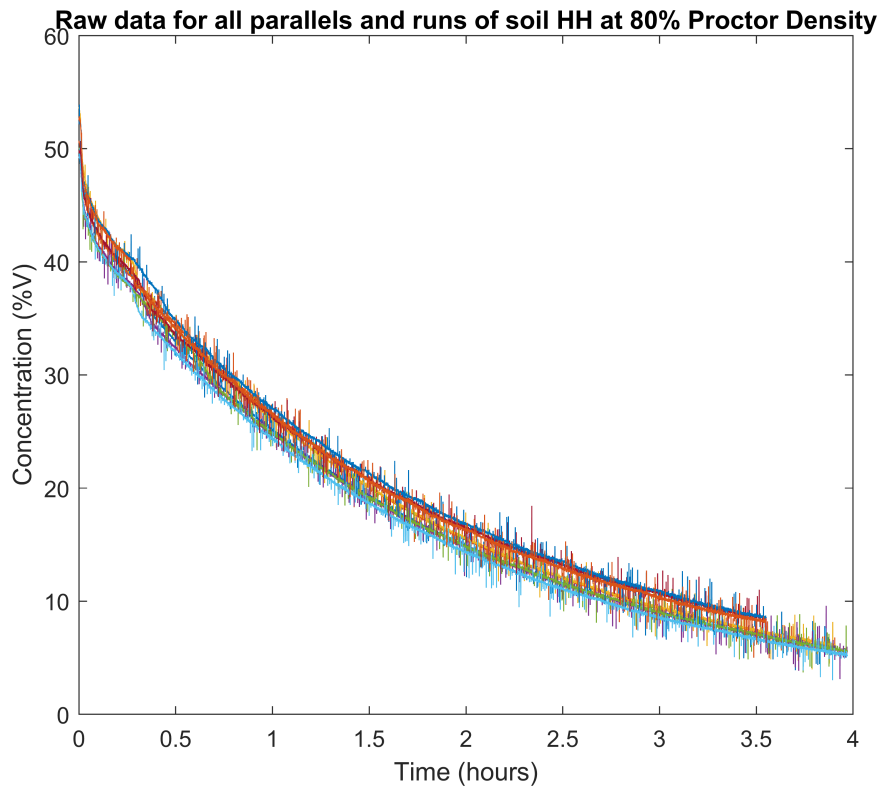


Figure E.7: Raw data for soil HH at 80% of the Proctor Density

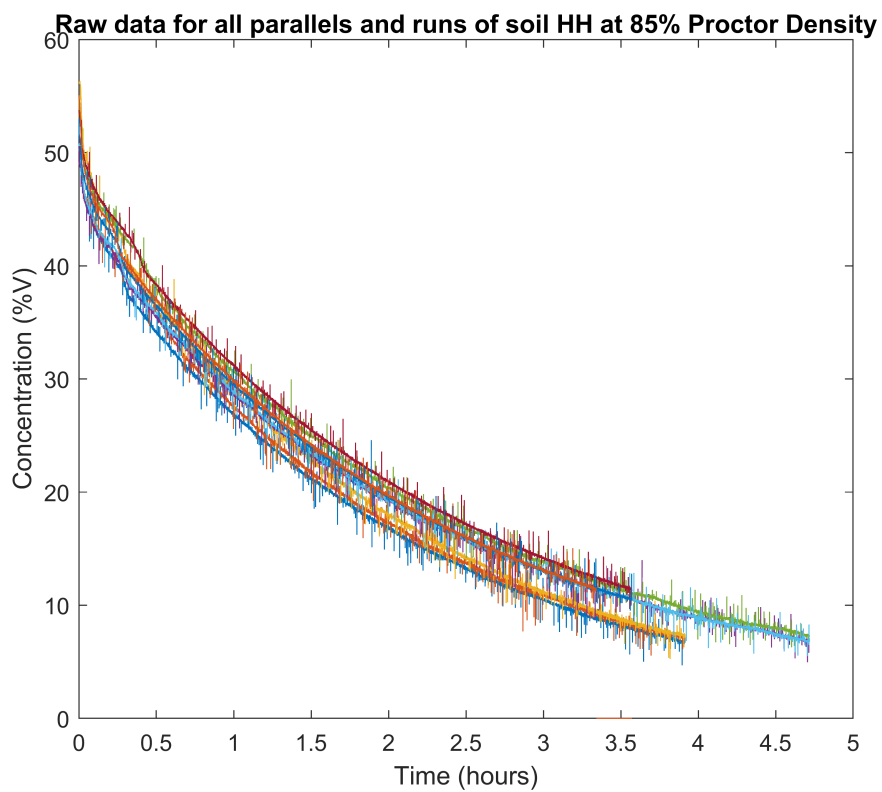


Figure E.8: Raw data for soil HH at 85% of the Proctor Density

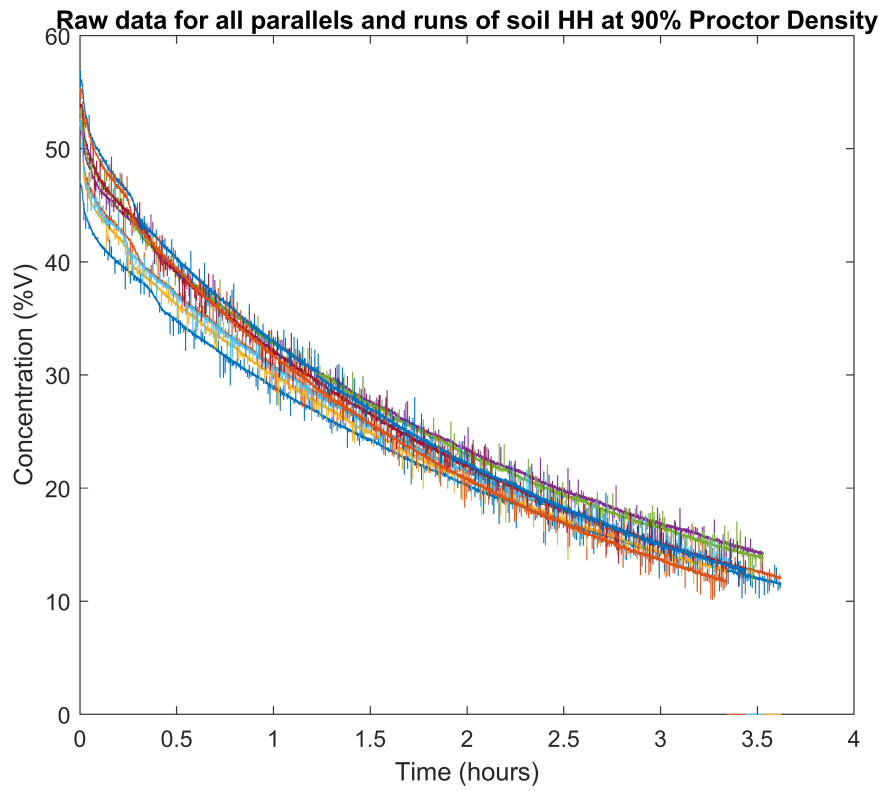


Figure E.9: Raw data for soil HH at 90% of the Proctor Density

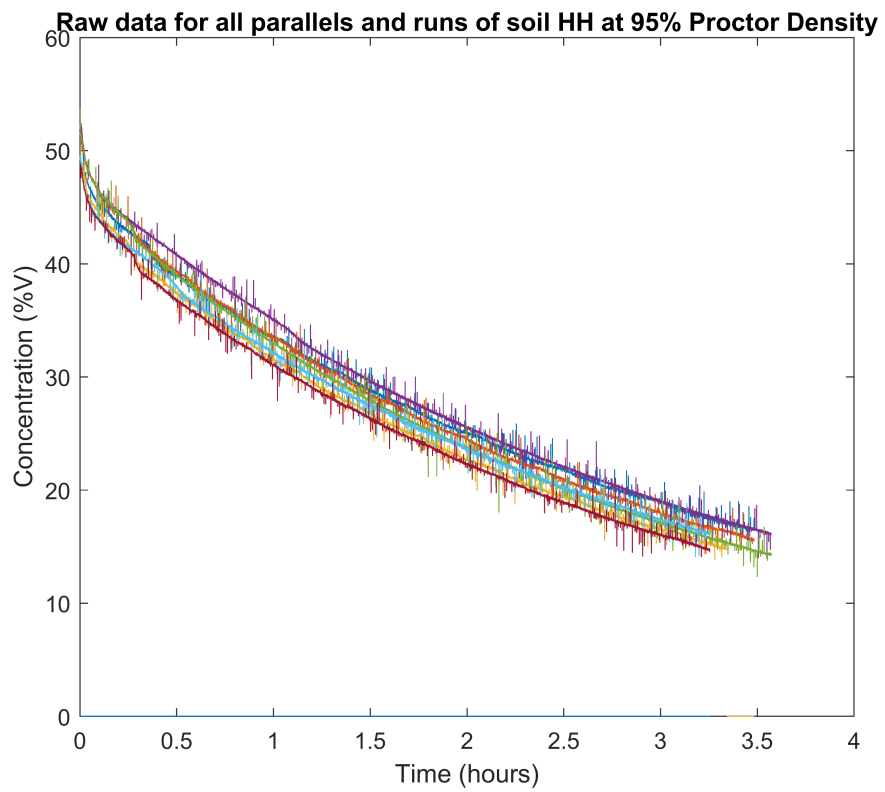


Figure E.10: Raw data for soil HH at 95% of the Proctor Density

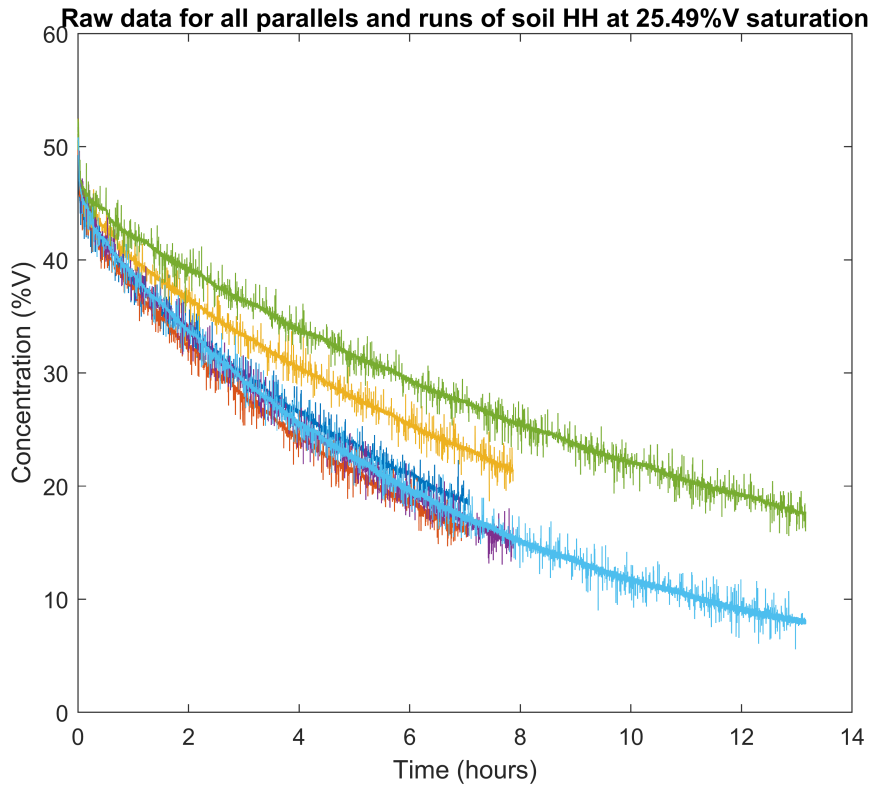


Figure E.11: Raw data for soil HH at 25.49%V saturation

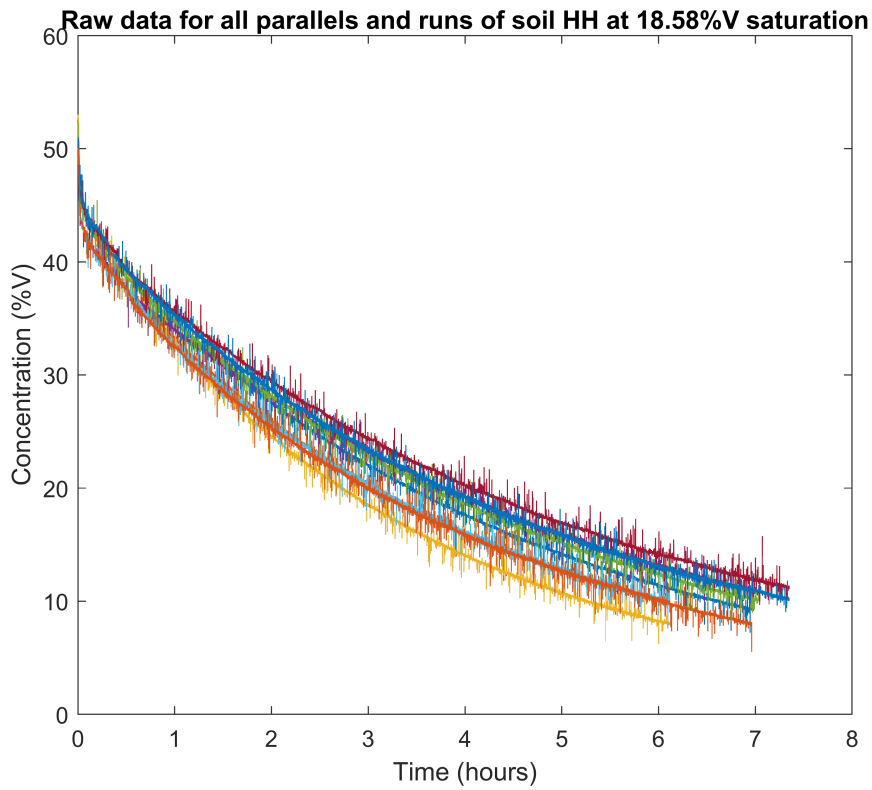


Figure E.12: Raw data for soil HH at 18.58%V saturation

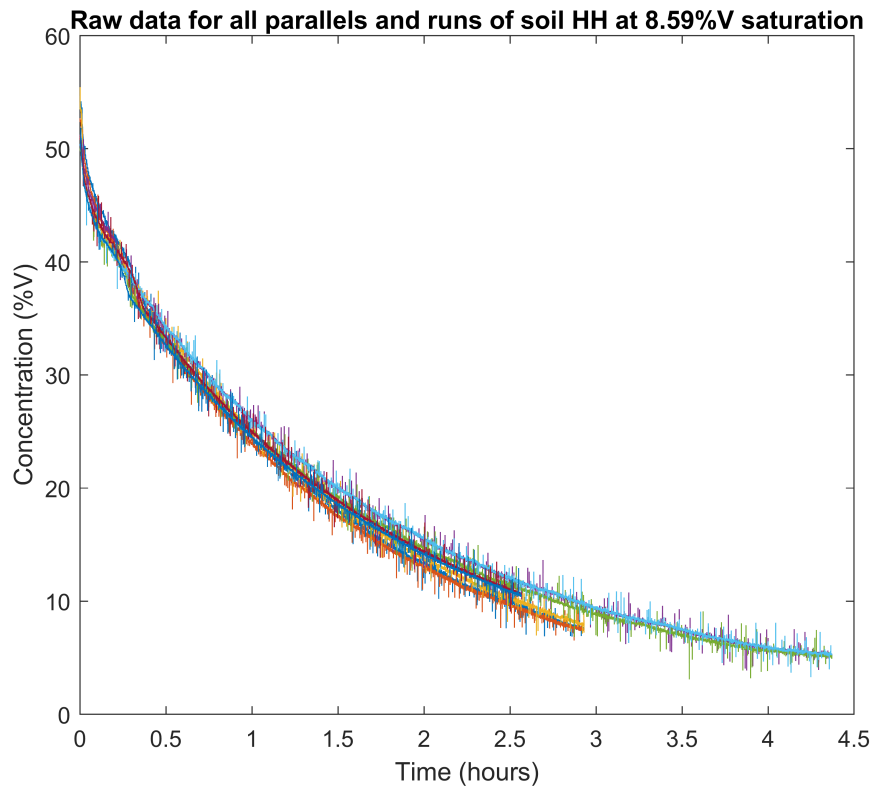


Figure E.13: Raw data for soil HH at 8.59%V saturation

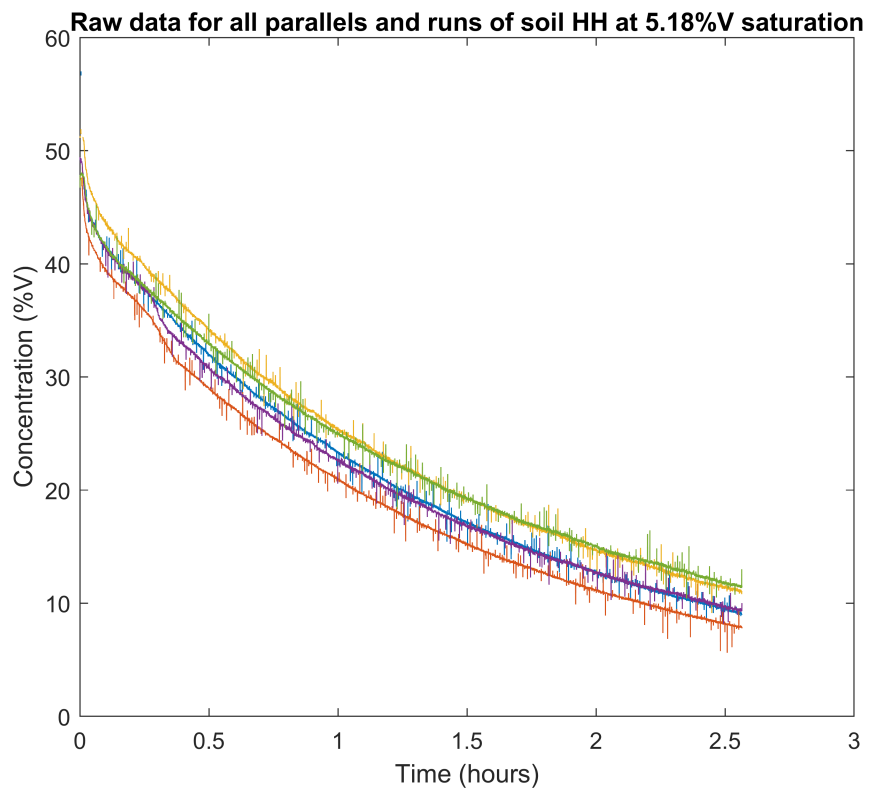


Figure E.14: Raw data for soil HH at 5.18%V saturation

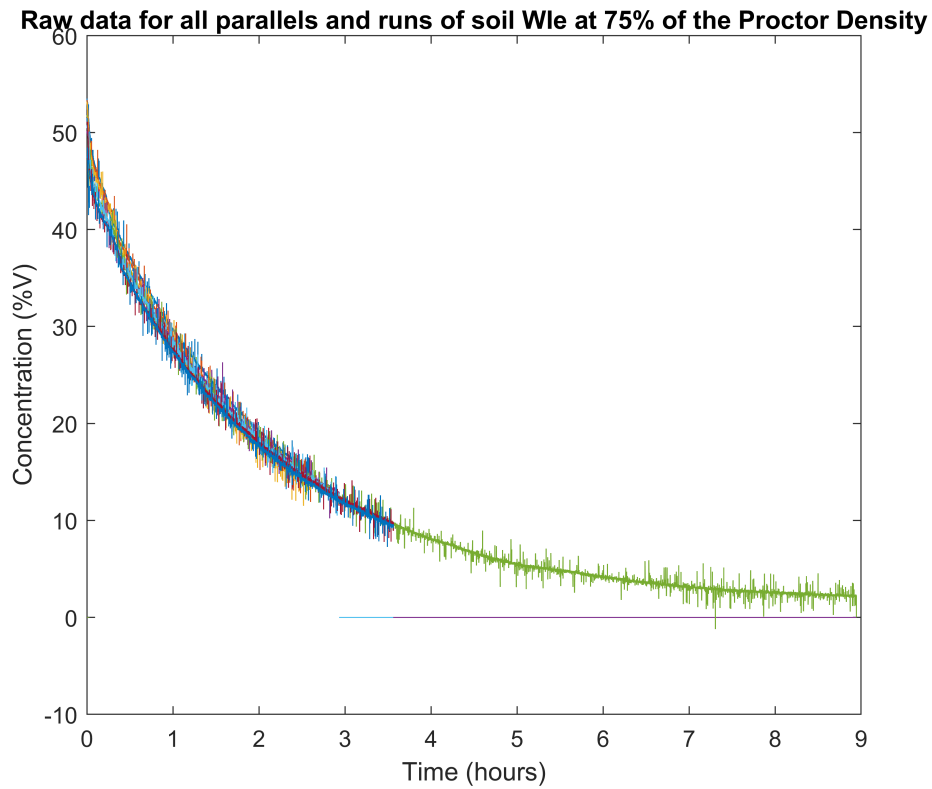


Figure E.15: Raw data for soil WIE at 75% of the Proctor Density

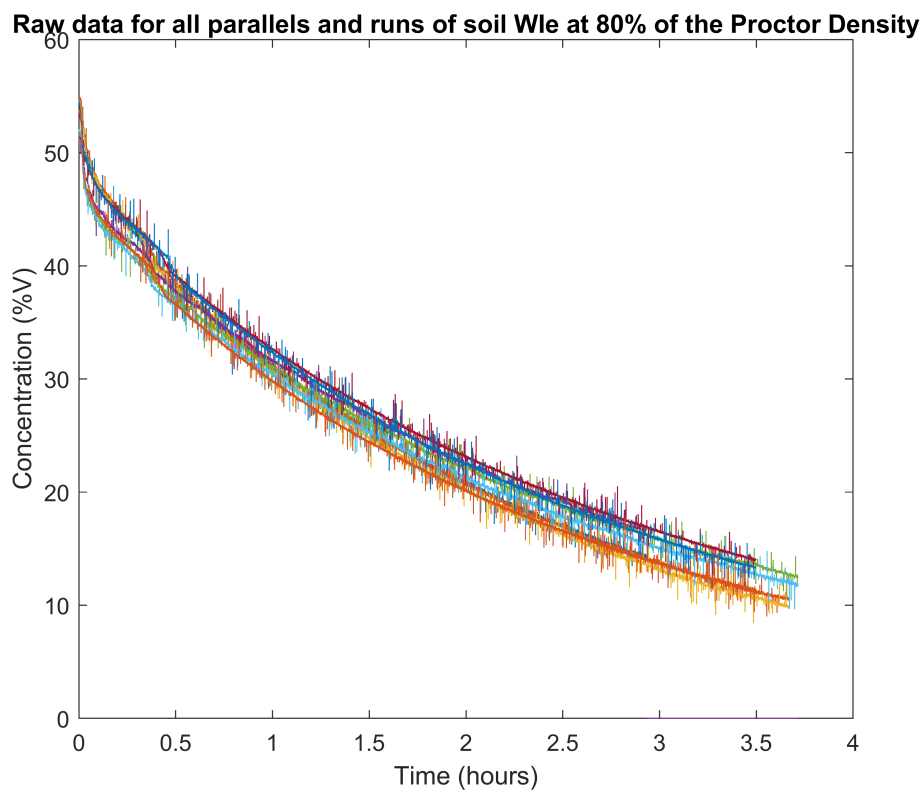


Figure E.16: Raw data for soil WIE at 80% of the Proctor Density

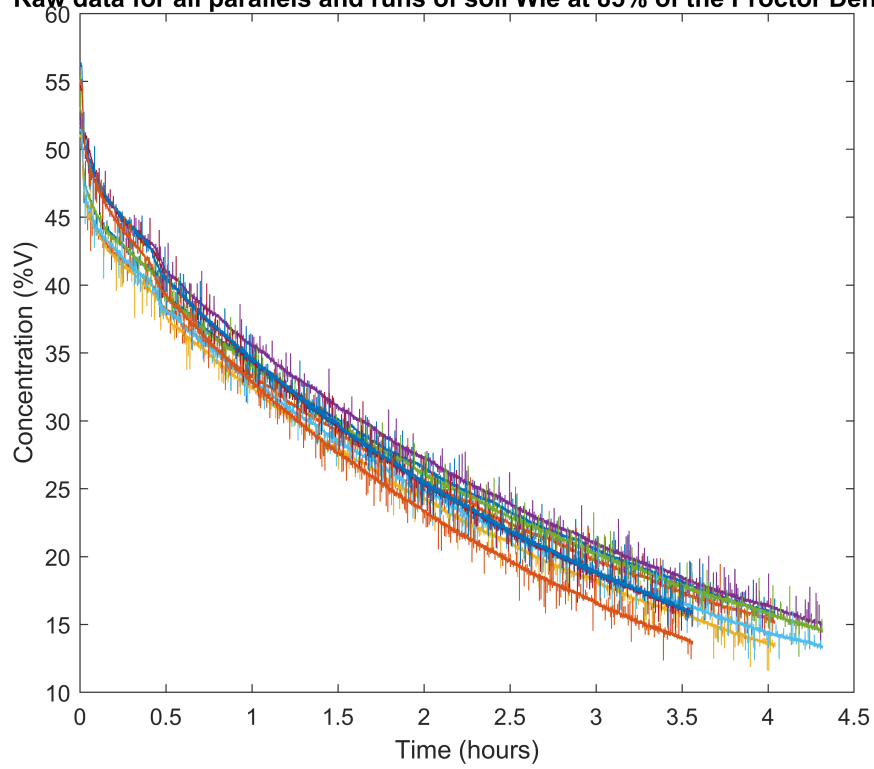
Raw data for all parallels and runs of soil WIE at 85% of the Proctor Density

Figure E.17: Raw data for soil WIE at 85% of the Proctor Density

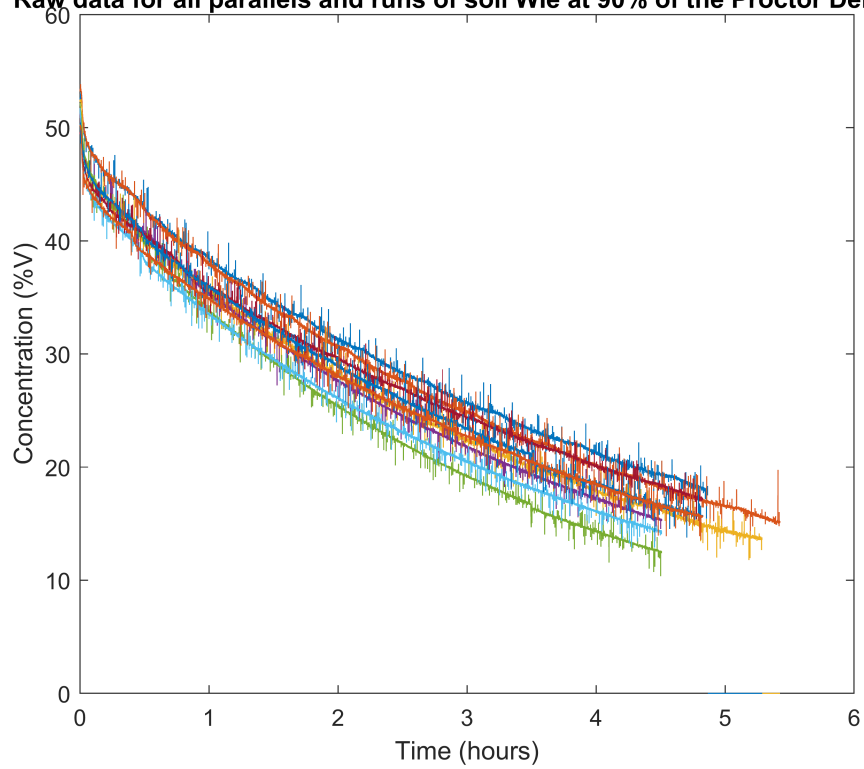
Raw data for all parallels and runs of soil WIE at 90% of the Proctor Density

Figure E.18: Raw data for soil WIE at 90% of the Proctor Density

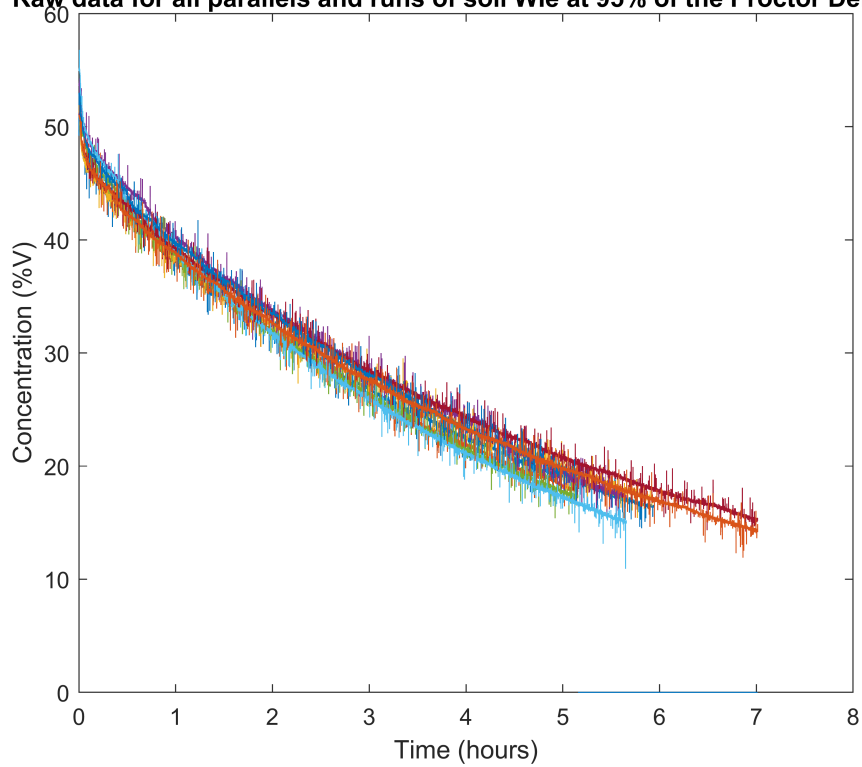
Raw data for all parallels and runs of soil WIE at 95% of the Proctor Density

Figure E.19: Raw data for soil WIE at 95% of the Proctor Density

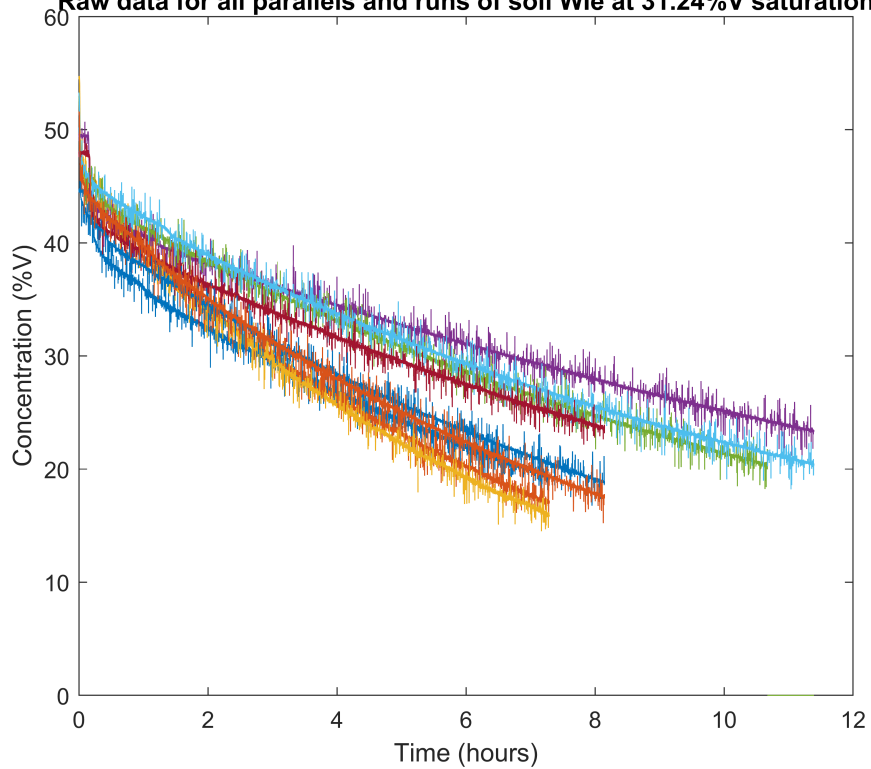
Raw data for all parallels and runs of soil WIE at 31.24%V saturation

Figure E.20: Raw data for soil WIE at 31.24%V saturation

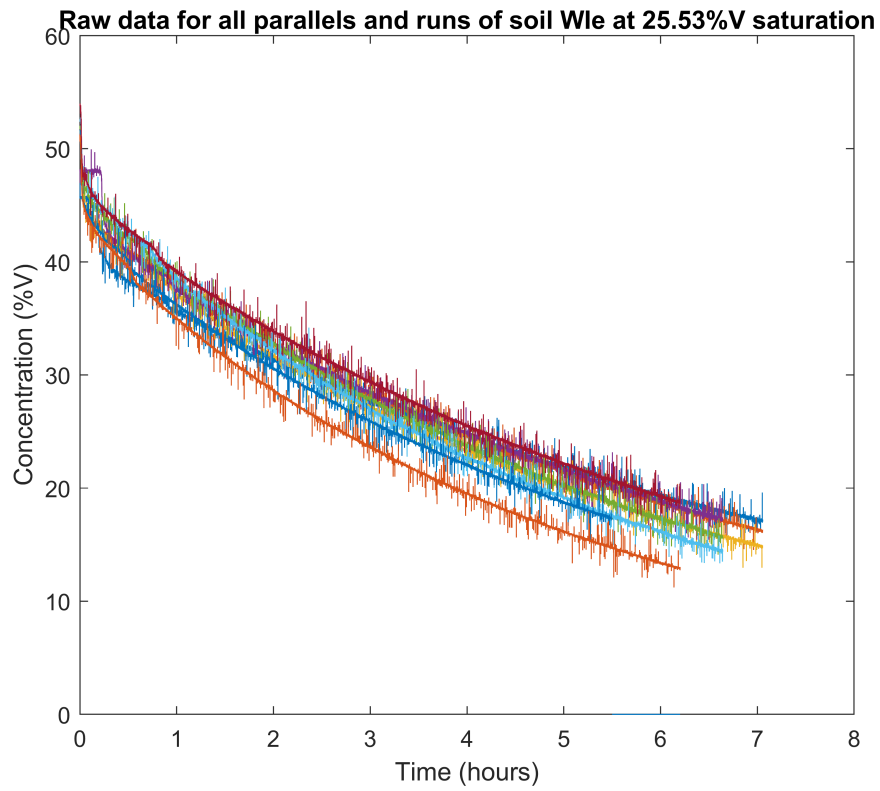


Figure E.21: Raw data for soil WIE at 25.53%V saturation

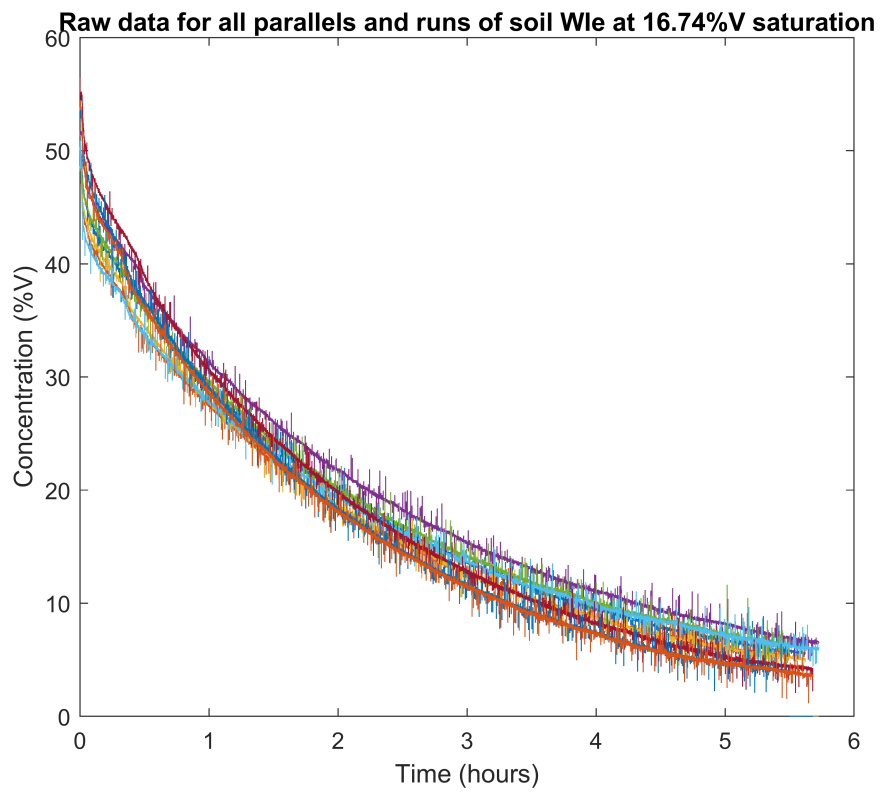


Figure E.22: Raw data for soil WIE at 16.74%V saturation

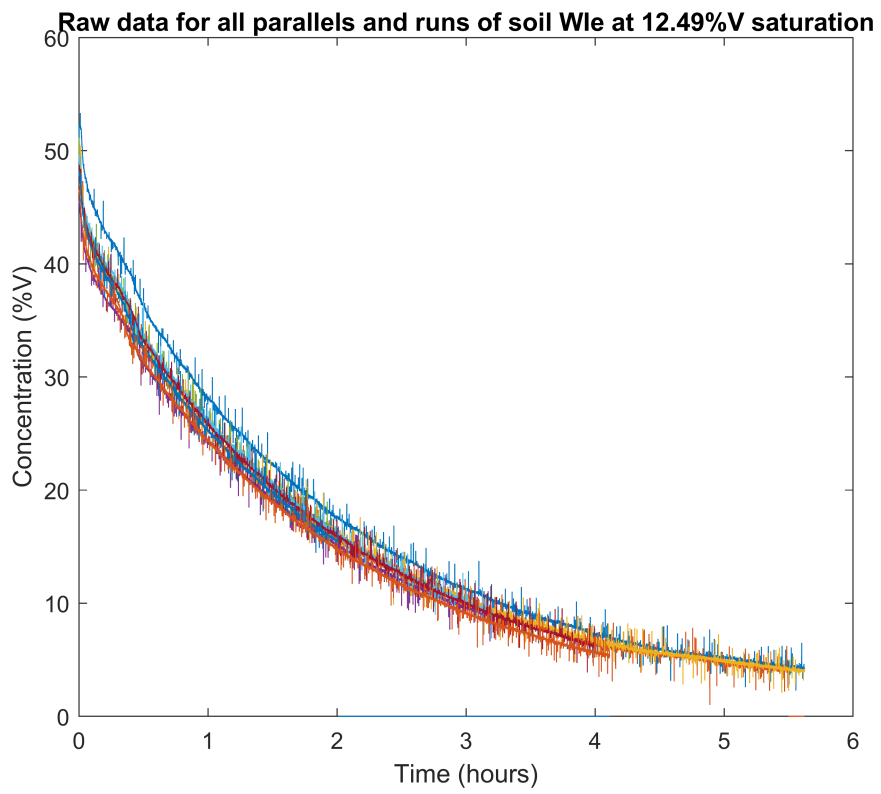


Figure E.23: Raw data for soil WIE at 12.49%V saturation

Determination of the fractionation factors

In this appendix the plots of $\delta^{13}C_t - \delta^{13}C_{t=0}$ versus the $\ln(M/M_0)$, from which the α_{trans} is determined, are given. These plots also contain a measure for the quality of the fit is given, this is the R^2 . The closer this value is to one, the better the linear trend fits the data. The slope of this line is used in equation 3.6 for the value of S .

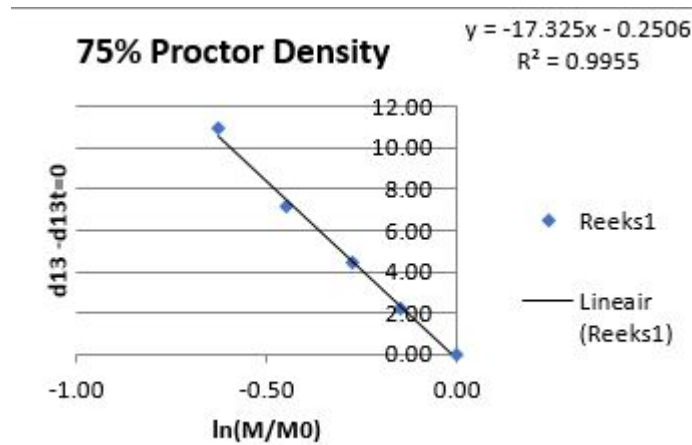


Figure E1: The fit of α_{trans} for the soil sample at 75% of the Proctor Density

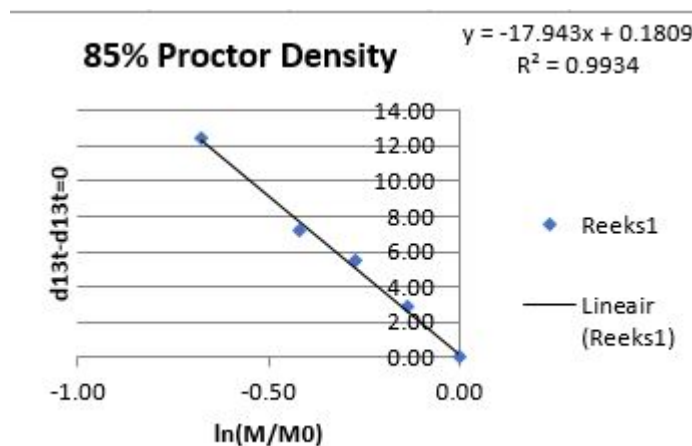
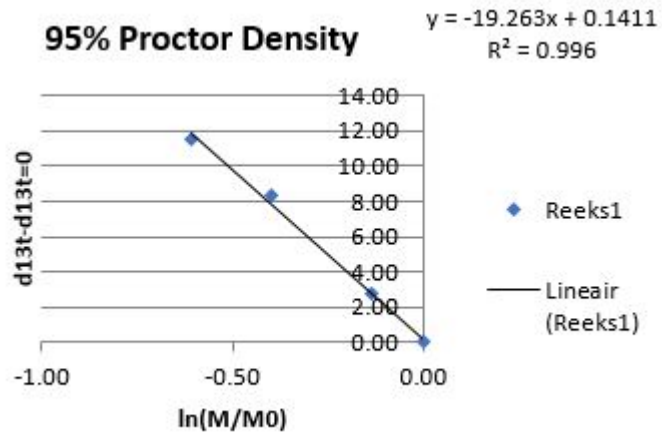
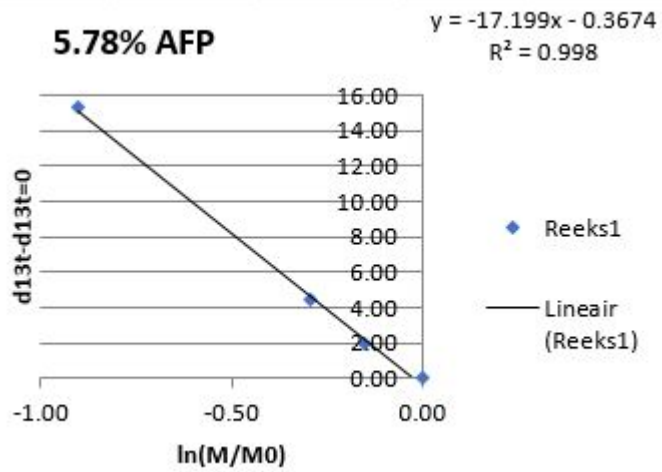
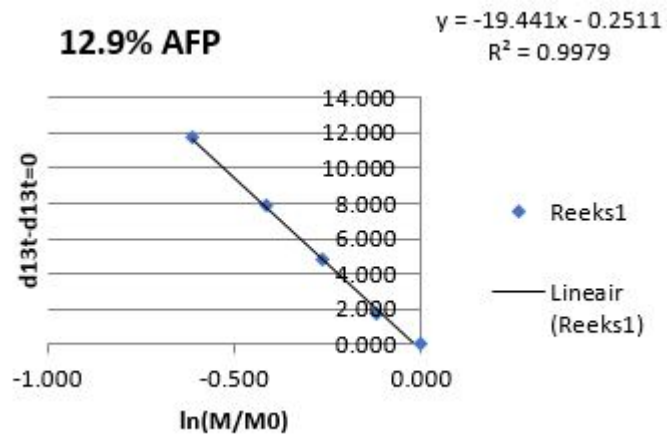


Figure E2: The fit of α_{trans} for the soil sample at 85% of the Proctor Density

Figure E3: The fit of α_{trans} for the soil sample at 95% of the Proctor DensityFigure E4: The fit of α_{trans} for the soil sample in the saturation series at 5.78% air-filled porosityFigure E5: The fit of α_{trans} for the soil sample in the saturation series at 12.9% air-filled porosity

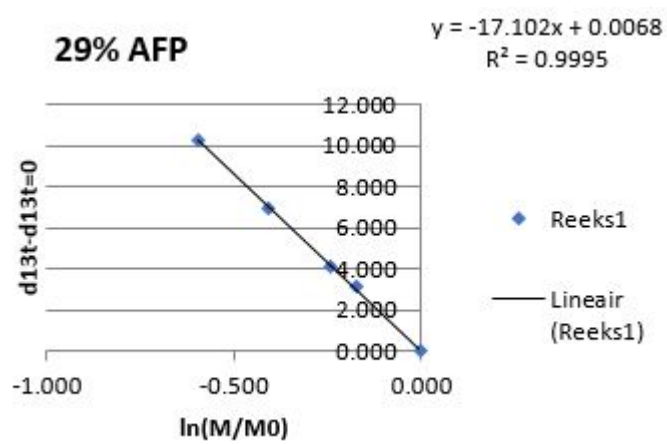


Figure E6: The fit of α_{trans} for the soil sample in the saturation series at 29.0% air-filled porosity

G

Statistical analyses

When assessing the statistical difference between the effective diffusion coefficients of the compaction and saturation series of both soils no difference was found. This is shown in Figures G.1 and G.2. However, in a t-test no statistical difference between the values of the effective diffusion coefficient for both soils was found; they both follow their own relation, as can be seen in Figure G.3. In Table G.1, the coefficients of determination are given. The relation with a value closest to 1 fits the data best, thus for both soils a linear relation is most suitable.

T-test: Deff for soil HH		
	<i>Variabele 1/ariabele 2</i>	
Mean	2.56E-06	2.07E-06
Variance	3.4E-13	1.41E-12
Observations	42	28
Hypothesized Mean Difference	0	
df	36	
t Stat	2.020143	
P(T<=t) one-tail	0.025429	
t Critical one-tail	1.688298	
P(T<=t) two-tail	0.050858	
t Critical two-tail	2.028094	

Figure G.1: Results of the t-test of the effective diffusion coefficients for the compaction and saturation series of soil HH

T-test: Deff for soil WIE		
	<i>Variabele 1/ariabele 2</i>	
Mean	1.72E-06	1.62E-06
Variance	3.3E-13	8.99E-13
Observations	45	36
Hypothesized Mean Difference	0	
df	55	
t Stat	0.575674	
P(T<=t) one-tail	0.283592	
t Critical one-tail	1.673034	
P(T<=t) two-tail	0.567184	
t Critical two-tail	2.004045	

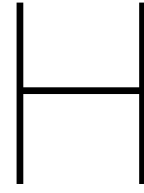
Figure G.2: Results of the t-test of the effective diffusion coefficients for the compaction and saturation series of soil WIE

T-toets: Deff between both soils		
	<i>Variabele 1/ariabele 2</i>	
Mean	2.36E-06	1.68E-06
Variance	8.12E-13	5.77E-13
Observations	70	81
Hypothesized Mean Difference	0	
df	136	
t Stat	5.005568	
P(T<=t) one-tail	8.47E-07	
t Critical one-tail	1.656135	
P(T<=t) two-tail	1.69E-06	
t Critical two-tail	1.977561	

Figure G.3: Results of the t-test of the effective diffusion coefficients for the compaction and saturation series of both soils

Table G.1: Coefficients of determinations for linear and exponential relations for both soils

Relation	R²
Soil HH linear	0.9253
Soil HH exponential	0.8585
Soil WIE linear	0.9484
Soil WIE linear	0.913



Data used to determine the increased predictions in Chapter 4.4

In this appendix the data used to determine the increased predictions given in Chapter 4.4 are given. Table H.1 shows the values from the paper by Cabral et al [9] and Table H.2 gives the values from the paper by Chanton et al [10]. In these tables the different values of α_{trans} for the different percentages that diffusive flux is of the total flux.

Table H.1: The values used for the increased values for oxidation efficiency, for the paper by Cabral et al [9]

D13C landfill	D13C atmosphere	α_{ox}	α_{trans} 2.5%	α_{trans} %7.5	α_{trans} %12.5	α_{trans} %17.5
-57.4	-56.7	1.0245	1.0003	1.0010	1.0016	1.0023
-58.2	-54.6	1.024	1.0003	1.0010	1.0016	1.0023
-57.6	-56.8	1.0219	1.0003	1.0010	1.0016	1.0023
-58.0	-55.5	1.024	1.0003	1.0010	1.0016	1.0023
-59.5	-53.9	1.0248	1.0003	1.0010	1.0016	1.0023
-57.2	-53.6	1.0263	1.0003	1.0010	1.0016	1.0023
-56.0	-42.4	1.0243	1.0003	1.0010	1.0016	1.0023
-56.0	-.59.6	1.024	1.0003	1.0010	1.0016	1.0023

Table H.2: The values used for the increased values for oxidation efficiency, for the paper by Chanton et al [10]

D13C landfill	D13C atmosphere	α_{ox}	α_{trans} 2.5%	α_{trans} %7.5	α_{trans} %12.5	α_{trans} %17.5
-54.59	-51.57	1.0235	1.0003	1.0010	1.0016	1.0023
-54.59	-51.36	1.0235	1.0003	1.0010	1.0016	1.0023
-54.59	-53.54	1.0288	1.0003	1.0010	1.0016	1.0023
-54.59	-52.51	1.0307	1.0003	1.0010	1.0016	1.0023
-54.59	-52.06	1.0311	1.0003	1.0010	1.0016	1.0023
-54.59	-52.52	1.0315	1.0003	1.0010	1.0016	1.0023
-54.59	-52.43	1.0307	1.0003	1.0010	1.0016	1.0023
-54.59	-53.39	1.0311	1.0003	1.0010	1.0016	1.0023
-54.59	-53.09	1.0307	1.0003	1.0010	1.0016	1.0023
-54.59	-54.28	1.0304	1.0003	1.0010	1.0016	1.0023
-54.59	-49.35	1.024	1.0003	1.0010	1.0016	1.0023
-54.59	-49.69	1.0266	1.0003	1.0010	1.0016	1.0023
-54.59	-50.23	1.0269	1.0003	1.0010	1.0016	1.0023